THE $N^{15} + H^1$ REACTIONS

Thesis by

Alois W. Schardt

In Partial Fulfillment of the Requirements

For the Degree of

Doctor of Philosophy

California Institute of Technology

Pasadena, California

1951

ACKNOWLEDGMENTS

It is a pleasure to acknowledge my gratitude to Dr. C. C. Lauritsen and Dr. W. A. Fowler. This research was started at their suggestion and completed with their guidance and help. I wish to thank Dr. R. F. Christy and Dr. T. Lauritsen for many illuminating discussions and suggestions.

The author is greatly indebted to Prof. Don Yost, Dr. David L. Douglas and Mr. Sidney Gibbins of the Chemistry Department for their help in finding suitable nitrogen targets and the preparation of TiN and CrN targets. Further thanks are due to Mr. E. J. Woodbury for operating the 100 kev generator, Mr. L. J. Gililland for supervising the construction of the counter and target arrangement, Mr. V. Ehrgott and J. Antz for executing the drawings.

This research was assisted by the joint program of the Office of Naval Research and the Atomic Energy Commission. The author was helped by Office of Naval Research assistantships from 1947 to 1950.

ABSTRACT

The excitation curve of the reactions (1) $N^{15}(p,\alpha)C^{12}$, (2) $N^{15}(p,\alpha')C^{12*}$, (3) $N^{15}(p,\gamma)O^{16}$ has been measured from 0.2 to 1.6 Mev. The thick target yield of reaction (1) was also measured at 100 kev. A special proportional counter was constructed for this purpose. Approximate theoretical and empirical expressions for some characteristics of proportional counters are given.

Cross sections and nuclear widths without barrier have been calculated for all resonances found. Using intensity arguments, an assignment of parity and total angular momentum is proposed for some levels in O^{16} and C^{13}. As these reactions are part of Bethe's carbon cycle in stellar energy production, the cross sections have been extrapolated to stellar energies.

TABLE OF CONTENTS

I. INTRODUCTION

On proton bombardment of N^{15} the following reactions are energetically possible

$$N^{15} + H^1 \longrightarrow (O^{16}) \begin{cases} \longrightarrow C^{12} + He^4 & Q = 5 \text{ Mev} \quad (1) \\ \longrightarrow C^{12*} + He^4 & Q = 0.53 \text{ Mev} \quad (2) \\ \longrightarrow O^{16} + \gamma & Q = 12 \text{ Mev} \quad (3) \end{cases}$$

Until separated isotopes became available, the study of these reactions was very difficult because N^{15} constitutes only 0.38% of ordinary nitrogen. The first to observe reaction (1) were Burcham and Smith[1]. They bombarded a mixture of oxygen and nitrogen with 0.5 Mev protons and found an alpha particle group of the correct energy. The intensity of this group varied with the nitrogen content of the gas used.

Fowler, Lauritsen, and Lauritsen[2],[3] observed reaction (2) for proton energies between 0.6 and 1.4 Mev using N^{15} enriched ammonium chloride. They observed the 4.5 Mev gamma rays and found resonances at 0.88, 1.03, and 1.20 Mev. Due to the energy spread of their beam, about 20 kev, they were not able to measure the width of these levels. Tangen[4] observed a gamma ray resonance at 0.428 Mev which he attributed to reaction (3)*.

Measurement of the absolute cross sections of these reactions became of interest when Bethe[5] suggested the carbon cycle as a source of stellar energy. This cycle is as follows:

$$(4) \quad C^{12} + H^1 \longrightarrow N^{13} + \gamma \qquad N^{13} \longrightarrow C^{13} + \beta^+ + \nu$$

$$(5) \quad C^{13} + H^1 \longrightarrow N^{14} + \gamma$$

$$(6) \quad N^{14} + H^1 \longrightarrow O^{15} + \gamma \qquad O^{15} \longrightarrow N^{15} + \beta^+ + \nu$$

$$(1),(2) \quad N^{15} + H^1 \longrightarrow C^{12} + He^4$$

In addition reaction (3) would remove carbon permanently from the cycle. The first attempt to measure the cross section of reaction (1) was made by Holloway and Bethe[6]. They measured σ_1 near 360 kev but did not measure the

---

* Our results indicate that this resonance is due to reaction (2).

energy accurately. As the cross section changes rapidly in this region (Figure 17), their measurement is not very significant. Cochrane and Hester[7] measured the excitation of reaction (1) from 0.2 to 0.5 Mev. They found a resonance at about 0.4 Mev. Unfortunately their statistics are insufficient to give a good value for the position or half width of this resonance.*

In order to calculate reaction rates under stellar conditions, it is necessary to know the cross sections at energies near 30 kev. At these energies a direct measurement of the cross sections is impossible because they are very small (e.g. $\sigma_1 = 4 \times 10^{-15}$ barns at 28 kev). It is necessary to know the excitation function in order to make a reasonable extrapolation from the smallest measurable cross sections ($\sim 10^{-7}$ barns) to stellar energies.

In this investigation accurate excitation curves for $N^{15} + H^1$ have been obtained. To measure the small cross sections at low bombarding energies it was necessary to develop a special proportional counter. As a part of this research the advantages and limitations of proportional counters in detecting heavy particles has been investigated.

The $N^{15} + H^1$ reaction belongs to a group of reactions leading to multiple alpha particle nuclei. Fairly complete nuclear models have been worked out for these nuclei by Wheeler[8], Hafstad and Teller[9], and Dennison[10]. The alpha particle nuclei are lighter than their neighbors; therefore the compound nucleus is formed in a highly excited state.

$H^3 + H^1 \longrightarrow (He^4)$	19.8 Mev excitation**
$Li^7 + H^1 \longrightarrow (Be^8)$	17.21 " "
$B^{11} + H^1 \longrightarrow (C^{12})$	15.96 " "
$N^{15} + H^1 \longrightarrow (O^{16})$	12.11 " "
$F^{19} + H^1 \longrightarrow (Ne^{20})$	12.90 " "

---

* The cross section they measured is also considerably smaller than the one found in this investigation.

** The excitation energies are taken from Hornyak and T. Lauritsen[11].

With the exception of $F^{19}(p,\gamma)Ne^{20}$, all reactions show strong capture radiation. In most cases the capture radiation competes with the (p,α) reaction. With the exception of the H^3 and Li^7 reactions, several groups of alpha particles are emitted corresponding to the ground and excited states in the residual nucleus.

Because of the large excitation, the alpha particle model cannot be expected to hold for the compound nucleus. It should, however, hold for the levels in the residual nuclei. In the case of O^{16*}, which is formed by the $F^{19}(p,\alpha)$ reaction, the lowest levels are 0(+) and 3(-) (Figure 25)[12]. Except for a slight displacement, this agrees well with the predictions made by Dennison[10]. The only excited state of C^{12} which can be reached by $N^{15}(p,\alpha)$ is at 4.47 Mev. An analysis of intensities at the different resonances (refer to Chapter VI), together with information from other reactions, indicate J = 2(+), again confirming the alpha particle model.

In the region which has been investigated (0.1 to ~1.6 Mev) the $B^{11}(p,\alpha)$, $N^{15}(p,\alpha)$, and $F^{19}(p,\alpha)$ reactions have a much greater width without barrier for short range alpha particle emission than for long range alphas. Thus the emission of short range alpha particles is inherently more probable. This manifests itself for the B^{11} and F^{19} reactions in a ratio of about 1 to 100 in the cross sections of the long to short range alpha particles. Because of a large barrier factor for the short range alpha particles, the cross sections are about equal in case of the $N^{15}(p,\alpha)$ reactions (Figure 16).

For bombarding energies in the range of 0 to 2 Mev the number of levels in the compound nucleus increases rapidly with atomic number. There is probably one in He^4, about three in Be^8 and C^{12}, six in O^{16} and a great multitude in Ne^{20} [11]. It is to be hoped that, as more information becomes available about these "simple" alpha nuclei, it will be possible to develop a more comprehensive theory.

II. PROPORTIONAL COUNTERS

Electron Collection and Pulse Shape.

Proportional counters have been investigated and described by many investigators[13],[14],[15]. The purpose of this investigation was to develop a heavy particle counter which had a large aperture and was insensitive to electric disturbances. Another counter desired was one sensitive to low energy alpha particles* and capable of measuring them in the presence of a proton background. A consideration of the mechanics by which pulses are formed is necessary in order to determine the design parameters.

The properties of different counter gases have not been investigated systematically. Most of the information available[15] is for 95 to 90% argon and 5 to 10% CO_2. Therefore only this filling is treated here; however, most of the considerations apply equally well to other gases. The particle to be counted produces heavy ionization along its path. Under the influence of the electric field in the counter the electrons move toward the collecting wire. A certain amount of recombination will occur if this field is too small. Rossi and Staub[16] have shown that for argon $E/p \geq 0.7$ volts/cm per mm Hg** is necessary for approximately 100% collection. If the pulse height is to be independent of the position of the track in the counter the above condition on E/p has to be satisfied.

In general it is desirable to collect the electrons quickly, in order to obtain fast pulses. For $E/p < 0.5$ volts/cm per mm Hg the electron velocity decreases rapidly.[17]. The electric field inside a counter is the same as for two concentric cylinders of radius a and b. (a = radius of central wire,

---

* Alpha energy between 0.6 to 2 Mev.

** E = electric field inside counter.
p = pressure of gas filling.

b of counter)

$$\frac{E}{p} = \frac{Vo}{\log b/a} \cdot \frac{1}{rp} \qquad (1)$$

Here Vo is the voltage across the counter, p the pressure, and r the distance from the central wire. Thus E/p is smallest at r = b. Typical operating conditions of the counter used (Figure 1) were Vo = 1000 volts, p = 200 mm Hg, and a = .005 inch and b = 0.50 inch; then $E/p \geq 0.87$. This shows that a counter to be operated with a high pressure needs a correspondingly high voltage.

Under the above conditions the electron velocity is about 5×10^6 cm/sec, and all electrons will be collected within 0.2 μ sec. Very close to the central wire secondary ionization occurs. Gas multiplication occurs so close to the central wire that the ions formed do not contribute to the pulse until the positive ions move toward the outer cylinder[14]. With a gas amplification of 50 or more the primary electrons contribute only a few per cent to the pulse height. The motion of the positive ion sheath produces the main part of the pulse.

If we assume that all primary electrons reach the central wire simultaneously and that the drift velocity of the positive ions is proportional to the electric field, it is possible to derive an expression for the pulse shape.* The change of voltage across the counter is given by

$$V_c = \frac{-\, m\, n_o e}{2C \log b/a} \log (1 + t/t_o) \qquad (2)$$

and

$$t_o = \frac{a^2 \log b/a}{2V_o(K/p)} \qquad (3)$$

$$V_{max} = -\frac{m\, n_o e}{C} \qquad (4)$$

---

* Refer to References (13), (14) and appendix.

m = gas multiplication, n_o = number of primary ions, e = electronic charge, C = total capacity across counter, t = time after collection, and K/p is the mobility of positive ions. For argon K/p is about 3 cm/sec per volt/cm per atmosphere. This expression holds true until the positive ions reach the outer cylinder several milli-seconds after the pulse started, then $V_c = V_{max}$.

In general the pulse is differentiated by a short time constant in the amplifier, which consists of a R_1C_1 network. Then the voltage developed across the resistance is given by

$$V = \frac{-m\, n_o e}{2C \log b/a}\, e^{-\frac{t + t_o}{\tau}} \left[\bar{E}_i\left(\frac{t + t_o}{\tau}\right) - \bar{E}_i\left(\frac{t_o}{\tau}\right) \right] \qquad (5)$$

where $\tau = R_1C_1$ and $\bar{E}_i(x)$ is the exponential integral tabulated in Jahke and Emde[18]. For the counter shown in Figures 1 and 3 V/V_{max} has been plotted (Figure 1). It should be noted that the pulse decays slowly compared to $e^{-t/\tau}$ and has a rather flat top. The experimental data agree with the theoretical curve, except during the first 0.3 μ sec; here the effect of electron collection is noticeable.

If one wants to estimate the effect of different values of τ equation (3) is inconvenient. In Figure 2 the ratio of maximum pulse height to pulse height for $\tau = \infty$ has been plotted as a function of τ/t_o.* Also given is the time (t_m) at which the maximum is reached. To use these curves one calculates t_o from equation (3) and V_{max} from equation (4). This theory breaks down if t_m is of the same order of magnitude as the electron collection time. In that case the experimental pulse height is smaller than given and t_m is larger.

The effect of space charge has been neglected. Since it takes several milli-seconds until the positive ions reach the cathode, a considerable charge

---

* b/a = 100 was used. For other values of b/a multiply the pulse height scale by log 100/log (b/a).

may build up at high counting rates. This is kept at a minimum by using only small pulses. However, the pulses should be 10 to 100 times noise. Generally 10 to 50 μ volts of noise is produced by the first tube and 80% of the pulse is lost by differentiation. Thus the pulse should be approximately 5 milli-volts. For an input capacity of 15 $\mu\mu$f this corresponds to 5×10^5 electrons. A particle loses 20 to 30 volts for every ion pair produced. Thus for a particle losing 200 kev in the counter, a gas amplification of 50 is needed.

Pulse Height.

As shown above the height of a pulse is ideally only a function of the number of primary ions formed. In the case of argon this is directly proportional to the energy lost in going through the counter gas[19]. Different groups of particles may thus be distinguished if they lose different amounts of energy in the counter. Depending on the specific experiment this difference can be increased by proper choice of gas pressure in the counter and of stopping foils.

Unless care is taken many factors will introduce a spread in pulse height. One would hope for equal pulses from a homogeneous group of particles, each particle traversing the same distance in the counter. Naturally some may be close to the center, others near the cathode of the counter. Let us consider briefly the different factors contributing to the spread in pulse height.*

1. Statistical fluctuations in the number of primary ions formed. If the particle loses about 0.3 Mev in the counter gas, more than 10,000 ion pairs are formed, and hence this effect is small.
2. Recombination. With sufficiently strong collection fields recombination can be practically eliminated.

* A more detailed discussion of most of these effects is given in Rossi and Staub[15].

3. Formation of negative ions. Electrons do not attach themselves to molecules of counter gases like A or CO_2. But if O_2 or H_2O are present some primary electrons are lost from the pulse by forming negative ions. Little quantitative data is available. However, a partial pressure as high as 10^{-2} mm Hg does not interfere with the operation of the counter.

4. End effects. The electric field is distorted near the end of the counter. Thus the gas multiplication varies along the wire, and some electrons may not even reach it. This can be minimized by using only the middle of the counter, at least one diameter away from each end. Alternately the counter may be especially designed to have a uniform field near the end[20].

5. Imperfections in central wire. The gas multiplication depends critically on the field within one diameter of the central wire. Variation in the diameter will cause trouble especially for thin wires. If the wire is not centered, the field will also be distorted. For formulas refer to Rossi and Staub[15].

6. Statistical fluctuations of gas multiplication. This has to be considered only if a small number of primary ions is collected. Hanna, et. al.[21] found that, for a mean number of primary ions between 10 and 700, the fluctuations in pulse height was only slightly larger than would be expected from the statistical fluctuation in the number of primary ions formed.

7. Space charge effects. At high counting rates or in the presence of X ray background, sufficient space charge may be built up to distort the counter field. Then the gas multiplication will

be a function of the local spare charge. This effect is not noticeable unless the counting rate is increased beyond 2,000 counts/sec, and then only if large pulses are used.

8. High voltage. The gas multiplication is practically an exponential function of counter voltage. For an A + CO_2 filling the multiplication may change as much as 1% per volt and even more rapidly at very high multiplication. Thus the power supply should be stable to better than 1 volt in about 1500 volts and have a minimum of ripple.

If the gas filling in the counter is unstable* the pulse height will drift slowly, although it is homogeneous at any instance. Unless very accurate pulse height analysis is needed this drift can be compensated by changing the voltage on the counter. If a very thin organic window is used, it may be necessary to flow gas through the counter continuously. The allowable variation in pressure may be computed as follows:

$$\frac{1}{M}\frac{\partial M}{\partial p} = \frac{1}{M}\frac{\partial M}{\partial V}\Big/\frac{\partial V}{\partial p} \qquad (6)$$

where M is the gas multiplication, V the voltage on the counter and p the pressure. Curves of M vs. V and V vs. p have been published[15]. $\partial V/\partial p \approx 25$ volts/cm over a pressure range of 10 to 40 cm. Thus for $M = 60$ $\frac{1}{M}\partial M/\partial p \approx 15$ to 20% per cm Hg. This indicates that the counter will operate satisfactorily if the pressure is kept within 1 mm Hg[22].

From the above one would expect that counters may be operated with only a few per cent spread in pulse height. Figure 4 shows several typical integral pulse height curves. Proportional counter #1 (Figure 3) was designed

---

* e.g. if organic vapors are given off by the window.

according to the above considerations. With 0.80 Mev protons only 5% spread in pulse height was observed.* In counter #2 (Figure 5) the end of the counter was used in order to obtain a larger solid angle, and the pulses are no longer of uniform height.

Description of Counters and Accessories.

Proportional counter #1 (Figure 3) was built primarily for use with a magnetic analyzer. It is designed to distinguish between different particles which are focussed by the same magnetic field. This can be done most easily by using the difference in specific ionization. Thus the path length in the counter is only 2.5 cm and the gas pressure 10 to 40 cm Hg. The particles enter the sensitive volume perpendicular to the counter axis through a 5/16 inch window. Mica, clamped between the two lead washers, was found to be very satisfactory for a window. Foils 1.5 mg per cm^2 (stopping power equivalent to 1 cm of air) could support atmospheric pressure in either direction and gave counters which showed no drift in pulse height for several months.

If the particles have a range smaller than 1 cm of air it is necessary to use thin organic foils. Supported by a grid they will hold atmospheric pressure in one direction. Figure 3 gives an enlarged drawing of such a support. A foil with a stopping power of 1.7 mm of air, made of our layers of New Skin,** was glued to this with a drop of shellac. A lead washer is used as a seal between support and counter. Before filling the counter has to be attached to the main vacuum system and cannot be removed from it until it is filled to atmospheric pressure. As the normal filling is only 20 cm Hg, the counter has to be refilled every time its window is exposed to atmospheric pressure.

---

* The 4% rise in counts at half pulse height is due to protons hitting the collecting wire.

** Manufactured by New Skin Company, Brooklyn, New York.

Frequent refilling* of the counter is desirable because the window gives off organic vapors. These do not increase the spread in pulse height but raise the operating voltage. For instance 1380 volts was needed one week after filling to give the same pulse height as 940 volts gave the first day. No attempt was made to use any thinner windows, although it is possible to use foils thinner than 0.5 mm air equivalent. In that case continuous gas flow through the counter is necessary, because foils of this thickness tend to leak.

For measuring small cross sections (10^{-31} cm^2) a counter with a large aperture is needed. Since the above design is not adaptable, an end-window counter** was used. As can be seen from Figure 4 counter #2 does not give pulses of uniform height. However, if only one group of particles is to be counted it is satisfactory. In order to prevent charging the window by scattered protons, the mica foil was coated with 0.2 mg/cm^2 of aluminum leaf. The counter was used at a high gas amplification in order to minimize interference from the accelerating column. Thus it is possible to mount the counter 0.8 inches from a target, bombarded with a 100 μ ampere beam, and detect counting rates as low as 2 counts per minute.

To amplify the counter pulses the amplifier described by Jordan and Bell (23) was used. It has a gain of 10,000, thus it will amplify 10 mv. pulses to 100 volts. A two tube pre-amplifier with a gain of 10 was mounted next to the counter. A 1.5 μ second clipping time together with a 0.15 μ second rise time gives best results. The clipping time is sufficiently short to eliminate microphonics and low frequency pickup, yet long enough to give about 20% of the maximum pulse height. The fast rise time is advantageous because a true

---

* If a mixture of A + CO_2 is available filling takes less than 10 minutes.

** A Radiation Counter Laboratory pressure seal mica window counter was refilled with 26 cm Hg of A + CO_2.

picture of the pulse can be observed in an oscilloscope, and improper operation of the counter is quickly spotted.

The high voltage power supply has to be stable and free of low or high frequency ripple. A shunt type regulator with a d.c. loop gain of over 1,000 was designed for this purpose. The output voltage is continuously variable from 600 to 1500 volts. It regulates against a 45 volt battery. The ripple at 1500 volts is less than 5 milli-volts rms. After a warm up period of one hour the output voltage drifts at most 0.056% per hour. Line voltage fluctuations have an even smaller effect. This power supply was used in all experiments and proved to be very satisfactory.

III. EXPERIMENTAL ARRANGEMENT AND PROCEDURE

A solid nitrogen compound enriched with N^{15} was bombarded with monoenergetic protons. The yield of alpha particles and quanta was then measured as a function of proton energy. For most of the work, the protons were accelerated by the 8 ft. by 13 ft. electrostatic generator of the California Institute of Technology[3]. Their energy is held constant to within 0.02 per cent. At 0.10 Mev the transformer rectifier set and RF ion source described by Hall[24] was used. It supplies over 200 μ amperes of beam current. The target arrangements are shown in Figures 5 and 6. The chambers are made out of brass. O-rings* are used for vacuum seals. This construction proved to be very satisfactory. Everything is readily accessible and can be assembled in a matter of minutes. Fourteen O-ring seals are used in the target chamber shown in Figure 6, yet none of them leaked during the course of the experiments.

100 Kev Apparatus

The target chamber (Figure 5) was designed for large solid angle and efficient cooling of the target. The counter aperture is 0.700 inches from the target spot. Apertures, 0.532 and 0.750 inches in diameter, were used giving solid angles of 0.40 and 0.75 steradians, respectively.

The target support is made from a 7/8 inch brass rod. Two 3/32 inch holes parallel to its axis are for air cooling. For 2 1/2 inches, half of it is machined off so that the target spot falls on the axis. The vacuum seals are arranged such that the support can rotate about its axis and be moved up and down. Lucite spacers insulate it from the main target chamber. A 1/8 inch rod, soldered to it, extends the axis of the main target holder. It keeps the target aligned. A pointer fastened to this rod rides on a

---

*Manufactured by Linear, Inc., State Road and Levick, Philadelphia, Pennsylvania.

protractor and is used to measure the angle between the target and the beam. Slots in the target holder can accommodate three round target pellets, 3/16 inch thick and 1/2 inch in diameter. Setscrews hold them in place and insure good thermal contact.

Since the target spot is very close to the counter, its position has to be well defined. This is accomplished by collimating the proton beam with 3/16 and 3/32 inch apertures, 5 1/2 inches apart. A 3/32 inch hole in the support may be put in the target position, and the beam allowed to pass through. The fluorescence in the quartz plate is used for visual alignment. These apertures cut down the beam current, but a current of 100 μ amp was sufficient to give statistical errors smaller than those due to other sources. A separate pumping connection to the main vacuum system is provided, because the pumping speed of the 3/16 inch hole is too small. To reduce the deposition of carbon by the beam a liquid air trap was provided as shown.

The beam current is measured from the target support, which is at +300 volts with respect to the target chamber to prevent emission of secondary electrons. A guard ring at -300 volts prevents secondary electrons, produced at the 3/32 inch aperture, from entering the target chamber. The current from the target chamber was also measured. It is practically zero for boron targets. However, in the case of TiN targets, at 45° with the beam, about 5% of the total beam current hits the target chamber. This is due to the large Coulomb scattering cross section at 0.10 Mev.

A polonium alpha source can be placed in the target position and the pressure in the chamber adjusted such that 3.7 Mev alpha particles entered the counter. A bias curve, as shown in Figure 4, was measured to ensure 100% efficiency of the counter. The over-all arrangement was checked by measuring the yield of the $Li^7(p,\alpha)\alpha$ reaction at 100 kev. The results agree within 10 per cent with the very accurate measurements of Haworth and King[25].

The $Li^7(p,\alpha)\alpha$ and $B^{11}(p,\alpha)Be^{8*}$ reactions have a very large yield compared to the $N^{15}(p,\alpha)C^{12}$ reaction. As slight impurities of boron could not be eliminated, two nitrided titanium pellets were mounted on the target support. One had been nitrided with atmospheric nitrogen, the other with nitrogen enriched to 31.5 atom per cent of N^{15}. Both targets were washed together with the same solutions to make sure that any boron contamination was distributed equally between the two targets.* After aligning the beam, the target was turned to 45°. First a blank run was made on the brass of the target support. Generally 30 to 60 counts for 0.06 Coulombs were observed. This gives a check on the boron content of the cleaning solutions and the stability of the counter. Then the two TiN targets were bombarded, each for 10 minutes. After 10 minutes (0.06 Coulombs) a visible black deposit had been built up on the target, and a slight loss in counting rate was noticeable. Since the beam spot is very small, three different spots could be used on each target. The difference of counts between the normal and enriched TiN targets was taken as due to $N^{15}(p,\alpha)C^{12}$. Measurements were also made with a thick boron target.

0.2 to 1.6 Mev Target Arrangement

At these higher energies cross sections are generally between 10^{-3} and 1 barn. Thus a beam current of less than 0.5 μ amp is sufficient. The KNO_3 used as target is somewhat unstable under prolonged bombardment, therefore it is desirable to have a fairly large solid angle subtended by the detector. Up to 0.85 Mev the elastically scattered protons can be stopped by foils which pass the long range alpha particles. A proportional counter with a mica window was used to count the alphas. At higher energies the heavy particle spectrograph described by Snyder, Rubin, Fowler, and Lauritsen[26] was employed

* The effect of boron will be discussed further in the section on targets.

to resolve protons and alphas.

The target arrangement is shown in Figure 6. The target chamber proper consists of a brass box 2 inches in diameter and 3/4 inch deep. The front face is made of dural with an O-ring seal at the side. The foil holder is supported by it and may be manipulated from outside the vacuum. A 3/4 inch glass window on the lid allows visual adjustment of the target. The proportional counter window, 0.317 inch in diameter, is 0.800 inch from the target spot, thus it subtends 0.94% of a sphere. The beam was collimated to 1/16 inch wide and 3/32 inch high.

The target support consists of a copper strip fastened to a 1/8 inch drill rod. It can be moved vertically between the furnace and the target chamber. It is insulated and centered by a lucite plug at the top and a spider at the bottom. A pointer, attached to the rod just below the lucite handle, indicates the angle between target and beam. For focussing the beam may be allowed to pass through a hole in the target support and can then be observed in the quartz window. Occasionally it was desirable to deposit the KNO_3 on a thin silver foil. In that case the beam passed through the foil and was collected on the quartz window.

The furnace, shown below the target chamber (Figure 6), is used to evaporate the KNO_3. No cooling is needed in the furnace because KNO_3 evaporates between 300° and 400° C. Since this is below red heat, it is necessary to be able to watch the salt in the furnace boat. A window, just behind the target support, gives a full view of the boat. The cap with the glass in it may be removed and washed without disassembling the furnace. The KNO_3 forms a clear, transparent deposit and does not obstruct the window until a thick coat has been evaporated. The heating element is made of 0.003 inch tantalum metal. About 20 amperes was needed to evaporate the KNO_3.

At bombarding energies above 0.85 Mev, the scattered protons block the counter. A magnetic spectrograph with scintillation counter[27] was used to

separate protons and alpha particles. The target arrangement has been described in detail by Snyder, et. al.[26]. It is very similar to Figure 6 except the vacuum chamber of the spectrograph joins at the place where the proportional counter is shown. A mica foil can be interposed between the target and the spectrograph to slow down the long range alpha particles from 5. Mev to below 2 Mev. The angle of observation was 137.8° with the beam. Observation in the backward direction is preferable, because in that case the target is at a large angle with the beam (62°), and small uneveness in the surface of the target does not affect the resolution. Also the proton scattering cross section is smaller in the backward direction.

The energy of the short range alpha particles decreases more rapidly than the energy of the scattered protons as the angle of observation goes from 0° to 180°. At 58° the alphas are focussed at a higher magnetic field than the protons. However, the scattering cross section is very large at this angle, and the tail of the Cu(p,p) curve extends about 0.15 Mev beyond the cut-off field (Figure 14). As the scintillation counter does not differentiate between protons and alpha particles, it was necessary to take counts with and without a 1 mg per cm^2 aluminum foil. This foil stops 100% of the alphas but only 22% of the protons. The C^{12++} are stopped by $\approx$0.2 mg per cm^2 aluminum foil.

The target makes an angle of 30° with the beam. Thus a very smooth target surface is required; otherwise the resolution of the spectrograph is masked by straggling in the target. To prevent this, the copper support was polished to a mirror finish, then a thin, uniform layer of KNO_3 evaporated.

The gamma rays were detected with the Geiger counter coincidence setup described by Fowler and Lauritsen[28]. In order to gain a larger solid angle, the two back counters were only 18 cm of the front counter. The sides of the front counter, not facing the back counter, were surrounded by .10 inch of aluminum tubing. The whole setup was placed in a lead house for shielding.

1 cm of aluminum converter was used in addition to conversion in the wall of the vacuum chamber. Under these conditions the front counter has practically the same efficiency as a counter surrounded by a saturation length of aluminum[28].

Cylindrical counters, made by the Radiation Counter Laboratory, were used. The active volume is 3 5/8 inches long and 23/32 inches in diameter. The center of the front counter was 1 1/2 inches from the target. This corresponds to poor geometry, and the solid angle has to be found empirically. The gamma ray yield was measured at the 0.898 Mev resonance in this position and with the counter at 9.8 cm from the target. In the latter position the solid angle can be calculated using standard formulas[28]. This gives 1.27% of a sphere at 9.8 cm, and from the ratio of yields 6.5% of a sphere at 1 1/2 inches.

Each time air was let into the system the target support was cleaned and polished. After a fresh target had been layed down, it was moved into bombarding position. The target thickness was measured at top, middle, and bottom using the 0.898 Mev gamma resonance. (Figure 19b). For the thicker targets the half width was used. For targets less than 5 kev thick the area under the curve was compared to the thick target step.* The thickness at other points of the target was found by interpolation. After a short bombardment, about 10 to 15% of the nitrogen is lost and the target has to be moved until a fresh spot is hit by the beam. Thus the curves are made up of measurements taken with many different spots, the thickness of which varies by about 15% from the mean.

Between 0.4 and 1.6 Mev the proton (H^+) beam of about 0.2 μ-amp was used. For lower energies it was necessary to use the molecular beam (HH^+). The deuterium contamination of the molecular beam caused no appreciable counts in the proportional counter. This was ascertained by running a semi-thick target curve with the proton beam.

---

* The area under a resonance curve is equal to the target thickness times the thick target yield.

down to 0.25 Mev. The current, however, was too small for thin target work. The gamma ray yield was greatly increased by the deuterium contamination and no measurements could be made below 0.4 Mev.

Targets

In experiments involving nitrogen as a target, it has always been difficult to find a suitable compound. Gas targets could not be used because the proton straggling in the entrance foil would distort the excitation curve. The 0.429 Mev resonance is only 0.9 kev wide and below 0.30 Mev the alpha cross section decreases very quickly, thus only a few kev straggling in the proton beam would change the yield significantly.

The nitrogen compound used must be stable in vacuum and should not decompose under bombardment. The other elements present should not effect the measurements to be made. Thus they should not give any alpha particles or gamma rays. At least, if they have a finite proton cross section, it should be small compared to the corresponding N^{15} cross section. As much nitrogen per unit stopping cross section as possible is desirable. Organic compounds and azides are too unstable. Certain nitrides have all the above qualifications. Titanium nitride (TiN) is very stable and easily made by heating titanium in a nitrogen atmosphere.

Sintered titanium metal was machined to small pellets (1/2 inch diameter, 3/16 inch thick) and then heated in an atmosphere of normal or enriched ammonia. Control pellets were also made out of chemically pure TiN powder. When the normal nitrogen targets were bombarded at 0.100 Mev, a large number of alpha particles was observed. Their yield varied between different targets and could not be attributed to the N^{15} content. With appropriate stopping foils their energy was found to be between 3 and 4 Mev. Among the light elements only the $N^{15}(p,\alpha)C^{12}$ and $B^{11}(p,\alpha)2\alpha$ reactions produced alpha particles in this energy range. A compressed amorphous boron target was bombarded and gave more than

10,000 times the yield expected from the N^{15} reaction. Thus traces of boron on the nitrogen targets were falsifying the results.

To be able to correct for the boron contamination two pellets were used. One had been nitrided with 31.5% enriched N^{15}, the other with ordinary nitrogen. They were washed together in the same solutions: first dilute HCL, distilled water, and finally ethyl alcohol. Thus it may be assumed that the same amount of boron was on both targets. Different spots on the same targets gave consistent results. The enriched target gave about twice as many counts as the normal TiN. The difference between the two has been taken as the effect due to $N^{15}(p,\alpha)C^{12}$.

To get more reliable results an attempt was made to eliminate B^{11} to 1 part in 100,000. Unfortunately boron is a fairly common element. It is in borax and generally found associated with sodium and potassium salts. For instance glass contains an appreciable amount. Chemical methods are not suitable for measuring such minute impurities; thus many targets were prepared, and the yield due to $B^{11}(p,\alpha)2\alpha$ was measured. It was found that the titanium metal was contaminated with boron. Members of the Department of Chemistry suggested using CrN instead. They were able to chromium plate and nitride copper pellets without picking up much boron. In the subsequent measurements, however, no effect due to $N^{15}(p,\alpha)C^{12}$ was detectable, although nitrogen enriched to 61% with N^{15} had been used.

At 0.10 Mev bombarding energy only the surface layer of the target contributes to the yield, because the stopping power is at its maximum and the cross section decreases rapidly with energy. But exactly the surface layer will not nitride properly if traces of more active gases are mixed with the ammonia in the nitriding furnace. In order to analyze this surface layer protons were elastically scattered by the target. If a homogeneous beam of protons hits a target, the energy of the scattered proton depends on the scattering nucleus. This method has been described by Rubin and Rasmussen[29].

The magnetic spectrograph described above was used with small slits to improve the resolution.

Figure 7 shows the number of protons scattered into the spectrograph by different targets. In order to have accurate calibration points chemically pure TiN^{14} and copper oxide were used first. At a fluxmeter reading between 43.0 and 43.5 the protons scattered by the heavy metal came in. At lower magnetic fields (larger fluxmeter readings) protons scattered by lower layers of the target reach the counter. At 46.8 the protons scattered by the oxygen at the surface of the target are noticeable as a step in the copper oxide curve. A similar step may be observed for the nitrogen in the TiN^{14} curve. The peak at 48.6 is due to a thin carbon layer deposited by the beam.

The nitrided chromium target has a step at the O^{16} position but not the slightest indication of either N^{14} or N^{15}. Presumably the process was not successful and all measurements made with it were disregarded. The nitrided titanium target has a step due to N^{14}, while the N^{15} is masked by a thin oxide layer. We can conclude that 31.5% N^{15} is in the target since the chemical activity of the two isotopes is practically the same.

In the region from 44 to 47, however, we notice a larger number of protons scattered by the titanium of the nitrided target than by the TiN^{14}. For fluxmeter readings larger than 45 it is almost the same as for pure Ti metal. As can be seen from the formulas developed by Fowler, et. al.[28], the yield of scattered protons from titanium is inversely proportional to the stopping cross section per scattering nucleus. Thus the proton scattered by the Ti of TiN are only 2/3 of those for Ti metal.* The knee of the scattering curve between 43.5 and 49.5 indicates the presence of nitrogen, but considerably less than in the case of TiN. To take account of this, the cross sections

---

* The stopping power of titanium is twice that of nitrogen.

measured with this target have to be increased. By comparing the gamma ray yield at the 0.898 Mev resonance with the thick target yield of a KNO_3 target, it was found that the surface layer has only 2/3 as much nitrogen as TiN for the same stopping power. Thus the results obtained at 0.10 Mev with this target have to be multiplied by 1.5.

The proton scattering analysis gives us only the surface composition of the target. This is sufficient in evaluating the 0.10 Mev data, because there the protons do not penetrate very deep into the target. At higher energies deeper layers contribute, and the target composition has to be known. Use was made of the 0.898 Mev gamma ray resonance (Figures 16 and 18). It has a width at half maximum of 2.2 kev and is responsible for most of the gamma ray yield up to 1.2 Mev. The quantum yield between 0.9 and 1.1 Mev is a measure of the N^{15} concentration at a distance of $(E_p - 0.898)$ Mev below the surface of the target.*

The chromium targets showed some N^{15} distributed over at least 0.3 Mev. Starting with none at the surface, it reached a maximum about 30 kev below the surface and then decreased slowly. The nitrogen concentration was always small compared to the nitrogen content of CrN. The titanium target had a yield corresponding to 2/3 of TiN at the surface. The nitrogen concentration decreases then approximately linearly for about 0.15 Mev. A small tail extends for at least 0.10 Mev more. This nitrogen distribution is to be expected from the diffusion of the ammonia into the heated titanium metal.

The nitrided titanium target is not very convenient for most of the work, because it integrates with the above nitrogen distribution as weight factor. Also the alpha particles, coming from the lower layers of the target, lose

---

* The distance expressed in Mev can be converted into cm by using the stopping cross section per atom at 0.9 Mev and the number of atoms per cm^3 of the target.

much energy in coming out. This makes it difficult to count all the alphas. After a survey of the region from 0.4 to 1.6 Mev bombarding energy, it was apparent that many details were obscured by the target structure.

For a complete investigation of the excitation curve, one needs a large number of different target thicknesses. A target is thin if the cross section is almost constant over the target thickness. With this limitation it should be as thick as possible to give maximum yield. A semi-thick target is thick compared to the resonance (about 10 width), but thinner than the distance between resonances. In that case one can measure the thick target yield of the resonance without interference from the other resonances. In alpha particle measurements, the target must be thin enough to alphas to avoid excessive energy spread. The nitrogen concentration should be constant throughout the target. These requirements are most easily satisfied if the target material can be evaporated or sublimed into a support.

Nitrogen compounds which sublime in a vacuum without decomposition are not numerous. Practically all nitrides decompose at least partially when heated. Gallium nitride may be an exception, but it is rather difficult to make. The cyanides look most hopeful. Both KCN and $CaCN_2$ were found to sublime satisfactorily. Unfortunately it was impossible to obtain either of them enriched with N^{15}. N^{15} is commercially available in the form of KNO_3.* This compound decomposes already at 400°C and is known to be somewhat unstable under bombardment[4]. To show that it evaporates without decomposition, a thin layer was deposited on silver leaf and analyzed with scattered protons. Figure 8 shows 1.61 Mev protons scattered by a clean silver foil and after $KN^{14}O_3$ had been deposited on it. The N^{14} peak is quite noticeable and decreased only slowly after prolonged bombardment.

---

* Eastman Kodak Company, Rochester, New York

The evaporation of KNO_3 has to be done rather carefully, since it decomposes before the filament shows any color. Until all the water has been boiled off, the melt in the furnace tends to sputter. If the target is exposed to air after evaporation, moisture is absorbed and the yield per kev of target thickness decreases. Only a slight increase in pressure accompanied the evaporation, thus decomposition should be small. Targets, evaporated after repeated heating of the furnace, did not show a marked decrease of nitrogen content. Boron compounds do not sublime at low temperatures, thus no trouble from boron contamination was encountered.

Under bombardment with 0.1 to 0.2 μ amp the KNO_3 targets were not very stable. The current density was not constant over the target area, therefore the central part lost nitrogen more quickly. Since the beam wanders slightly when the voltage is changed, the counting rate showed appreciable fluctuations. In most of the graphs the fluctuations are primarily due to this cause. The target was frequently changed to minimize this effect, but then the variation in thickness of the target became bothersome. The loss of nitrogen was assumed to be proportional to the total charge collected. The rate of loss was checked frequently by comparing yields at selected bombarding energies.

The target thickness in kev was always measured by means of the 0.898 Mev resonance, either by width at half maximum or by the area under the curve. It should be accurate to better than 10%. This was converted into a number of N^{15} atoms by dividing the width by the stopping cross section per N^{15} nucleus. For KNO_3 enriched to 61% with N^{15} this cross section is equal to 5.57×10^{-17} kev cm at 0.90 Mev. On all graphs the target thickness has been given at 0.90 Mev.

IV. EVALUATION OF EXPERIMENTAL DATA

The raw data consists of counts per microcoulomb as a function of bombarding energy. This is sufficient to give the position and width of resonances if they are not too wide. In general, however, the quantities of primary interest are cross sections and the partial widths without barrier for the different competing processes.

As long as the angular distribution of the reaction products is not known, it is most convenient to express the results as 4π times the differential cross section per unit solid angle in the direction of observation.

$$\sigma_{eff} = \frac{4\pi}{\Omega_c} \frac{N_o}{nt} = \frac{Y}{nt} \tag{7}$$

N_o is the number of disintegrations counted per proton, Ω_c is the solid angle subtended by the detector in the center of mass system, and nt is the number of N^{15} nuclei per square centimeter of target. For thin targets and isotropic distribution this is identical with the integrated cross section. Different detecting methods and target thicknesses have been used. Each one requires a rather special treatment.

100 Kev Data

At this low bombarding energy the variations of the cross section with energy is primarily determined by the Gamow penetration factor. Its rapid variation (10% per kev), and the fact that the stopping power for protons is at its maximum, makes it impossible to use thin targets. Neglecting the effect of resonance factors, Hall and Fowler[30] have derived an expression for the cross section using the thick target yield.

$$\sigma = \frac{0.993\ \varepsilon\ Z_o\ Y}{2E^{3/2}} \left(1 + \frac{E^{1/2}}{Z_o} + \ldots\right) \tag{8}$$

where E is the proton energy in Mev, Y the thick target yield in disintegrations per proton, ε the stopping cross section per active nucleus in Mev-cm^2, and Z_o

the atomic number of the target nucleus. If we have isotropic distribution of the emitted particles, Y can be computed from the number of counts "N" as follows:

$$Y = \frac{N}{6.24 \times 10^{12}\ q\ (\text{fraction of sphere})(\text{efficiency})} \qquad (9)$$

q is the charge in microcoulombs giving N counts. The efficiency of the counter will in general be 100% for heavy particles and 3% to 10% for quanta.

For the $N^{15}(p,\alpha)$ measurement a target of enriched TiN was used. At 100 kev $\epsilon = 3.8 \times 10^{-20}$ Mev cm^2 per nitrogen atom. This value for ϵ is not very accurate since there are only a few good measurements of stopping power at low energies. The value for the cross section computed in this way was multiplied by 1.5 to correct for the incomplete nitration of the target. This gives $\sigma = 5 \times 10^{-7}$ barns at a bombarding energy of 101.5 kev. Because of a thin oxide layer on the target the actual energy may be slightly lower ($\sim$ 2 kev)*.

For $B^{11}(p,\alpha)Be^{8}$* a thick target of pressed amorphous boron was used. The large yield of this reaction made it possible to obtain a large number of counts ($\sim$1000) down to 60 kev. Alpha particles of energies greater than 2.6 Mev were counted. About 98% of the alpha particles in this energy range are due to the reaction leaving Be^8 in the 2.9 Mev excited state. This was also checked experimentally by counting only alphas of energy greater than 4.5 Mev. About 65% of the alpha particles from $B^{11}(p,\alpha)2\alpha$ have an energy greater than 2.6 Mev[31] and are counted. $\epsilon = 1.34 \times 10^{-20}$ Mev cm^2 per boron atom, and 81.6% of B^{11} is in natural boron. Log(E σ) vs. $E^{-1/2}$ has been plotted (Figure 23) for comparison with the penetration factor.

The accuracy of these measurements depends primarily on the condition of the target. Very thin surface layers will decrease the proton energy by several kev ($\sim$20% error). Only the data obtained during the first ten minutes of bombardment have been used. Otherwise the effect of carbon layers

* Refer to discussion of targets, Chapter III.

decreases the yield markedly. In the case of the N^{15} target the effect of boron contamination limits the accuracy to about 50%. In all runs statistical and geometric errors are negligible compared to these factors.

Long Range Alpha Particle Data

Up to a bombarding energy of .85 Mev the alpha particles were counted at 90° with a proportional counter. Equation (2) gives the yield per proton.* The effective cross section as defined by equation (7) has been computed. In general the targets were sufficiently thin that the cross section could be considered constant over the target.** Points are plotted at an energy one half the target thickness below bombarding energy.

Below 0.25 Mev a 60 kev target was used. It gives about 85% of the thick target yield. The cross section may be expressed as the derivative of the thick target yield.

$$\sigma = \varepsilon \frac{dY_{\infty}}{dE} \tag{10}$$

$$Y_{\infty}(E) = \sum_{n=0} Y(E - n\xi) \tag{11}$$

where Y is the yield of a target ξ kev thick. Then

$$\sigma = \varepsilon \sum_{n} \frac{dY(E - n\xi)}{dE} \tag{12}$$

Since the yield decreases very rapidly with energy, only the first two terms are significant. The second term was at most 10% of the first. ε was computed from the stopping power of air[32]. The stopping power relative to air of KNO_3 per nitrogen nucleus equals 5.4 in the region of 0.2 to 0.4 Mev.

At 0.195 Mev the cross section was also computed using equation (8). This gives $\sigma = 2.5 \times 10^{-4}$ barns compared to 2.7×10^{-4} barns obtained by the

---

* Again isotropic distribution in C.M. system is assumed. Correction from C.M. to lab system is less than 0.2%.

** Target was 2 kev at 0.9 Mev or 6 to 7 kev between 0.2 and 0.3 Mev.

above differentiation method.

Above 0.85 Mev separation of protons and alpha particles was accomplished with a magnetic spectrograph[26]. Since its maximum field bends alpha particles of only 2 Mev, stopping foils had to be placed before the aperture of the spectrograph. Mica foils of 1.69 and 2.00 cm air equivalent were mounted on a foil holder and could be turned in front of the spectrograph as needed. Protons, scattered by a thin silver foil, were allowed to enter the spectrograph (a) directly, (b) after passing through one of the mica foils (Figure 9). The energy of the protons (1.190 Mev) was chosen to give the same velocity as the velocity of the long range alpha particles. The number of protons scattered into the spectrograph with and without the mica foil is the same within 5%.* The displacement of the proton peak gives the energy loss in the foil. The width of the profile gives the straggling.

The number of doubly charged alpha particles entering the spectrograph per proton may be computed using formulas given in references[26][34].

$$N_o(\alpha^{++}) = 1.602 \times 10^{-13} \frac{R}{q} \int \frac{N(I)}{I} \, dI \qquad (13)$$

In this equation $R = p/\delta p$ is the resolution of the spectrograph. $N(I)$ is the number of alpha particle counts at a given magnetometer current I[33] for a charge of q microcoulombs of protons. As long as the angular distribution of alpha particles is not known, it is best to find $4\pi \Omega_c^{-1} N_o$. Where Ω_c is the acceptance angle in the center of mass system. The quantity $4\pi R \Omega_L^{-1}$ is most easily found from Rutherford scattering on copper. This value is slightly larger than that obtained from geometric measurements because it corrects for the counter efficiency. The scintillation counter[27] used was 90% efficient. This gives $4\pi R \Omega_L^{-1} = 2.93 \times 10^5$ as compared to 2.63×10^5.

---

* Equation (13) was used in the computation.

Alpha particle profile curves (Figure 9) were measured every 0.12 Mev. In the graphical integration the following approximate formula was used:

$$\int \frac{N(I)}{I}\, dI \approx \frac{\Delta I}{I} \sum_n N_n(I) \qquad (14)$$

As long as the shape of the alpha profile curve is determined primarily by the straggling in the mica foil, one would expect that the ratio of maximum height to area is approximately constant.

$$n = \frac{\int \frac{N(I)}{I}\, DI}{N_{max}} . \qquad (15)$$

This proved to be the case within the experimental error of 5%.* n = .0605 for mica foil #1 (1.69 cm of air), and 0.106 for foil #2 (2.00 cm of air). Only the maximum height was measured at intermediate points and multiplied by n.

The solid angle of the spectrograph (Ω_L = .0061 steradians) is quite small; therefore it is possible to use $d\Omega_C/d\Omega_L$ in the conversion from center of mass to laboratory angles.

$$\frac{d\Omega_C}{d\Omega_L} = 1 + 2\beta \cos\theta_L + \beta^2 (\cos^2\theta_L - \frac{1}{2}\sin^2\theta_L) + \ldots \qquad (16)$$

$$\beta = \left[\frac{M_1 M_2 E}{(M_1 + M_o) M_3 Q + M_o M_3 E}\right]^{1/2}$$

θ_L is the laboratory angle between beam and direction of observation. M_o, M_1, M_2, and M_3 are the masses of the target nucleus, incident and ejected particles, and of the residual nucleus respectively. E is the proton energy in the laboratory system and Q the reaction energy. This correction is at most 10%. The fraction of singly ionized alpha particles was taken into account as described by Thomas, et. al.[35]. The ratio of α^+/α^{++} varies between 0.15

* The target used was 25 kev thick for protons at 0.9 Mev.

and 0.35 depending on the energy of the alpha particles, 1.6 to 1.1 Mev.

The final formula used in computing the cross section is as follows:

$$\sigma_{eff} = \frac{1.602 \times 10^{-13}}{q\, nt} \frac{4\pi R}{\Omega_L} \left(\frac{d\Omega_c}{d\Omega_L}\right)^{-1} (1 + \alpha^+/\alpha^{++}) n \; N_{max} \qquad (17)$$

The effective cross section computed in this way is not greatly distorted by target thickness since the target used was 25 kev thick. Only at the 1.21 Mev resonance is the effect of target thickness significant. Here the resonance cross section was calculated by assuming that the half width is the same for both long and short range alpha particles. The effect of interference (Figure 21b) should not change this appreciably.

The accuracy is again determined primarily by the target deterioration. With the exception of the region 1.3 to 1.6 Mev at least 100 and generally over 500 counts were taken at each point; thus statistical errors are negligible. The data taken with the proportional counter is more consistent, because less bombardment was needed for the desired number of counts. In the region where proportional counter and spectrograph data overlap, the agreement is better than expected (Figure 17), especially since the data correspond to two different angles of observation. The stopping cross section enters into all the computations. It has not been measured for potassium but extrapolation between measured elements should be accurate to 10%. Thus the over-all accuracy is approximately 15%.

Cochrane and Hester[7] have measured the long range alpha cross section from 0.2 to 0.5 Mev. Within experimental errors their excitation curve agrees with our results. However, their cross section at the low resonance is only .013 compared to 0.09 barns obtained in this investigation. This discrepancy is not too surprising if one considers the difficulties associated with nitrogen targets, especially since only small quantities of separated isotopes are available. Cochrane and Hester started with $N^{15}H_4N^{14}O_3$ and transformed it

by Kjeldahl's method into NH_4Cl. From this they evolved NH_3 for use in a gas target. The amount of $N^{15}H_4N^{14}O_3$ available to them was sufficient for only one target and no check could be made on the efficiency of the chemical process. On the other hand, we were able to use $KN^{15}O_3$ which had been analyzed by Eastman Kodak Company. Three different KNO_3 targets gave consistent results and agree with preliminary data taken with the TiN target.

Gamma Ray Data

The curves given by Fowler, Lauritsen, and Lauritsen[28] were used in determining the quantum efficiency of the Geiger counter. It is 3.0% for the 4.5 Mev and 9.7% for the 13 Mev radiation. The absorption of the gamma radiation in the converter and target chamber was calculated using the absorption coefficients of Streib[36]. This increased the cross section by 10% and 7% for the 4.5 and 13 Mev radiation, respectively.

For the analysis of coincidence absorption measurements Bleuler and Zünti[37] have used the absorber thickness d_n which gives 2^{-n} times zero absorber coincidences. The energy of mono-energetic gamma radiation is found by reading the energies corresponding to the different d_n values on Figure 10. If the radiation is not mono-energetic, different energies are obtained at each d_n reading. This was found to be the case with the radiation at 1.05 Mev bombarding energy (Figure 12). Fortunately the cut-off of secondaries from mono-energetic radiation is sharp. Thus beyond d_7 the contribution of any soft components can be neglected.

Let $A_1(L)$ equal all the electrons from the converter of range greater than L, A_1 and A_2 the components from the two gamma rays. The plot of $\left\{ \log \left[A_1(1) + A_2(L) \right] - \log \left[A_1(0) + A_2(0) \right] \right\}$ vs. L has the same shape as $\log A_2(L)$ for $L > d_7$ of the soft radiation. Thus for large absorbers the shape of the curve will be the same as that of a mono-energetic gamma ray, except the zero on the log scale is shifted. By extrapolating the standard curve back to zero absorber one finds the fraction of zero absorber coincidences due to the hard radiation. Since the ratio of zero absorber coincidents to front counter counts is approximately independent of gamma ray energy[28], one

can compute the yield of the hard component. The counts due to the soft component are then obtained by subtraction. In principle any number of component can be separated this way. Actually it is difficult to get experimental data accurate enough to carry out the analysis if more than two components are present.

Fowler, et. al.[28] have shown that d_7 and d_6 are independent of the counter geometry while d_1, etc. do depend on it. This particular setup was calibrated using the ThC'', $N^{15}(p,\alpha\gamma)$, and $D(p,\gamma)$ radiations. The $N^{15}(p,\alpha\gamma)C^{12}$ radiation was measured by Thomas and T. Lauritsen[11] at the 1.21 Mev resonance with a β-ray spectrometer. It consists only of 4.465 ± .020 Mev quanta. Coincidence absorption curves on the $D(p,\gamma)$ radiation, 6.2 Mev, have been published by Fowler, et. al.[38]. For the high energy points the $Li^7(p,\gamma)$ data with absorber near front counter given by Fowler[28] was used. This geometry corresponds closely to the present setup. Since the lithium radiation is a mixture of 17.5 and 14.8 Mev quanta, 16.5 Mev is its effective energy. From this data Figure 10 was drawn, which in turn was replotted as shown in Figure 11.

The experimental data after subtraction of background counts (Figure 12) was recomputed and plotted on semi-log paper (Figure 13). According to the above theory, the thick absorber end of the curve has to correspond to one of the standard curves. Figure 11, plotted on transparent paper, was then moved vertically across Figure 13 until agreement was reached in the 9 to 16 mm region. The experimental points fall right between the 12 and 14 Mev curves, when the 100% point on the standard curve falls on the 15% point on the experimental curve. By trying other positions, it can be seen that the quantum energy falls certainly between 11 and 15 Mev and is most probably at 13 Mev.* From mass differences the energy of the capture radiation leading

* This wide limit is necessary because of the extrapolation employed in plotting the standard curves.

to the ground state in O^{16} should be 13 Mev.

The analysis of the soft component is more difficult. The experimental points for small absorbers may be fitted satisfactorily by assuming it to be only 4.5 Mev radiation. However, if some of the capture radiation cascades to the ground state one would expect also 6 and 7 Mev quanta. From the shape of Figure 13c this seems to be improbable. Further discussion of this point will be given in the next section.

To measure the excitation curve of the hard component, coincidents were measured with 8.9 mm of aluminum absorber. This gives 27% of zero absorber coincidences for 13 Mev but only 0.1% for 4.5 Mev radiation. On a typical run the background amounted to 4 counts out of 25. Thus even a 50% error in background will not change the results significantly. To check this excitation curve, a coincidence absorption curve was also taken at 1.12 Mev. It showed the expected decrease in hard quanta.

The accuracy of the gamma ray cross sections cannot be as good as that for alpha particles. There is always an uncertainty in the Geiger counter efficiency and its sensitive volume. Measurements on the thick target yield of the 0.898 Mev resonance varied as much as 15%. The solid angle measurement at the 1 1/2 inch position is only accurate to 10%. Thus the over-all accuracy is about 25% for the 4.5 Mev gamma rays and somewhat poorer for the hard component. At the 0.898 Mev resonance the short range alpha particles were measured at 58° simultaneously with the gamma rays at 90°. The ratio turned out to be 0.85 alpha per quantum. The position of the two sharp resonances 0.429 and 0.898 Mev is good to 1 kev, since they were compared directly with the 0.8735 Mev F^{19} resonance.

Short Range Alpha Particle Data

The yield of alpha particles from $N^{15}(p,\alpha\gamma)C^{12}$ is large enough for observation with the spectrograph at the 0.898 and 1.21 Mev resonances.

Figure 14 shows the profile curve of a thin KNO_3 target taken with 0.899 Mev protons.

For positive identification of these alpha particles, their and the gamma ray excitation were measured simultaneously at the 0.898 Mev resonance (Figure 21a). From Figure 14 the alpha particle yield was computed as previously described (Equations 13 to 16). The quantum yield was computed as described above. This gives 0.85 alpha particles per quantum. The thick target alpha particle yield was measured by bombarding a thick target above the resonance. Then the area under the alpha profile curve corresponds to the thick target yield. This gives about 90% of the thick target gamma ray yield. The discrepancy is probably due to experimental error or angular distribution factors.* This does not exclude the possibility of another group of short range alpha particles, but no such group was found in front of the scattered protons.

In measuring the alpha particle energy, one has to take into account the resolution width of the spectrograph. Since the 0.898 Mev resonance is only 2.25 kev for protons, the alpha particles will not fill the spectrograph window. In order to obtain a known distribution of alpha particles, a thick target was bombarded at or slightly above resonance. The spectrograph window may be represented by a rectangle having a width ξ_α. The energy resolution used is 1/64, that is $\xi_\alpha/E = 1/64$.

Let E_α be the energy of an alpha particle produced at the surface of the target. The energy the spectrograph measures for an alpha particle produced inside the target is $E_\alpha - \delta E_\alpha$. This δE_α is composed of the energy loss of the alpha particle as it leaves the target and the decrease in alpha energy due to the energy loss of the proton (ΔE_p).

---

* The alpha particles were observed at 58° and the quanta at 90°.

$$\delta E_a = \frac{dE_a}{dE_p} \Delta E_p + \frac{\varepsilon_a}{\varepsilon_p} \Delta E_p \tag{18}$$

Here it is assumed that the alpha particle travels the same distance in leaving the target as the proton in entering. dE_a/dE_p can be computed from the expression for Q (Equation 23). Thus a proton energy corresponds to each alpha energy. The spectrograph width for alpha particles can be replaced by an equivalent width for protons.

$$\xi_p = \frac{\Delta E_p}{\delta E_a} \xi_a \tag{19}$$

where ξ_p gives the energy range for protons from which alpha particles can enter spectrograph. Thus the maximum alpha particle yield is equal to the maximum yield of a target ξ_p kev thick. Let E_p and E_R be the energy of the incident proton and resonance energy, respectively. Then, provided $E_p - E_R \leq \frac{1}{2} \xi_p$, the maximum yield is given by[28].

$$Y_{max} = \frac{\omega_R \Gamma}{2\varepsilon} \arctan \frac{1}{2} \xi_p \Gamma \left[(E_p - E_R)(E_p - E_R - \xi_p) + \frac{1}{4}\Gamma^2 \right]^{-1} \tag{20}$$

When the alpha particles leaving the front of the target have the average $H\rho$ (that is go through the middle of the spectrometer window), the fluxmeter will read the true alpha particle energy. Thus we get the yield of a target $\frac{1}{2} \xi_p$ thick.

$$Y_Q = \frac{\omega_R \Gamma}{2\varepsilon} \arctan \frac{1}{4} \xi_p \Gamma \left[(E_p - E_R)(E_p - E_R - \frac{1}{2}\xi_p) + \frac{1}{4}\Gamma^2 \right]^{-1} \tag{21}$$

The point on the front of the profile curve where the yield has risen to Y_Q/Y_m of the peak value gives the true alpha particle energy.

$$\frac{Y_Q}{Y_m} = \frac{\tan^{-1} \frac{1}{4} \xi_p \Gamma \left[(E_p - E_R)(E_p - E_R - \frac{1}{2}\xi_p) + \frac{1}{4}\Gamma^2 \right]^{-1}}{\tan^{-1} \frac{1}{2} \xi_p \Gamma \left[(E_p - E_R)(E_p - E_R - \xi_p) + \frac{1}{4}\Gamma^2 \right]^{-1}} \tag{22}$$

This expression reduces to 1/2 if $\xi_p << \Gamma$. At the 0.898 Mev resonance ξ_p turned out to be 2.2 kev or just equal to Γ. In Figure 15 little arrows

indicate the points used in computing E_α. A constant background corresponding to the foot of the curve was assumed.

The Q of the reaction can be computed using the standard non-relativistic formula:

$$Q = M_3^{-1} \left[(M_2 + M_3) E_2 - (M_3 - M_1) E_1 - 2 \sqrt{M_1 M_2 E_1 E_2} \cos \theta \right] \qquad (23)$$

where the subscripts have the same significants as in Equation (16). From the three measurements made at the 0.898 Mev resonance, the following values were obtained: 0.5281, 0.5361, and 0.5302 Mev. At the 1.21 Mev resonance 0.5226 Mev was measured. This is probably not as accurate as the results at the lower resonance because the scattered protons interfered slightly with the alpha particle measurement. The average is $0.529 \pm .004$ Mev. The deviations are within fluctuations found previously in similar measurements. Thus we can conclude that the two resonances decay to the same excited state in C^{12}.

The accuracy of the above Q value is decreased by systematic errors. The angle of observation is known to $\pm 1/2^\circ$. Then there is the calibration of the flummeter, proton energy, carbon layers, etc., which decrease the accuracy. Thus $Q = 0.529 \pm .008$ Mev.

V. RESULTS AND DISCUSSION

Identification of Observed Radiation.

The over-all picture of the cross sections is given in Figure 16. For graphical purposes the width of the two narrow resonances (at 0.429 and 0.898 Mev) has not been drawn to scale. Details of the curves with experimental points are given by Figures 17 to 21 inclusive. The curves give 4π times the cross section per unit solid angle in the direction of observation. All gamma ray measurements were made at 90°, so were the long range alpha particles up to 0.85 Mev. Between 0.7 and 1.6 Mev the long range alphas were observed at 137.8°.

Figure 17 shows the excitation curve for long range alpha particles. The measurements with the spectrograph showed that their energy agrees within .1 Mev with the energy to be expected using masses given by Bethe[42]. The alphas observed with the proportional counter had an energy greater than 3 Mev. No increase in counts was observed if all alphas with energy greater than 2.2 Mev were counted. The yield is also linear in the N^{15} content of the target.

Figures 18, 19, and 20 were prepared from gamma ray measurements. Coincidence absorption measurements at the resonances show primarily 4.5 Mev radiation. At the 1.21 Mev resonance Thomas and Lauritsen[11] measured the quantum energy with a β-ray spectrometer and obtained $4.465 \pm .020$ Mev. Buechner, et. al.[11] measured 4.468 Mev for the excitation energy of the lowest excited state in C^{12}. The short range alpha particles, corresponding to $N^{15}(p,\alpha)C^{12*}$, have been observed (Figure 14). At the 0.898 Mev resonance they show the same excitation (Figure 21a) and cross section as the gamma rays.

Around 1.05 Mev coincidence absorption measurements show the presence of some 13 Mev radiation. Capture radiation to the ground state in O^{16} is

the only process which is sufficiently energetic. The other part of the radiation is probably mostly 4.5 Mev. Unfortunately the measurements are not very energy sensitive, and a large fraction of 6 or 7 Mev quanta cannot be ruled out. One would expect approximately 7 Mev quanta if cascading occurs in some of the capture radiation. Theoretical considerations indicate that cascading is rather improbable.* Thus the 4.5 Mev component may be smaller in the 0.95 to 12. Mev region than has been shown on the graph.

Since the target contained other nuclei besides N^{15} one has to check whether any of them influence the measurements. Both KNO_3 and TiN targets were used above 0.4 Mev. The results agree if the variation of nitrogen concentration with depth in the TiN target is taken into account. At the bombarding energies used, the Coulomb barrier of both titanium and potassium is large; therefore their transmutation cross sections are small. The $N^{14} + H^1$ cross sections have been investigated by Duncan and Perry[39] and were found to be much smaller than the N^{15} cross sections. For $N^{14}(p,\gamma)O^{15}$ the largest resonance is at 1.065 Mev with a cross section of 3.5×10^{-28} cm^2 and $\Gamma = 5$ kev. Thus it is about 1/3 of the $N^{15}(p,\gamma)O^{16}$ cross section, but because of its small width the yield was negligible compared to the N^{15} reaction. Blank runs with normal KNO_3 showed no measurable gamma radiation. For the measurements below 0.4 Mev, special care was taken to eliminate B^{11} contaminations. All measurements were reproducible in both yield and position of resonances. Data taken with different target thickness showed the expected differences.

Discussion of Resonances.

As can be seen from Figure 16 most of the resonances of the short and

---

* Refer to next chapter.

long range alpha particles are not common. The 1.210 Mev resonance, however, is common to both reactions. Figure 21b shows the yields of the two reactions plotted on a relative scale. Since both yields were measured together, the displacement of a few kev should be real. The cross section curve (Figure 18) for the short range alpha particles indicates a small resonance around 1.1 Mev which is masked by the tail of the 1.210 Mev resonance.

To interpret these excitation curves it is necessary to use a Breit-Wigner multi-level dispersion formula. This should be possible since there is very little, if any, non-resonance radiation. Unfortunately a knowledge of the angular distribution of the cross sections is necessary. With the results obtained until now, one is limited to the single level formula applied at each resonance plus an argument as to possible interference terms.

The single level formula is

$$\sigma = \pi \lambda^2 \frac{\omega \Gamma_p \Gamma_x}{(E_R - E)^2 + \Gamma^2/4} \qquad (24)$$

where λ is the wave length of the incident proton in CM system, Γ_p the proton width, Γ_x the width of emitted radiation, Γ the full width at half maximum of the resonance, E and E_p are the proton energy and resonance energy respectively. ω is a statistical factor given by $\omega = (2J + 1)/\left[(2s + 1)(2i + 1)\right]$. J is the total angular momentum of the compound nucleus, s and i are the spins of the incident and target nucleus respectively. Γ_p and Γ_x are not constant due to the barrier penetration factors. In the notation of Christy and Latter[40] $\Gamma = \sqrt{E/E_1}\, PG$. Here P is the Gamow penetration factor. $\sqrt{E/E_1}$ gives the velocity normalization. G is the width at 1 Mev without barrier, provided E_1 = 1 Mev for protons and 4 Mev for alpha particles.

The dispersion formula is most easily applied to the narrow resonances of the $N^{15}(p,\alpha\gamma)C^{12}$ reaction (Figures 19 and 20). Here the variation of

penetration factors over the resonance width is negligible. The non-resonant radiation is small; thus interference terms are not important. The wide resonances of $N^{15}(p,\alpha)C^{12}$ are not as readily interpreted. The proton penetration factor changes greatly over the resonance width. In general it is necessary to know the partial wave responsible for the resonance in order to compute the penetration factors. In the low energy region the s-wave Gamow factor and the proton wave length were divided out.* Figure 22 shows that at low energies a good fit can be obtained with the single level dispersion formula, but above 0.4 Mev the experimental points deviate markedly.

The asymmetry of the next resonance, at about 1.02 Mev, is even more marked after a penetration factor is taken out. This behavior can be explained by interference between the three long range alpha resonances. Constructive interference between the low and 1 Mev resonances is indicated in the region from 0.4 to 1 Mev (Figures 17 and 22). Since there is a phase shift of 180° in going through a resonance, the interference is destructive below 0.3 and above 1 Mev. The sharp decrease of the cross section between 1 and 1.1 Mev can be explained by destructive interference between the 1.0 and 1.2 Mev resonances. This would also explain the slight displacement between the maxima of the long range alpha particle and gamma ray yield at the 1.21 Mev resonance (Figure 21b). Above 1.4 Mev we would have again destructive interference. The surprisingly low value of the cross section at 1.6 Mev is thus explicable. Single level dispersion formulas were approximately fitted at the three resonances. The effect of interference terms can be estimated by taking differences of the amplitudes. This showed that the above explanation is possible. The true resonance

---

* More detailed discussion is given in the next section.

position of the 1 Mev resonance could be shifted to a considerably higher or lower energy. Naturally until phase factors are taken into account no quantitative calculation is possible.

Between 1.0 and 1.1 Mev all three reactions show a resonance (Figures 17, 18). Their widths are about 150 kev, although none of them can be measured very accurately. The present data is consistent with the assumption that all three correspond to only one state in O^{16}. The capture radiation gives the true position of the resonance, 1.05 Mev. The maximum of the long range alpha yield is displaced toward lower energies by the interference with the 1.21 Mev resonance. The maximum of the short range alpha particles is displaced toward higher energies by the penetration factor of the alphas. The exact position and width of this resonance is masked by the tail of the 1.21 Mev resonance.

The pertinent experimental information about the resonances has been summarized in Table I. The thick target yield is given only for the narrow resonances. The $N^{15}(p,a\gamma)$ resonance above 1.6 Mev has not been included. The gamma ray yield was rising rapidly at the highest energy obtainable. The long range alpha particles do not participate in this rise.

Extrapolation to Stellar Energies.

For stellar energy production only the value of the cross sections around 30 kev is important. This can be estimated by extrapolating the dispersion formula. At low bombarding energies the energy dependence of the cross sections is primarily determined by the Gamow penetration factor of the protons. At low energies $\sqrt{E}\ P$ is proportional to $\exp\left[-0.992\ Z_o E^{-1/2}\right]$,* this holds true regardless of the proton wave[30] or of the nuclear radius. If there is a low energy resonance, however, the resonance

---

* E is in Mev., Z_o = nuclear charge.

denominator cannot be neglected. This introduces complications because it is to be expected that the interference terms between the different resonances change due to phase shifts.

The results with the $B^{11}(p,\alpha)2\alpha$ reaction illustrate the difficulties. Because of the large cross section it was possible to make measurements down to about 50 kev. This reaction has a resonance at 0.162 Mev which is 5 kev wide[11]. There is a considerable non-resonant background, but as yet no quantitative information is available to separate the two. From this one would expect the experimental curve to decrease faster than the Gamow factor and slower than Gamow plus resonance factors. This is actually the case (Figure 23). Here $E\sigma$ has been plotted to take account of the energy dependence of λ^2. The curves were normalized to fit at 0.1 Mev. This curve illustrates the relative effects of the penetration and resonance factors.

The analysis of the $N^{15}(p,\alpha)C^{12}$ reaction is considerably more certain. Since the alpha yield is almost zero at 1.6 Mev we have to consider only the three resonances. Neglecting interference the contribution of the 1.05 and 1.21 Mev resonances is negligible, and the cross section is determined primarily by the low resonance. To show its true resonance shape the cross section (Figure 17) was divided by the proton Gamow factor and $4\pi\lambda^2$. Then equation (24) takes the following form:

$$\frac{\sigma}{4\pi\lambda^2\sqrt{E/E_1}\,P} = \frac{\frac{1}{4}\omega\,\Gamma_p\,\Gamma_\alpha}{(E-E_R)^2 + \Gamma^2/4} \qquad (25)$$

Since the alpha particle energy is larger than the potential barrier Γ_α may be considered constant. $\Gamma = \Gamma_\alpha + \Gamma_p \sim \Gamma_\alpha$ provided $\Gamma_p << \Gamma_\alpha$. In computing Figure 22 the curves of Christy and Latter[40] for s-wave protons on nitrogen were used. The experimental points can be fitted by a resonance curve with the maximum at 0.338 Mev and a width of 94 kev. The agreement

is rather remarkable considering the large change in cross section (Figure 17). At low energies this gives

$$\sigma_\alpha(E) = \frac{110}{E} e^{-6.95E^{-1/2}} \qquad (26)$$

σ_α is in barns provided E is in Mev.

The above expression would be quite accurate except for two facts. Even though the contribution of the 1.05 Mev resonance is small compared to that of the 0.338 Mev resonance, their amplitudes are almost comparable. This could change the cross section easily by a factor of 1.5. The interference is probably destructive, thus the above value might be high. From the present experiments no information can be gained regarding resonances below 0.1 Mev. It has been assumed that no such resonance exists. In neutron experiments where no potential barrier is present many low lying resonances have been found. Thus until more is known about the levels in O^{16} no final cross section can be computed.

Compared to $N^{15}(p,\alpha)C^{12}$ the $N^{15}(p,\alpha\gamma)C^{12}$ reaction gives no appreciable contribution to stellar energy production. Its resonances are very narrow (Table I), and no non-resonant radiation was found (Figure 18). An extrapolation of the $N^{15}(p,\gamma)O^{16}$ cross section to stellar energies is of interest, because this process removes nitrogen permanently from the carbon cycle. The reaction could be observed only at the 1.05 Mev resonance, because its yield is small. There is no reason to suppose, however, that it does not have other resonances. For instance it may compete with the long range alpha particles at the 0.338 Mev resonance. This could not have been detected, but would have a significant contribution at 30 kev.

In extrapolating from 1.05 Mev to 0.03 Mev it is important to use the correct proton wave. This resonance is probably also due to s-wave protons.*

---

* Refer to next chapter and Figure 25.

Equation (24) was used in the extrapolation. In order to get a low estimate $\Gamma = 135$ kev was used. (Γ cannot be measured accurately). This together with values given in Table I gives

$$\sigma_\gamma(E) = \frac{0.009}{E} e^{-6.95E^{-1/2}} \tag{27}$$

This is only the contribution of one resonance and the actual value of σ_γ is probably larger. Combining equations (26) and (27) one gets $\sigma_\gamma/\sigma_a \geq 0.8 \times 10^{-4}$. This value is larger than assumed by Bethe[5] but still small enough as not to interfer with the carbon cycle during the age of the sun.

VI. NUCLEAR WIDTHS

Calculations

Much information has been obtained regarding cross sections and resonance widths for nuclear reactions. In order to compare results one has to calculate quantities directly related to nuclear properties. The nuclear width without barrier, G, can be computed from the dispersion formula provided the levels involved are known. Conversely the angular momentum of the levels can be determined if G is known. From the consideration of the transit time of a heavy particle through a nucleus one can say that G is at most a few Mev, but generally smaller. Available experimental data show that with a few exceptions G has a value between 1 kev and 1 Mev for heavy particle reactions. By making certain level assignments, a value for G can be calculated. If this is larger than the maximum possible value of G the assumed assignment may be ruled out.

First Γ_p and Γ_x of equation (24) have to be calculated. If $E = E_R$ and $\Gamma = \Gamma_p + \Gamma_X + \ldots$*, then

$$\sigma_R = 4\pi\lambda^2 \omega \Gamma_p \Gamma_X / \Gamma^2 \tag{28}$$

---

* $\Gamma = \sum$ partial width of all competing processes.

Using results of Table I, Γ_P and Γ_X may be computed provided ω is known. It should be mentioned that if Γ_P is of the same order of magnitude as Γ_X, its value depends critically on σ_R. Two solutions are obtained, and it is difficult to say whether Γ_P or Γ_X is the larger one. If the solution is complex the measured cross section is larger than the maximum possible cross section for the assumed statistical factor ω. This was used to rule out certain level assignments. However, if a decrease of σ_R within experimental error gave a real result, the assignment was considered.

The nuclear width for charged particles is then obtained by dividing the partial width by the Gamow factor. The normalization given by Christy and Latter[40] has been adopted.

$$\Gamma_X = \sqrt{E/E_1}\, P_X G_X \qquad (29)$$

The term $(E/E_1)^{1/2}$ takes care of the velocity normalization. E_1 equals 1 Mev for protons and 4 Mev for alpha particles has been used in the calculations. The penetration factor for protons can be taken directly from the curves of Christy and Latter. The long range alpha particles have an energy above the barrier. Their penetration factor is unity unless very high angular momenta are involved. Also $(E/E_1)^{1/2}$ is almost equal to one, thus $\Gamma_{\alpha o}$ and $G_{\alpha o}$ are practically equal.

In case of the short range alphas the penetration factor was calculated using the WKB approximation. With the same normalization as in equation (29) one gets

$$\sqrt{E/E_1}\,P = \sqrt{\frac{E_B}{E_1}}\, e^{-2C_\ell}\ , \qquad (30)$$

where E_B is the barrier height, 4.21 Mev. Bethe[41] gives equation (631) and (600a) for calculation of C_ℓ. The only modification needed is to use the sum of the N^{15} and He^4 radii, since the alpha particle radius is not negligible as in the case treated by Bethe. The penetration factors have been calculated at the short range alpha resonances and are given in Table II.

For a table of the nuclear widths all possible combinations of angular momenta and spin have to be considered. To start with, the spins of the ground state of C^{12}, N^{15}, and O^{16} are known to be 0, 1/2, and 0 respectively. The high degree of symmetry of the C^{12} and O^{16} nuclei gives even parity. It is generally assumed that the parity of N^{15} is odd(42). The spin of the incoming protons is 1/2, their parity is the same as that of the partial wave considered. Therefore s-wave protons may form either 0(-) or 1(-) states in O^{16}. Similarly P protons lead to 0(+), 1(+), or 2(+) and D protons give 1(-), 2(-), 3(-) levels. Alpha particles have zero spin and even parity; therefore in alpha emission the parity change depends only on the partial wave considered.

At least one of the resonances is common to both short and long range alpha particles. Therefore some states in O^{16} are able to decay to the ground and first excited state in C^{12}. This eliminates 0(-) as a possible assignment for C^{12*}. The resonances which cannot decay by long range alpha particles must correspond to 1(+), 2(-), 3(+), etc., levels in O^{16}, because those cannot decay to 0(+) in C^{12}. Levels in O^{16} are not observed unless they can be excited by s, p, or d-wave protons. The barrier factor for the higher waves makes Γ_p too small compared to Γ_α.

Results and Comparison of Widths.

Table III gives the nuclear widths for all levels up to $J = 3$. If a state in O^{16} can be formed or decay by several partial waves only the one with the smallest barrier factor was considered. Since isotropic distribution has been assumed in calculating Table I, the results have to be corrected for any angular distribution factors. In general these will not change the answers significantly.

At the 0.338 Mev resonance only long range alphas were found. The

small value of Γ_p and the barrier factor for short range alpha particles explain their absence. Also capture radiation cannot compete to any degree because Γ_p/Γ is small. Only s protons forming a 1(-) level in O^{16} give a reasonable value for G_p. The next value, $G_p = 1.8$ Mev, is rather improbable.

The absence of long range alphas at the 0.429 Mev resonance is only explainable if transitions to 0(+) in C^{12} are forbidden. The 2(-) state in O^{16} makes G_p too large. 3(-) cannot be the excited state in C^{12} because the corresponding G_α, is too large. 0(-) and 1(+) assignments in O^{16} give reasonable values for most widths. Neither of these levels can decay by electric dipole to the ground state in O^{16}, thus 13 Mev radiation is not to be expected.

The 0.898 Mev resonance cannot be due to a 0(-) level in O^{16} because the observed cross section is four times the maximum theoretical value. Only the 2(-) level gives a reasonable value for G_p. 1(+) gives an extremely small while 3(+) gives too large values for G_p. With this assignment the 1(-) and 3(-) states in C^{12} have extreme alpha widths.

At the 1.05 Mev resonance all three reactions were observed. The 3(-) assignment for O^{16} may be ruled out because it requires electric octapole capture radiation and an extreme proton width. The gamma ray width indicates electric dipole radiation. The quadrupole width is smaller than the maximum theoretical value, but larger than would be expected.

At the 1.21 Mev resonance levels in O^{16} with $J = 0$ or 1 would give too small a cross section. The best value for G_p is obtained if the level in O^{16} is 3(-). All short range alpha widths for an assignment of 1(+) in C^{12} are rather large.

Unfortunately too little is known about nuclear widths to make a definite level assignment. However, the above discussion indicates that the excited state in C^{12} is not 3(-), 1(+), or 1(-). If the capture radiation is

electric dipole then the 3(+) and 2(-) levels in C^{12} have also excessive widths at the 1.05 Mev resonance. This leaves only 2(+) for the excited state in C^{12}; the same value as the alpha model predicts. The most probable level assignment and nuclear widths are given in Figure 25 and Table IV.

The angular momentum and parity of the excited state in C^{12} may also be obtained from other reactions. For instance $B^{11}(p,\gamma)C^{12}$ shows transitions to the ground state and predominantly cascading through the 4.47 Mev level[43]. Unfortunately the excitation has not yet been determined, thus it is impossible to draw conclusions from the relative intensities of the two components. In any case angular distribution measurements are necessary before definite level assignments can be made.

Since the pair state in O^{16} has the same angular momentum and parity as the ground state, one would expect transitions to that level. If the capture radiation is electric dipole about 10% of the radiation should go to it.* No pairs could be observed in the experiments because a thick aluminum converter was used in all measurements. Since the next level at 6.13 Mev is 3(-), higher order transitions are needed and it cannot compete. Thus it is improbable that more than a small fraction of the capture radiation cascades. On the other hand if the 13 Mev radiation is electric quadripole from a 2(+) level then a transition to the 3(-) state would be electric dipole and much cascading is to be expected. Unfortunately the experimental results (Figure 13) are not sufficiently accurate to eliminate this alternative.

The width for long range alpha particles is narrow compared to that for protons or short range alphas. A similar situation exists in the case of $B^{11}(p,\alpha)Be^{8}$ and $F^{19}(p,\alpha)O^{16}$. The first reaction has a resonance only 5 kev wide at 0.162 Mev[11]**. A check of the fluorine reaction showed a

---

* For a given oscillator strength Γ_γ is proportional to E^3.

** The nuclear width and resonance width are practically the same since these alpha particles are emitted with an energy larger than the potential barrier.

new resonance at 0.78 Mev (Figure 24) which is less than 10 kev wide. It had been missed in previous investigations[36] because of spread in proton beam energy. The widths for $F^{19}(p,\alpha\pi)O^{16}$ resonances are also surprisingly small compared to $F^{19}(p,\alpha\gamma)O^{16}$. In all four cases the compound nucleus is formed in a highly excited state and decays to a 0(+) level. However, alpha particles decaying to states of higher angular momentum in the residual nucleus show larger natural widths. This holds true for $F^{19}(p,\alpha\gamma)O^{16}$ 3(-), $N^{15}(p,\alpha\gamma)C^{12}$ 2(+), $B^{11}(p,\alpha)Be^{8*}$ not known. The alpha particle model does not apply to the highly excited states in the compound nucleus, and an explanation has to wait for a more complete nuclear theory.

REFERENCES

1. Burcham and Smith, Nature 143, 795 (1939).
2. Fowler and Lauritsen, Phys. Rev. 58, 192A (1940).
3. Lauritsen, Lauritsen, and Fowler, Phys. Rev. 59, 241 (1941).
4. R. Tangen, Kgl. Nord. Vid. Selsk. Skr. No. 1 (1946).
5. H. A. Bethe, Phys. Rev. 55, 103, 434 (1939), and Astrophys. J. 94, 37 (1940).
6. Holloway and Bethe, Phys. Rev. 57, 747 (1940).
7. Cochrane and Hester, Proc. Roy. Soc. 199, 458 (1949).
8. J. A. Wheeler, Phys. Rev. 52, 1083 (1937).
9. Hafstad and Teller, Phys. Rev. 54, 681 (1938).
10. D. M. Dennison, Phys. Rev. 57, 454 (1940).
11. Hornyak and Lauritsen, Rev. Mod. Phys. 20, 191 (1948); Rev. Mod. Phys. 22, (1950).
12. D. R. Inglis, Phys. Rev. 78, 616 (1950).
13. Corson and Wilson, Rev. Sci. Inst. 19, 207 (1948).
14. Wilson, Corson, and Baker, Preliminary Report No. 7, Nuclear Science Series.
15. Rossi and Staub, Ionization Chambers and Counters: Experimental Techniques, National Nuclear Energy Series V-2, (McGraw-Hill, 1949).
16. Ref. 15, page 58, Fig. 3.10.
17. Ref. 15, page 14, Fig. 1.6.
18. Janke and Emde, Tables of Functions, (Dover, 1945).
19. Jesse, Forstat, and Sadauskis, Phys. Rev. 77, 782 (1950).
20. M. Biachman, Rev. Sci. Inst. 20, 477 (1949).
21. Hanna, Kirkwood, and Pontecorvo, Phys. Rev. 75, 985 (1949).
22. Ter-Pogossian, Robinson, and Townsend, Rev. Sci. Inst. 20, 289 (1949).
23. Jordan and Bell, Rev. Sci. Inst. 18, 703 (1947).
24. R. N. Hall, Rev. Sci. Inst. 19, 905 (1948).
25. Haworth and King, Phys. Rev. 54, 38 (1938).
26. Snyder, Rubin, Fowler, and Lauritsen, Rev. Sci. Inst. 21, 852 (1950).

27. Tollestrup, Lauritsen, and Fowler, Phys. Rev. 76, 428 (1949).

28. Fowler, Lauritsen, and Lauritsen, Rev. Mod. Phys. 20, 236 (1948).

29. Rubin and Rasmussen, Phys. Rev. 78, 83 (A) (1950).

30. Hall and Fowler, Phys. Rev. 77, 197 (1950).

31. H. A. Bethe, Rev. Mod. Phys. 9, 217 (1937).

32. H. A. Bethe, BNL-T-7.

33. Lauritsen and Lauritsen, Rev. Sci. Inst. 19, 916 (1948).

34. Chao, Tollestrup, Fowler, and Lauritsen, Phys. Rev. 79, 108 (1950).

35. Thomas, Rubin, Fowler, and Lauritsen, Phys. Rev; 75, 1612 (1949).

36. Streib, Fowler, and Lauritsen, Phys. Rev. 59, 253 (1941).

37. Bleuler and Zünti, Helv. Phys. Acta. 19, 376 (1946).

38. Fowler, Lauritsen, and Tollestrup, Phys. Rev. 76, 1767 (1949).

39. Duncan and Perry, Bull. A.P.S. 25-4, 21, (1950).

40. Christy and Latter, Rev. Mod. Phys. 20, 185 (1948).

41. H. A. Bethe, Rev. Mod. Phys. 9, 178 (1947).

42. H. A. Bethe, Elementary Nuclear Theory. (John Wiley & Sons, Inc., New York, 1947).

43. R. L. Walker, Phys. Rev. 79, 172 (1950).

APPENDIX

Shape of Proportional Counter Pulses

In deriving the pulse shape, a number of simplifying assumptions were made. In the ideal case all primary electrons arrive at the central wire simultaneously, each producing (m-1) secondary electrons. The positive ions are produced so close to the central wire that the pulse is formed by their motion toward the cathode[14] rather than by the motion of the electrons toward the collecting wire. The electric field of the ions is small compared to the static field in the counter. Thus, in calculating the action of the field on the ions, only the forces due to the constant voltage V_o across the counter has to be considered.

The voltage produced across an isolated counter* by the motion of an ion may be derived by setting the work done on the ion equal to the loss of electrostatic energy of the counter.

$$V_c = \frac{Q\,V(r)}{CV_o} \tag{31}$$

V_c equals the change in voltage due to the motion of the charge Q from the central conductor to position r. $V(r) = \frac{V_o}{\log b/a} \log \frac{a}{r}$ is the electrostatic potential in the counter and C the capacity of the counter. a and b are the radii of the central wire and counter, respectively. To a good approximation the drift velocity of positive ions is proportional to the electric field.

$$\frac{dr}{dt} = \frac{K}{P} E \tag{32}$$

For argon K/P is about 3 cm/sec per volt/cm per atmosphere[14]. Substituting for E from equation (1) and integrating one gets

---

* Neglect the current from power supply or grid current of first tube.

$$r = a\sqrt{1 + t/t_o}$$

$$t_o = \frac{a^2 \log b/a}{2 V_o(K/P)} \tag{33}$$

Substitute everything back into equation (31).

$$V_c = A \log (1 + t/t_o)$$

$$A = \frac{-Q}{2C \log b/a} = \frac{-mn_o e}{2C \log b/a} \tag{34}$$

Q is the total charge of the positive ions, which is the number of primary ions formed (n_o) times the gas multiplication (m). V_c will reach its maximum value, $V_m = -Q/C$, when all ions are collected.

The pulse actually observed at the output of the amplifier has been differentiated by a series R_1C_1 network. The differential equation applying to the network is

$$R_1 \frac{di}{dt} + \frac{i}{C_1} = \frac{dV_c}{dt} \tag{35}$$

i is the current through the network. The voltage observed is $V = i R_1$. Substitute from equation (34) and rearrange into standard form of a linear equation.

$$di + \left[\frac{i}{\tau} - \frac{A}{R_1(t + t_o)}\right] dt = 0 \tag{35'}$$

where $\tau = R_1C_1$. The particular solution giving $i = 0$ at $t = 0$ is given by

$$\begin{aligned} V = i R_1 &= A e^{-t/\tau} \int_o^t \frac{e^{x/\tau}}{x + t_o} dx \\ &= A e^{-\frac{t + t_o}{\tau}} \left[\bar{E}_1\left(\frac{t + t_o}{\tau}\right) - \bar{E}_1\left(\frac{t_o}{\tau}\right)\right] \end{aligned} \tag{36}$$

$\bar{E}_1(x)$ is the exponential integral tabulated by Janke and Emde[18].

The maximum will be at $di/dt = 0$. From equation (35)

$$V_h = R_1 i_m = \frac{A\tau}{t_m + t_o} \tag{37}$$

where V_h = pulse height, i_m = maximum current and t_m = time of maximum. A direct solution of equations (36) and (37) for V_h and t_m proved to be impractical. By introducing the parameter $u = (t_m + t_o)/\tau$, it is easy to find V_h and t_m as a function of τ/t_o. Then equations (36) and (37) become, after rearrangement

$$E_1\left(\frac{t_o}{\tau}\right) = \bar{E}_1(u) - \frac{e^u}{u} \tag{38}$$

$$t_m = \tau u - t_o \tag{39}$$

$$\frac{V_h}{V_m} = \frac{1}{2u \log b/a} \tag{40}$$

Using these equations, Figure 2 has been computed.

DESCRIPTION OF FIGURES

1. Dimensions of proportional counter #1 and comparison of experimental and theoretical pulse shape. The ordinate of the theoretical curve is fraction of maximum pulse height.
2. Theoretical curve giving fraction of maximum pulse height and time at which it is reached as a function of counter and circuit constants.
3. Drawing of proportional counter #1 with detail of thin window support.
4. Discriminator bias curves for proportional counter #1 and #2. It shows the distribution of pulse height under different operating conditions.
5. Experimental setup used in the 100 kev measurements of long range alpha particles.
6. Experimental setup used in the 0.20 to 0.85 Mev measurements of long range alpha particles.
7. Analysis of nitride targets using high resolution scattering. ~~(Replaced the work nitrated in the legend by nitrided)~~
8. Analysis of a thin KNO_3 target deposited on a silver foil.
9. Calibration of mica stopping foils and typical long range alpha particle profile curve. These curves show primarily the straggling of the protons and alpha particles. Foil #1 is equivalent to 1.69 cm of air, #2 is 2.00 cm.
10. The absorption of secondary electrons produced in a thick aluminum converter by gamma radiation. d_n indicates the absorber thickness which reduces the coincidence counts to 2^{-n} of the number without absorber.
11. Standard absorption curves for the geometry used. They have been plotted from Figure 10.
12. Absorption of the secondaries produced in a thick aluminum converter by the $N^{15}(p,\gamma)$ radiation.
13. Per cent of zero absorber counts computed from Figure 12 plotted on semi-log paper for comparison with standard curves.

14. Calibration of fluxmeter and profile curve of alpha particles from $N^{15}(p,\alpha\gamma)C^{12}$. A polished copper surface was used for the calibration, and a thin KNO_3 layer on copper for the alpha particle profile. ~~($\theta = 58^\circ$ instead of $\theta = 60^\circ$.~~

15. Curves for measuring the energy of the alpha particles from $N^{15}(p,\alpha\gamma)C^{12}$, angle of observation is 58°. A thick KNO_3 target was used. Proton background has been subtracted.

16. $N^{15} + H^1$ reactions. The width of the resonances has been increased for easier reading of graph.

17. Excitation curve of long range alpha particles. The angle of observation is 90° for points designated by open circles and crosses O and X, and 137.8° for points designated by solid circles. Target thickness was measured at 0.90 Mev. The yield is given for a KNO_3 target enriched to 61% with N^{15}. Target thickness distorts the shape of the curve only at the 1.21 Mev resonance.

18. Excitation curve of gamma radiation. All measurements were made at 90°. Target thickness was measured at 0.90 Mev. The yield is given for a KNO_3 target enriched to 61% with N^{15}.

19. Gamma radiation was measured at 90° for both thick and thin targets. (a) 0.429 Mev resonance. The thin target is 0.57 kev thick at this energy. (b) 0.898 Mev resonance. The thin target is 0.72 kev thick at this energy.

20. Gamma radiation was measured at the 1.21 Mev resonance at 90°. The 51 kev (at 0.90 Mev) target was used to compute the thick target yield at this resonance.

21. (a) This curve shows that the short range alpha particles and gamma rays of $N^{15}(p,\alpha\gamma)C^{12}$ follow the same excitation at the 0.898 Mev resonance.

21. (b) This curve shows the slight displacement of the excitation of gamma radiation and long range alpha particles at the 1.21 Mev resonance. A 30 kev (at 0.90 Mev) target was used.

22. Excitation curve of long range alpha particles after barrier factors have been taken out. S-wave protons were assumed. (~~Replace 0.090 in the expression for the solid curve by 0.0090~~).

23. Alpha particles from $B^{11}(p,\alpha)Be^{8*}$ observed at 90°. Notice that experimental points follow closely the Gamow penetration factor.

24. Long range alpha particles from $F^{19}(p,\alpha)O^{16}$ observed at 90°. This is only a preliminary curve.

25. Energy level diagram of O^{16}. Proposed angular momentum and parity assignments have been shown. With the exception of the 6.05 and 6.13 Mev levels in O^{16} they are based on intensity arguments.

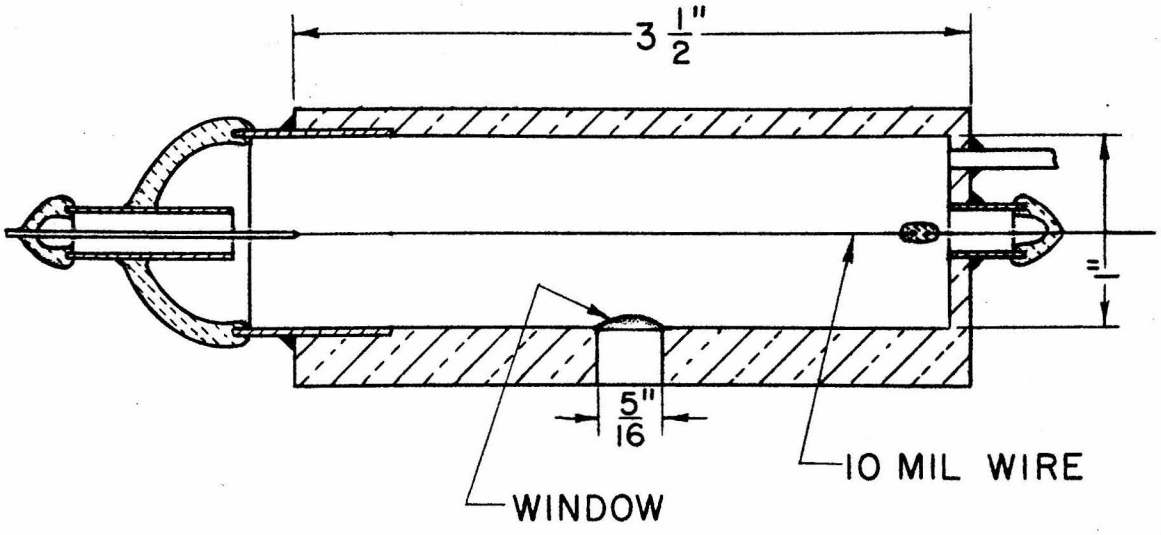

PROPORTIONAL COUNTER NO. 1

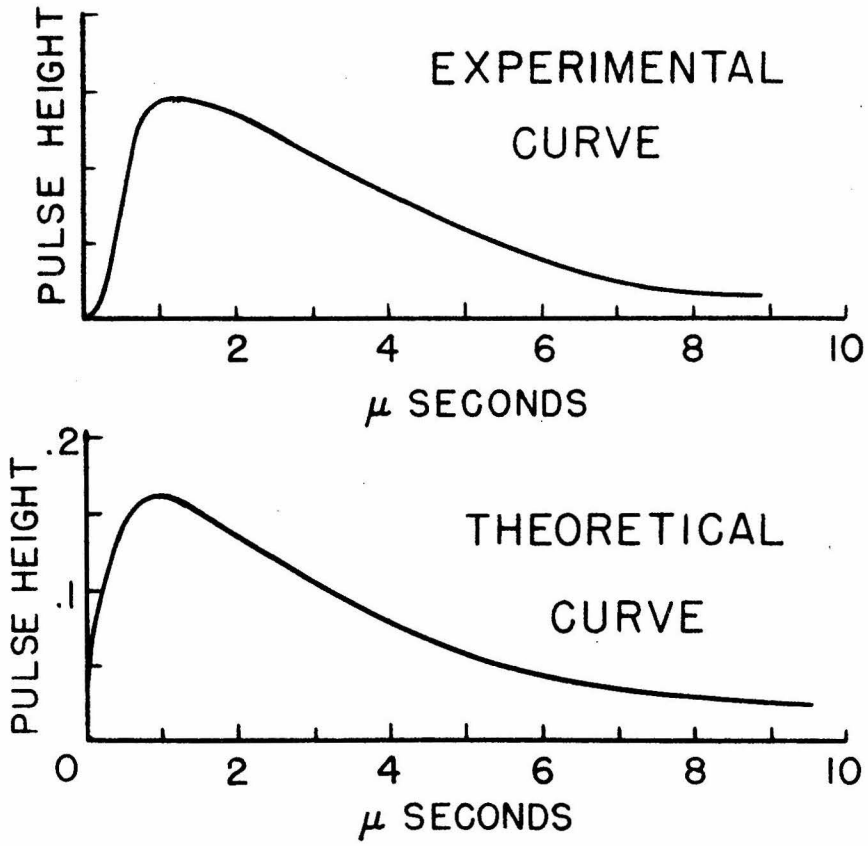

t_0= 0.12 μ SECONDS

τ = 1.6 μ SECONDS

V = 1000 VOLTS

FIGURE 1

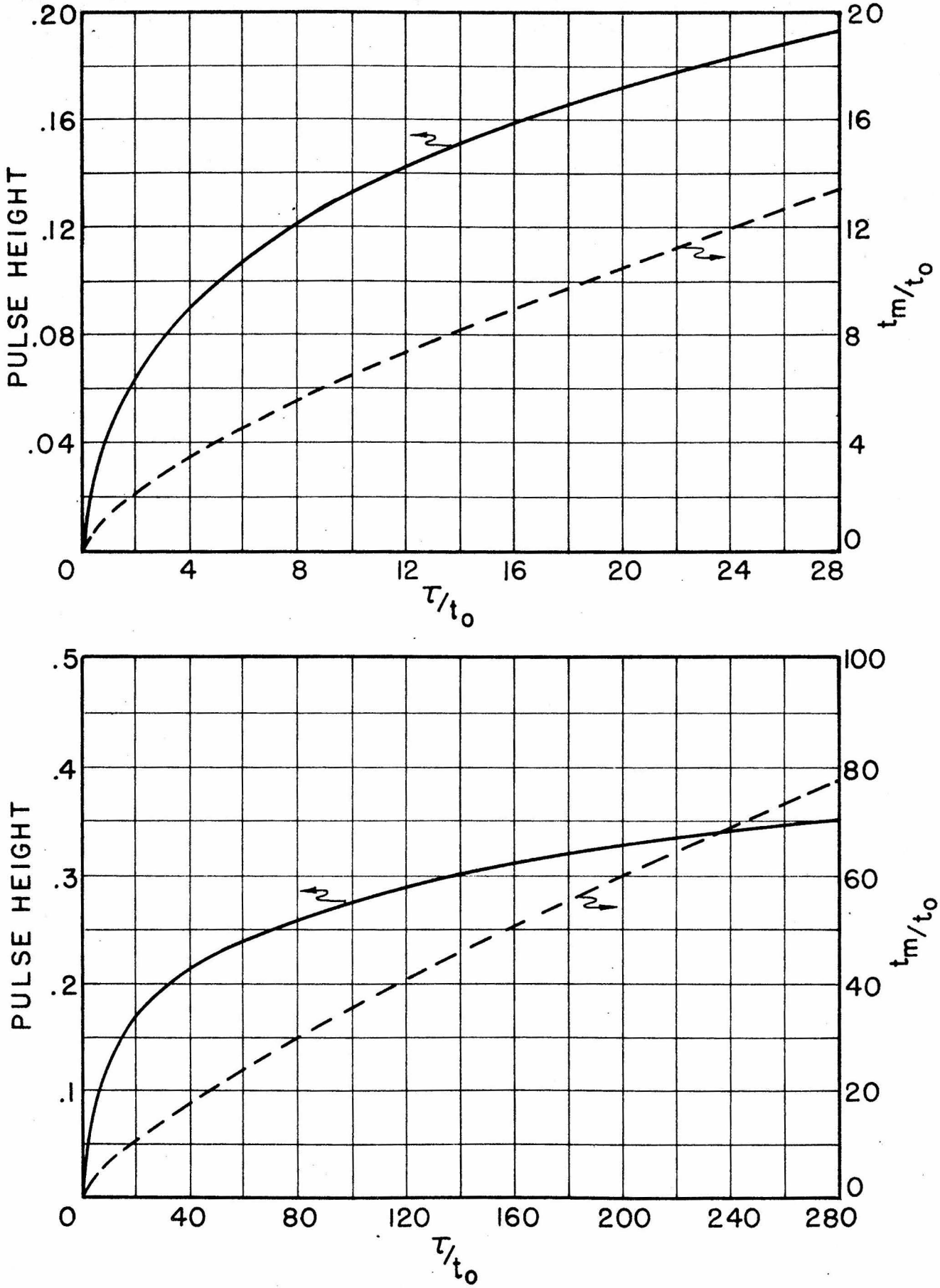
PULSE HEIGHT
.20
.16
.12
.08
.04
0
4
8
12
16
20
24
28
τ/t_o
20
16
12
8
4
0
t_m/t_o
PULSE HEIGHT
.5
.4
.3
.2
.1
0
40
80
120
160
200
240
280
τ/t_o
100
80
60
40
20
0
t_m/t_o

FIGURE 2

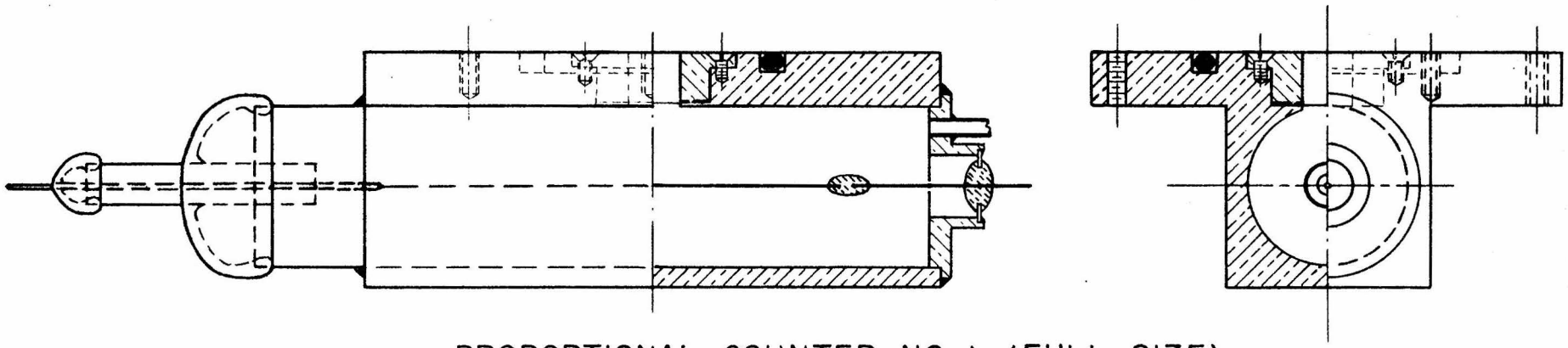

PROPORTIONAL COUNTER NO. 1 (FULL SIZE)

THIN-WINDOW
SUPPORT
(4 x SIZE)

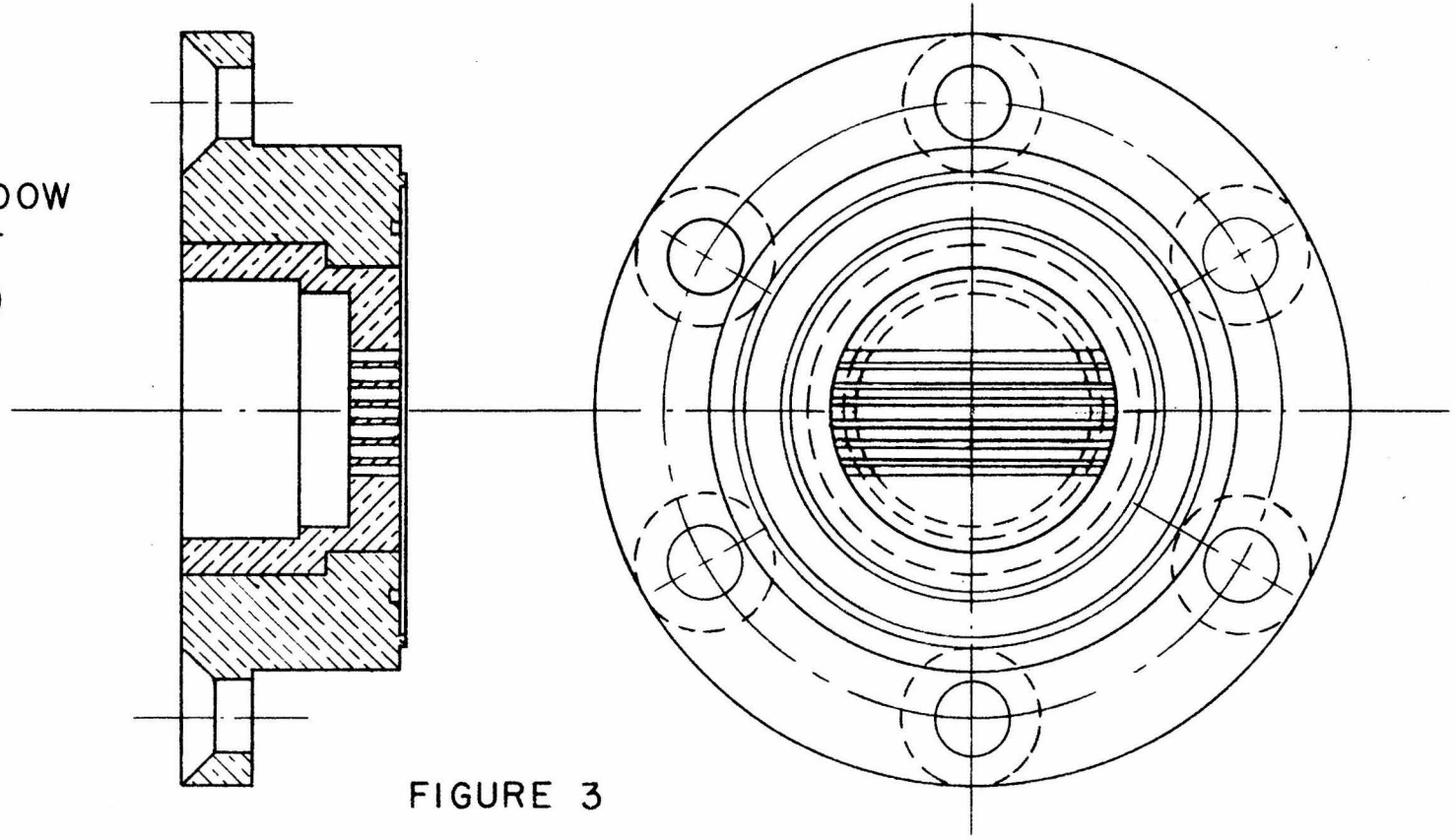

FIGURE 3

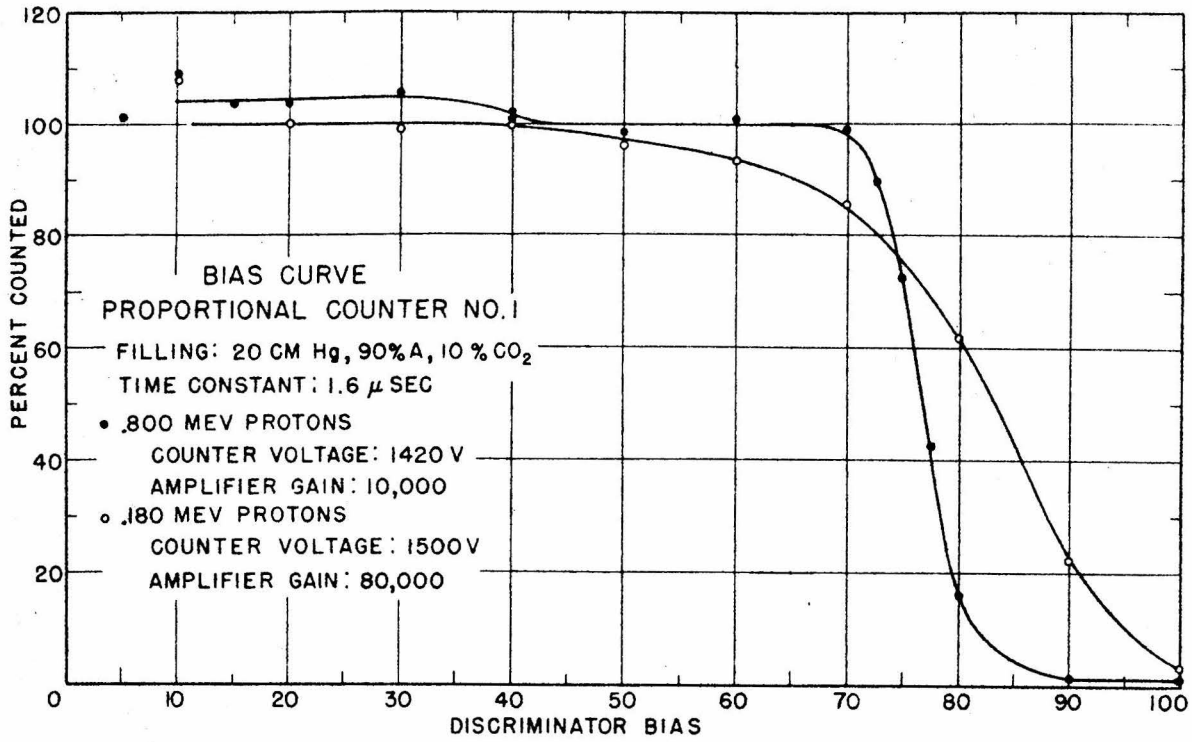
BIAS CURVE
PROPORTIONAL COUNTER NO. 1
FILLING: 20 CM Hg, 90% A, 10 % CO_2
TIME CONSTANT: 1.6 μ SEC
• .800 MEV PROTONS
COUNTER VOLTAGE: 1420 V
AMPLIFIER GAIN: 10,000
∘ .180 MEV PROTONS
COUNTER VOLTAGE: 1500 V
AMPLIFIER GAIN: 80,000
PERCENT COUNTED
DISCRIMINATOR BIAS
0
10
20
30
40
50
60
70
80
90
100
120

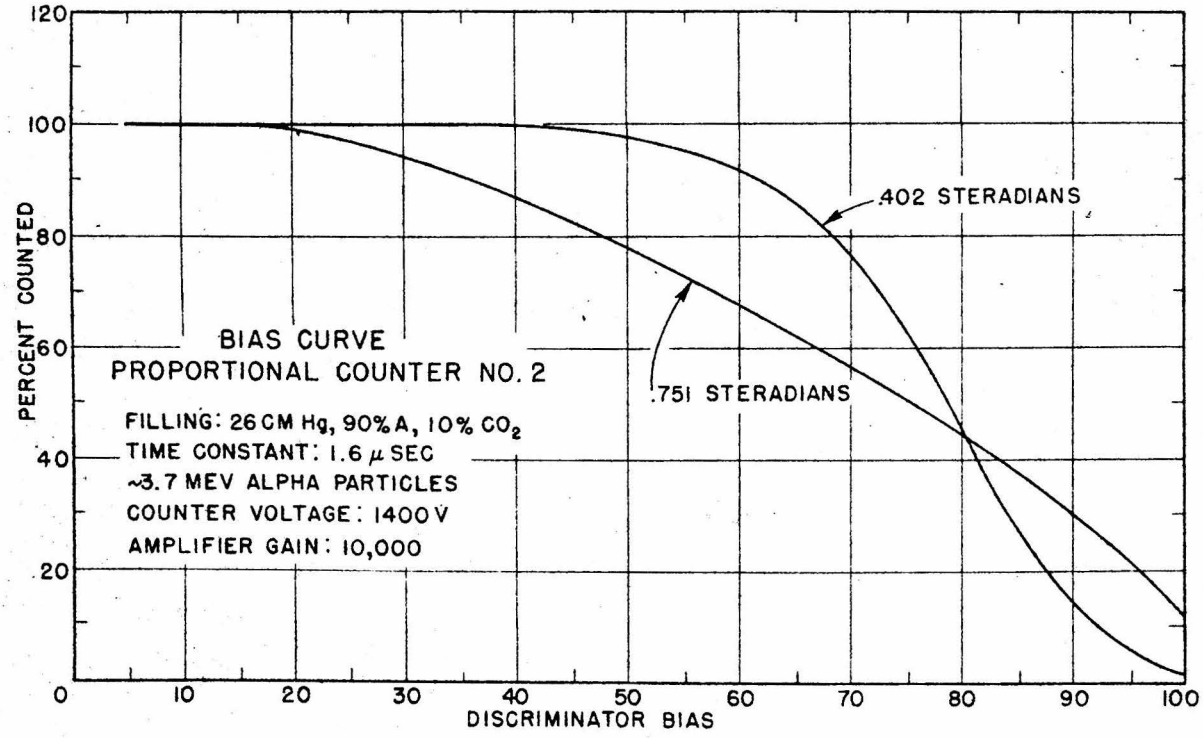
BIAS CURVE
PROPORTIONAL COUNTER NO. 2
FILLING: 26 CM Hg, 90% A, 10% CO_2
TIME CONSTANT: 1.6 μ SEC
~3.7 MEV ALPHA PARTICLES
COUNTER VOLTAGE: 1400 V
AMPLIFIER GAIN: 10,000
.402 STERADIANS
.751 STERADIANS
PERCENT COUNTED
DISCRIMINATOR BIAS
0
10
20
30
40
50
60
70
80
90
100
120

FIGURE 4

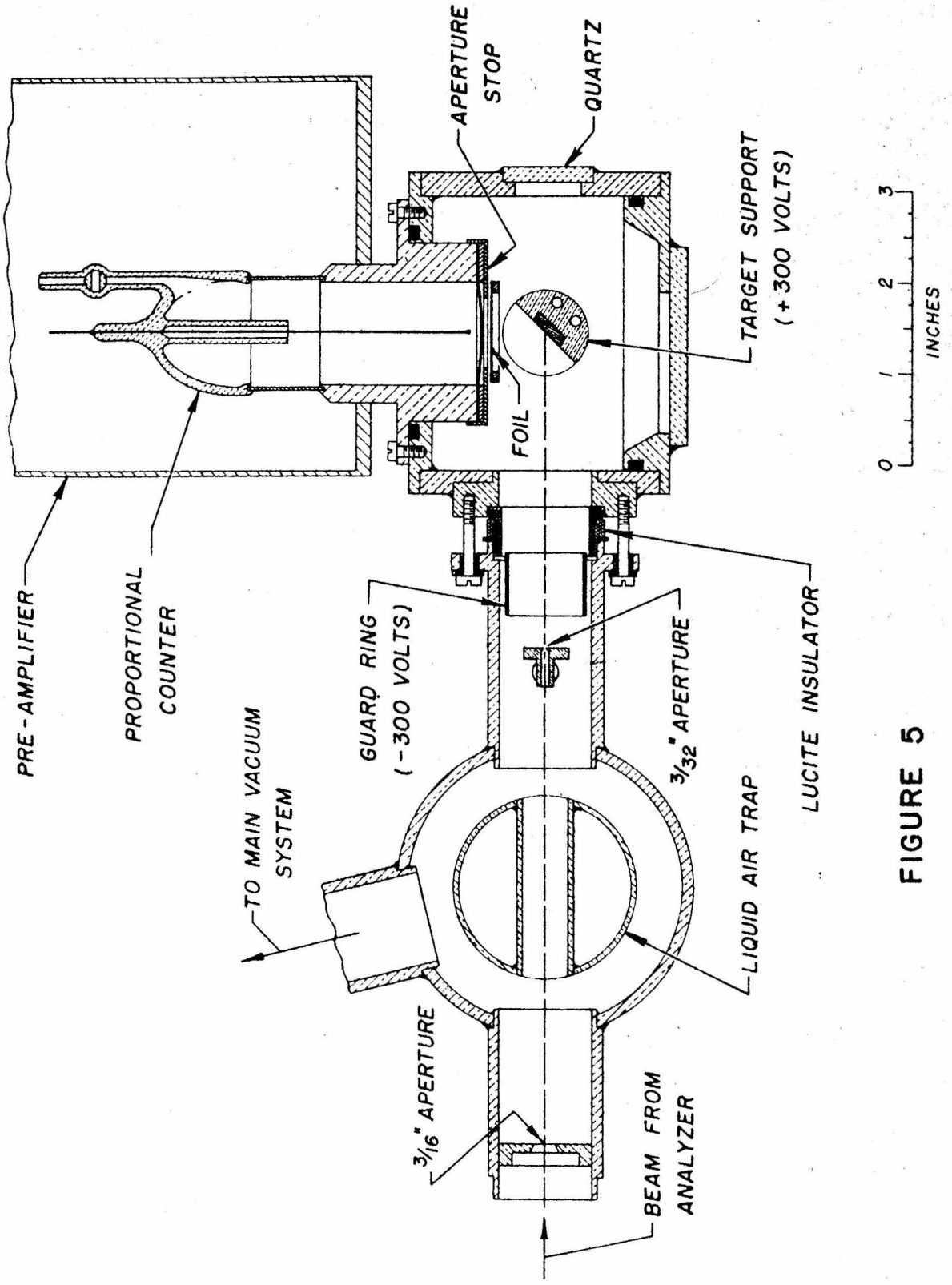
PRE-AMPLIFIER
PROPORTIONAL COUNTER
APERTURE STOP
QUARTZ
FOIL
TARGET SUPPORT (+300 VOLTS)
GUARD RING (-300 VOLTS)
LUCITE INSULATOR
TO MAIN VACUUM SYSTEM
3/32" APERTURE
LIQUID AIR TRAP
3/16" APERTURE
BEAM FROM ANALYZER
0
1
2
3
INCHES

FIGURE 5

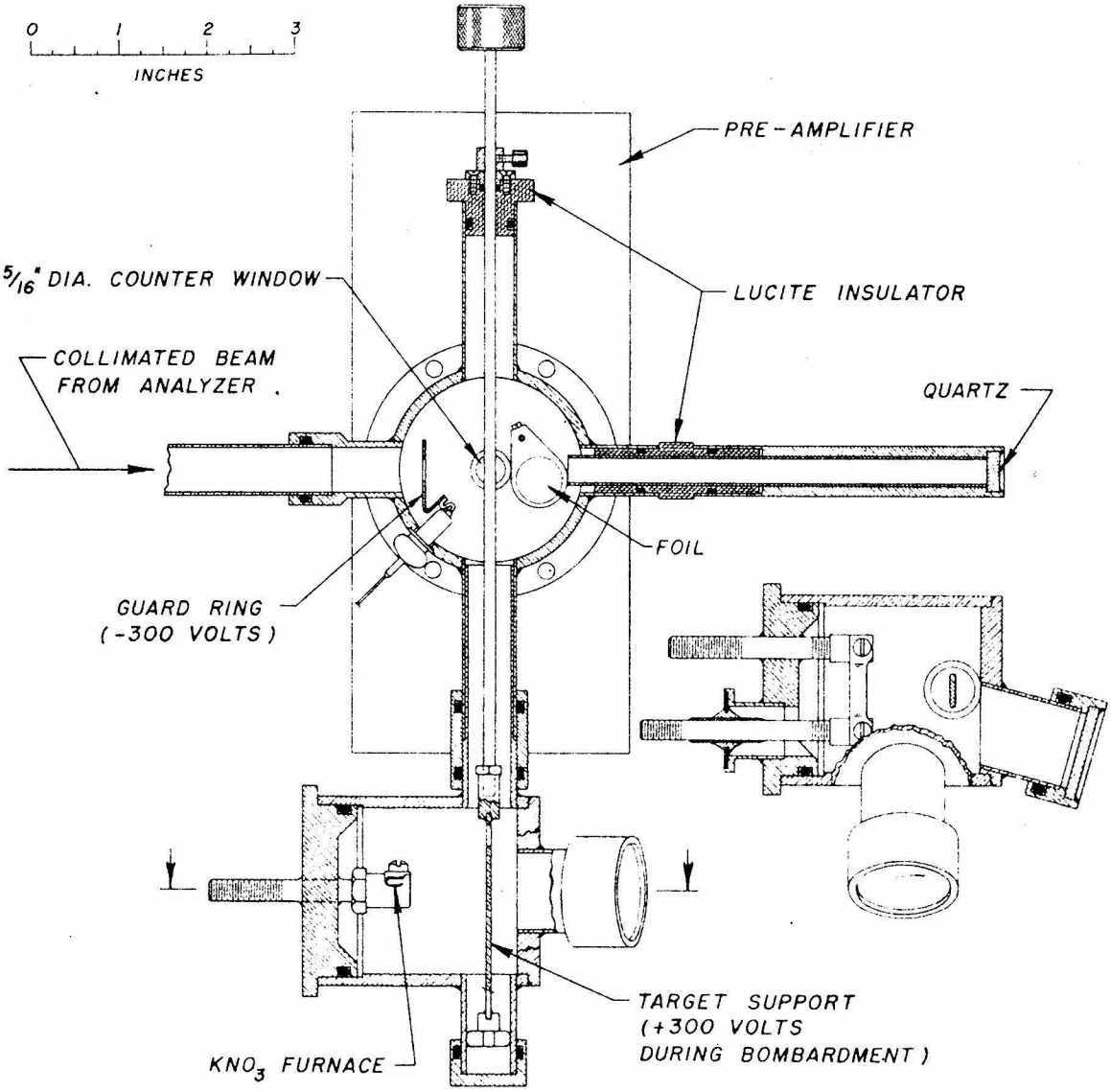
0 1 2 3
INCHES
PRE-AMPLIFIER
5/16" DIA. COUNTER WINDOW
LUCITE INSULATOR
COLLIMATED BEAM FROM ANALYZER
QUARTZ
FOIL
GUARD RING (-300 VOLTS)
TARGET SUPPORT (+300 VOLTS DURING BOMBARDMENT)
KNO3 FURNACE

FIGURE 6

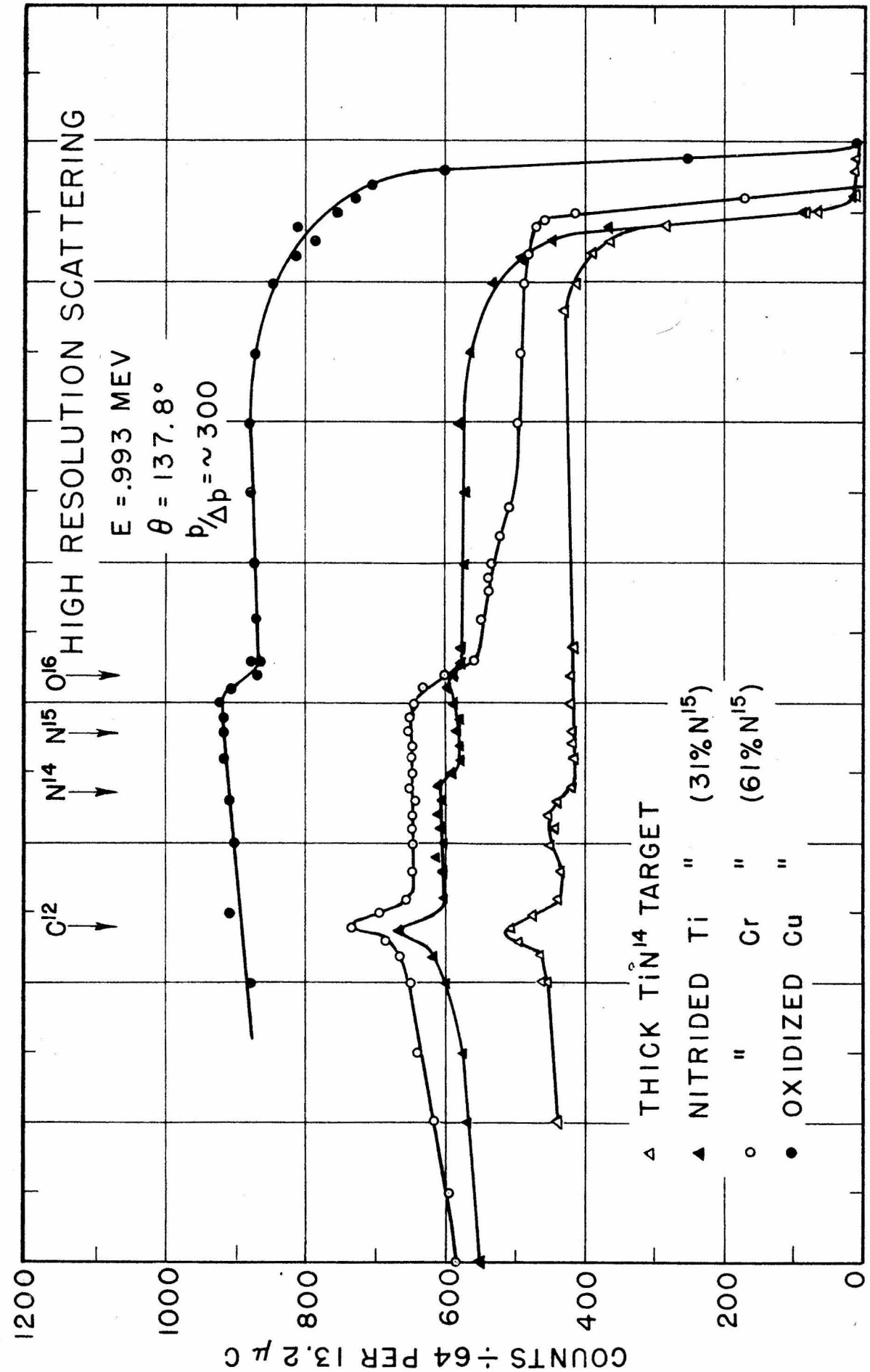
HIGH RESOLUTION SCATTERING
E = .993 MEV
θ = 137.8°
p/Δp = ~ 300
C12
N14 N15
O16
THICK TiN14 TARGET
NITRIDED Ti " (31% N15)
" Cr " (61% N15)
OXIDIZED Cu "
COUNTS ÷ 64 PER 13.2 μ C
FLUXMETER READING
0
200
400
600
800
1000
1200
42
43
44
45
46
47
48
49
50
51

FIGURE 7

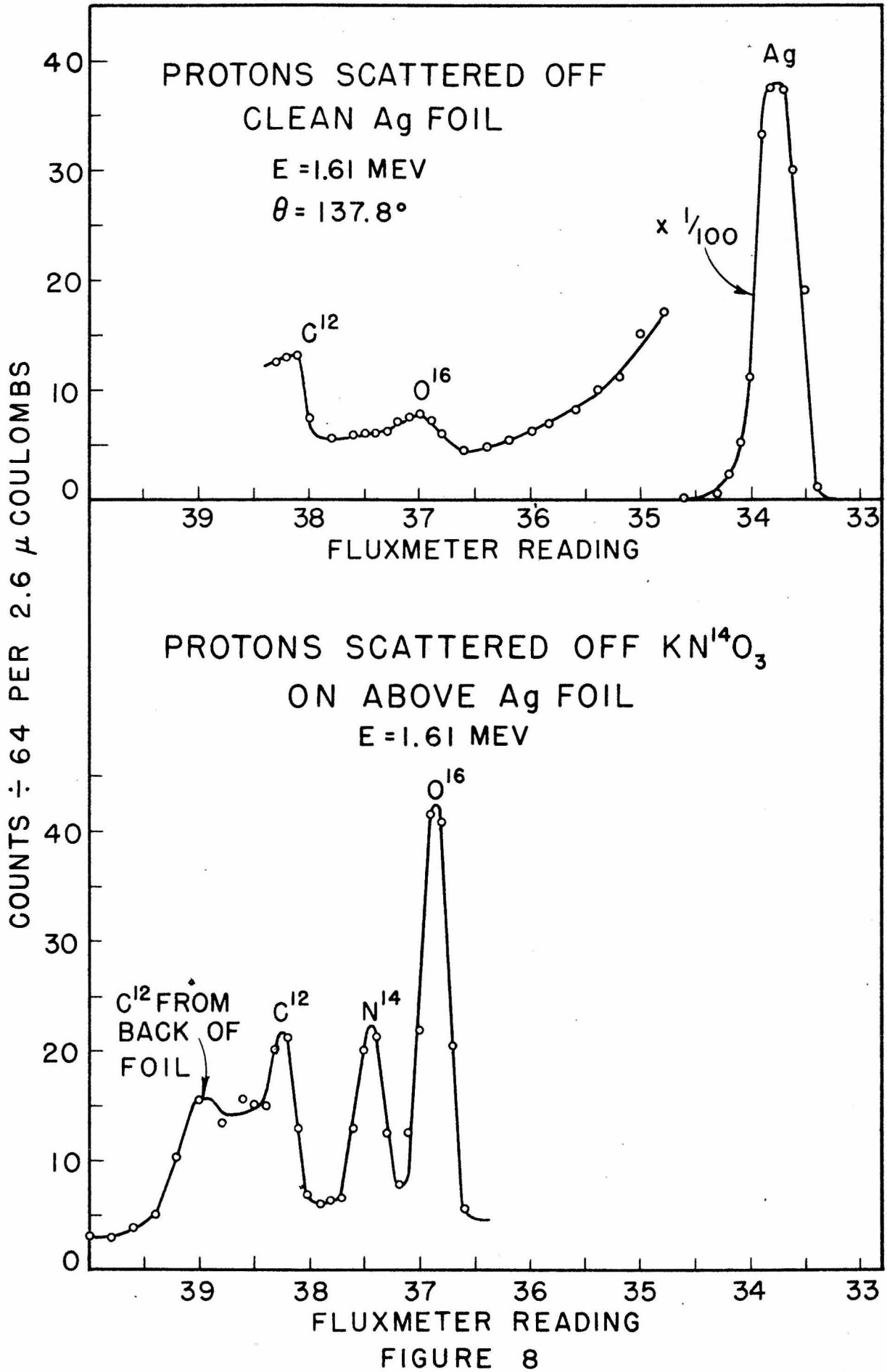
PROTONS SCATTERED OFF
CLEAN Ag FOIL
E = 1.61 MEV
θ = 137.8°
x 1/100
Ag
C12
O16
40
30
20
10
0
39
38
37
36
35
34
33
FLUXMETER READING
PROTONS SCATTERED OFF KN14O3
ON ABOVE Ag FOIL
E = 1.61 MEV
O16
C12 FROM
BACK OF
FOIL
C12
N14
COUNTS ÷ 64 PER 2.6 μ COULOMBS
40
30
20
10
0
39
38
37
36
35
34
33
FLUXMETER READING

FIGURE 8

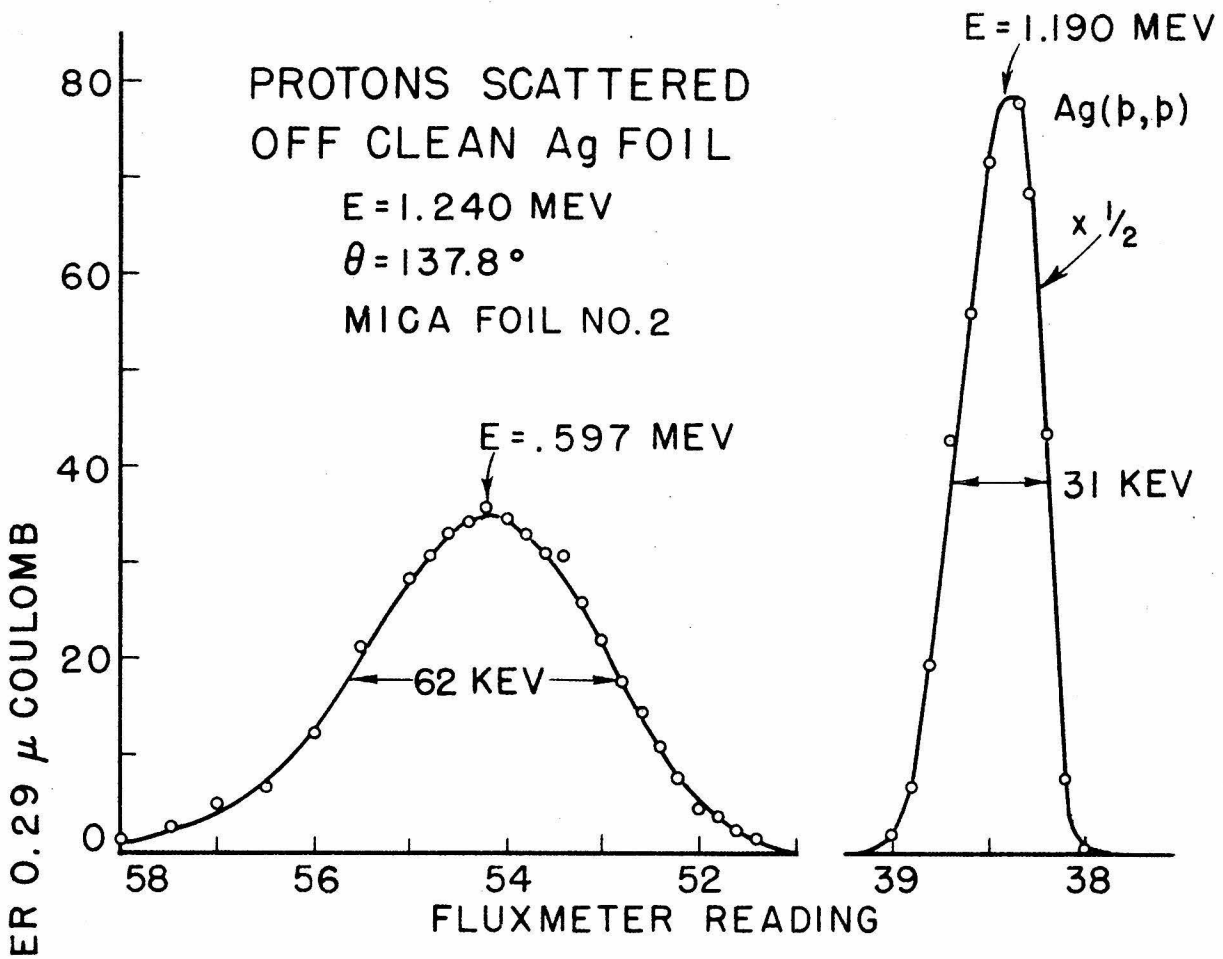
PROTONS SCATTERED
OFF CLEAN Ag FOIL
E = 1.240 MEV
θ = 137.8°
MICA FOIL NO.2
E = .597 MEV
62 KEV
E = 1.190 MEV
Ag(p,p)
x 1/2
31 KEV
COUNTS ÷ 100 PER 0.29 μ COULOMB
FLUXMETER READING

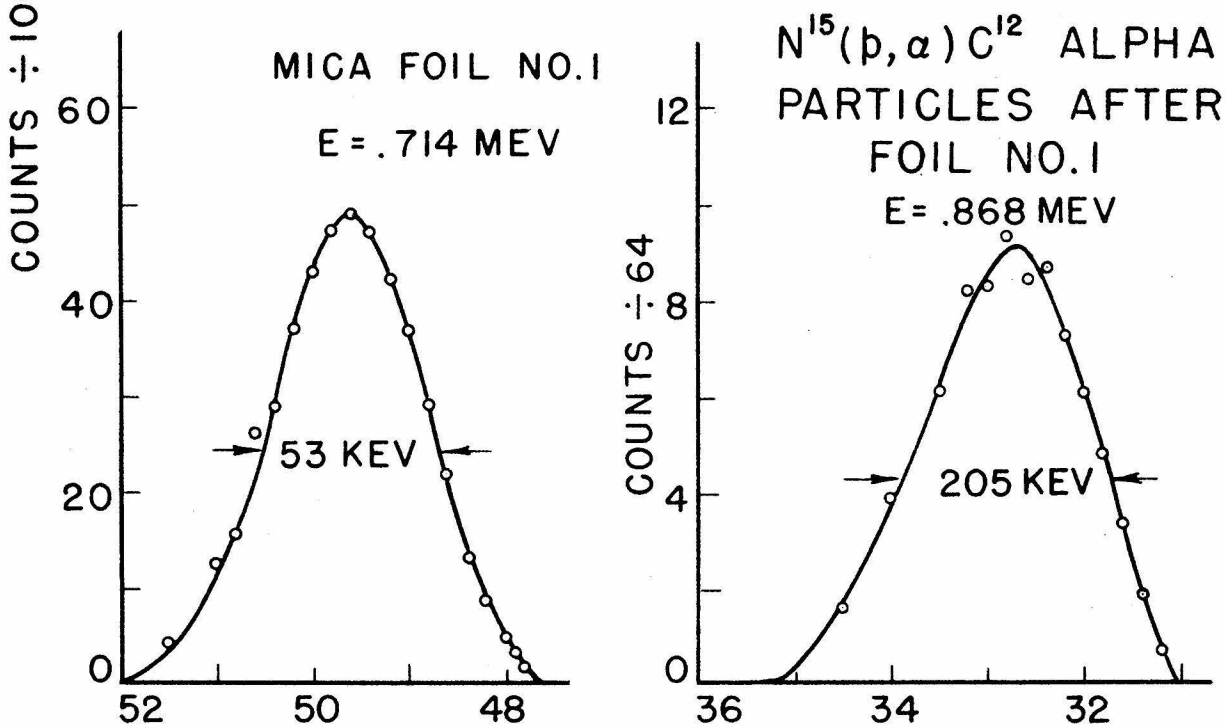
MICA FOIL NO.1
E = .714 MEV
53 KEV
N15(p,α)C12 ALPHA
PARTICLES AFTER
FOIL NO.1
E = .868 MEV
205 KEV
COUNTS ÷ 64
COUNTS ÷ 8
FLUXMETER READING

FIGURE 9

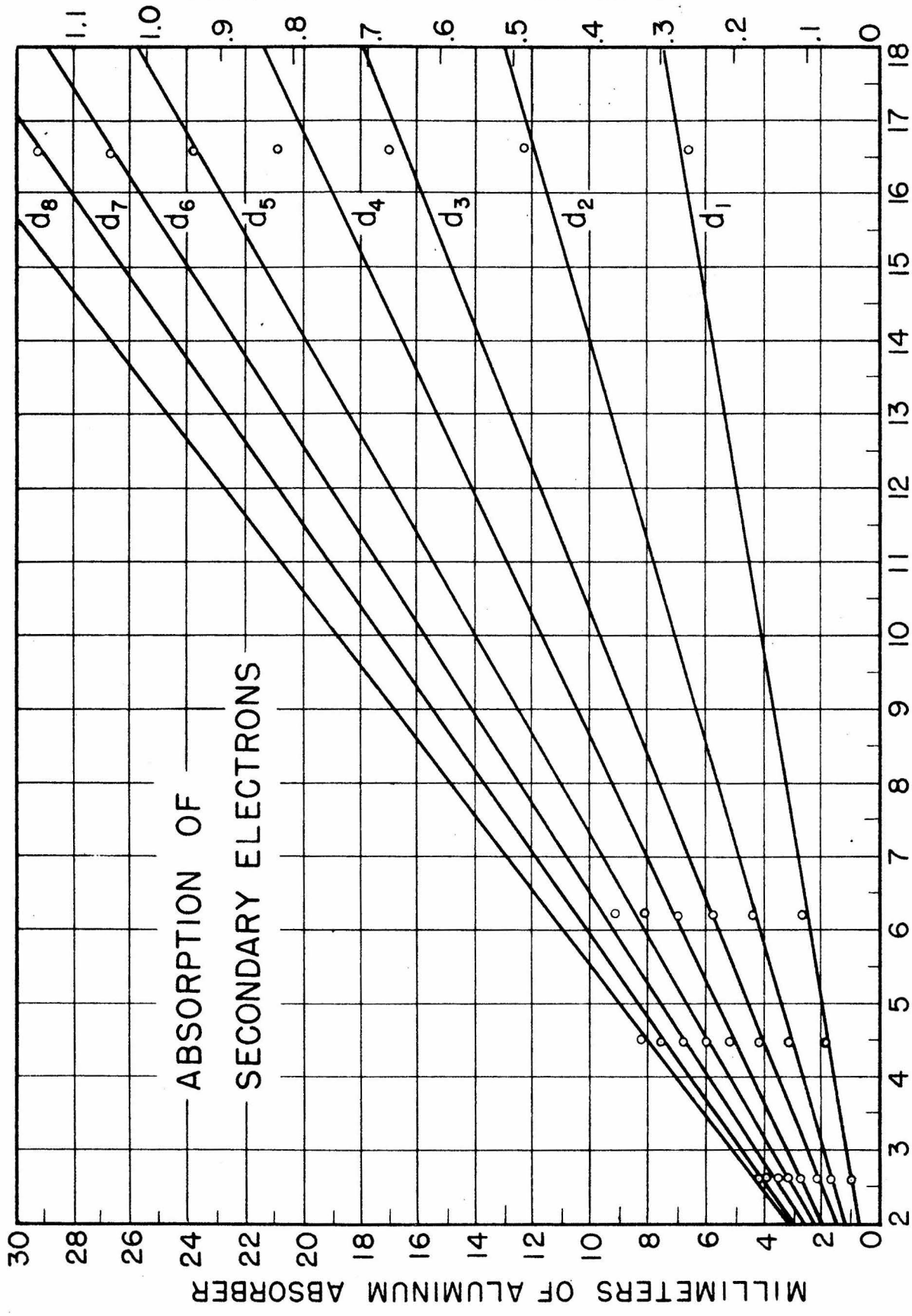
ABSORPTION OF SECONDARY ELECTRONS
d_8
d_7
d_6
d_5
d_4
d_3
d_2
d_1
MILLIMETERS OF ALUMINUM ABSORBER
INCHES OF ALUMINUM ABSORBER
QUANTUM ENERGY (MEV)

FIGURE 10

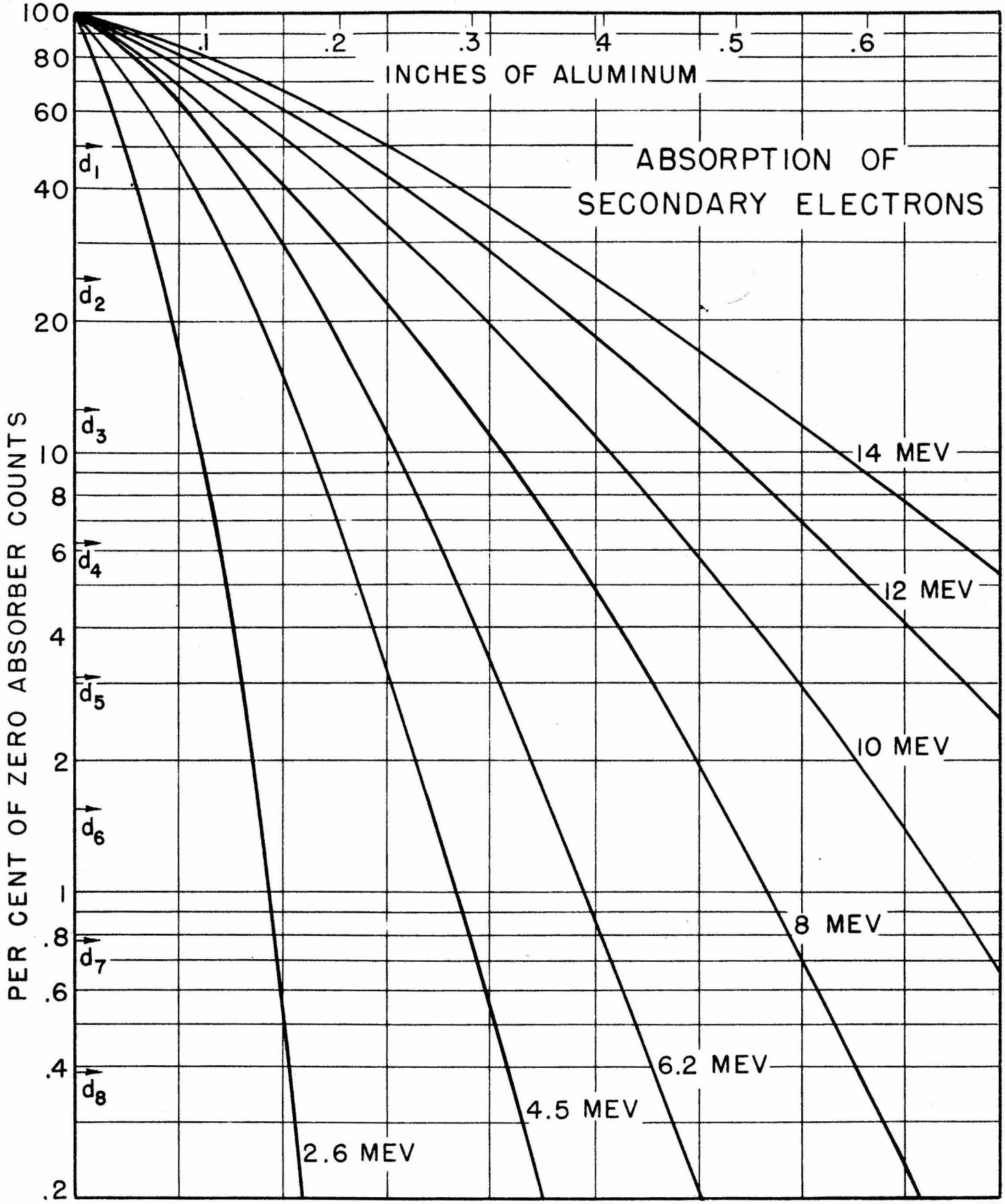
ABSORPTION OF
SECONDARY ELECTRONS
INCHES OF ALUMINUM
.1
.2
.3
.4
.5
.6
PER CENT OF ZERO ABSORBER COUNTS
100
80
60
40
20
10
8
6
4
2
1
.8
.6
.4
.2
d_1
d_2
d_3
d_4
d_5
d_6
d_7
d_8
14 MEV
12 MEV
10 MEV
8 MEV
6.2 MEV
4.5 MEV
2.6 MEV
0
2
4
6
8
10
12
14
16
18
MILLIMETERS OF ALUMINUM

FIGURE 11

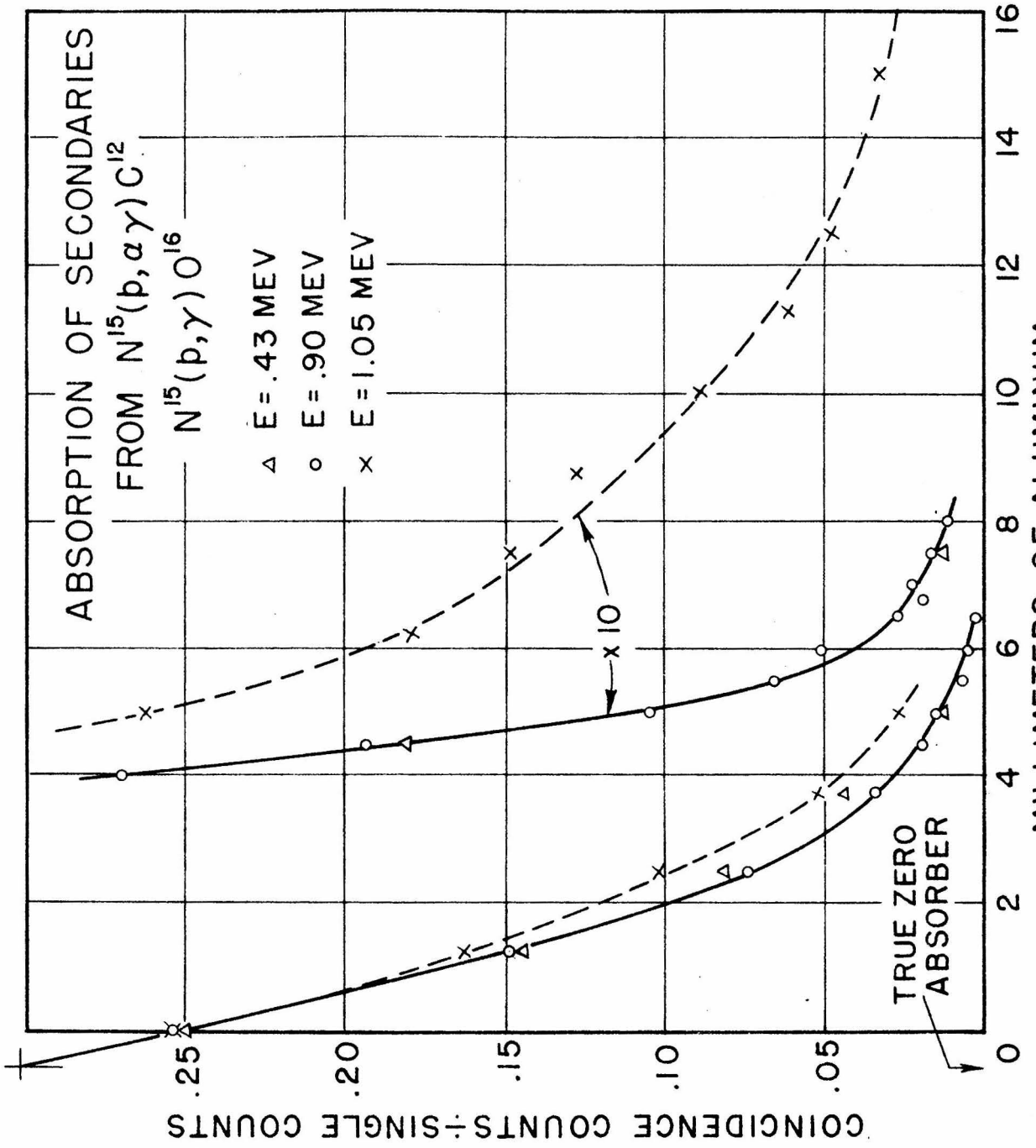
ABSORPTION OF SECONDARIES
FROM $N^{15}(p,\alpha\gamma)C^{12}$
$N^{15}(p,\gamma)O^{16}$
△ E=.43 MEV
○ E=.90 MEV
× E=1.05 MEV
× 10
TRUE ZERO ABSORBER
COINCIDENCE COUNTS÷SINGLE COUNTS
.25
.20
.15
.10
.05
0
2
4
6
8
10
12
14
16
MILLIMETERS OF ALUMINUM

FIGURE 12

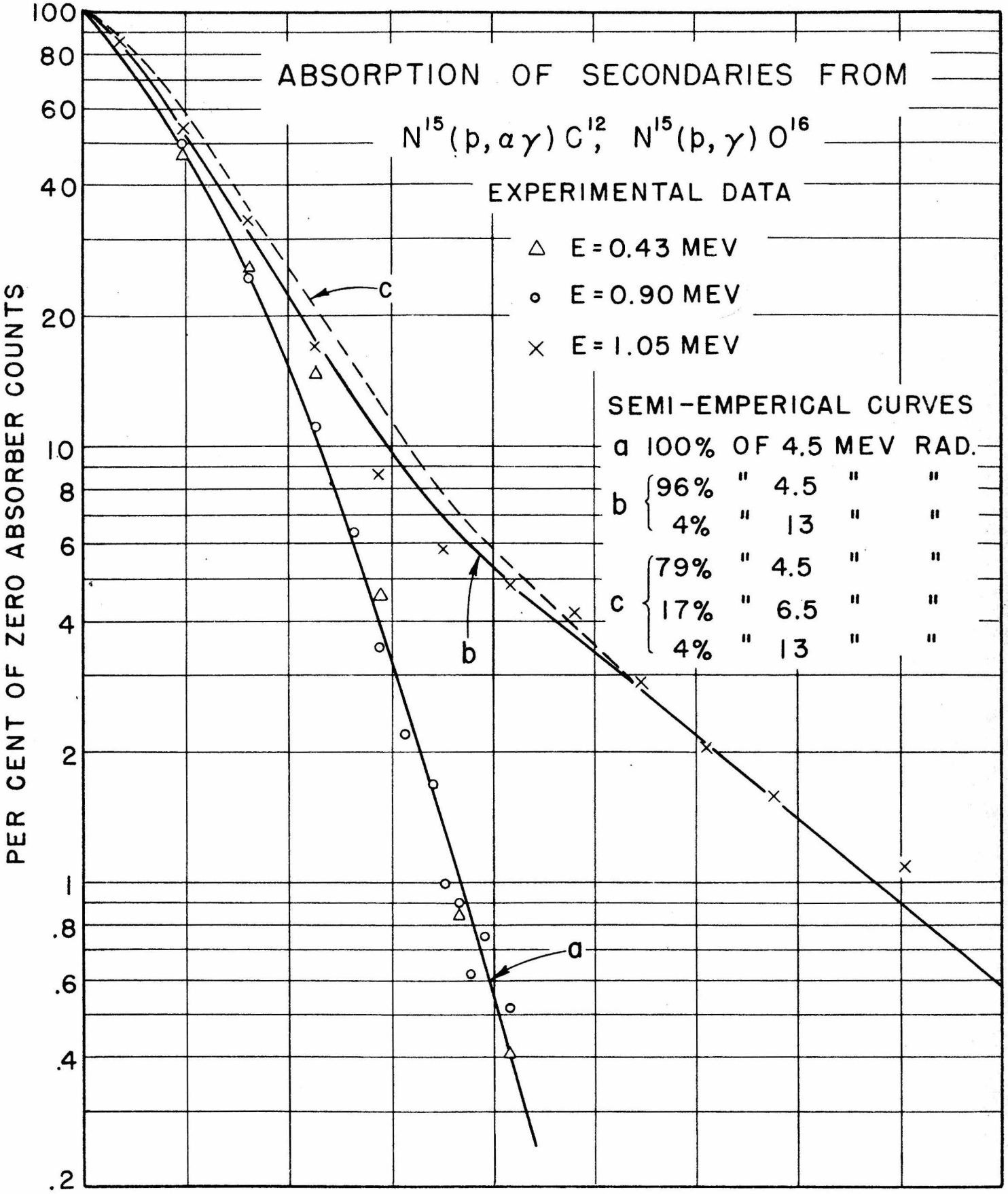
ABSORPTION OF SECONDARIES FROM
$N^{15}(p,\alpha\gamma)C^{12}$; $N^{15}(p,\gamma)O^{16}$
EXPERIMENTAL DATA
△ E = 0.43 MEV
o E = 0.90 MEV
× E = 1.05 MEV
SEMI-EMPERICAL CURVES
a 100% OF 4.5 MEV RAD.
b 96% " 4.5 " "
4% " 13 " "
c 79% " 4.5 " "
17% " 6.5 " "
4% " 13 " "
a
b
c
PER CENT OF ZERO ABSORBER COUNTS
100
80
60
40
20
10
8
6
4
2
1
.8
.6
.4
.2
0
2
4
6
8
10
12
14
16
18
MILLIMETERS OF ALUMINUM

FIGURE 13

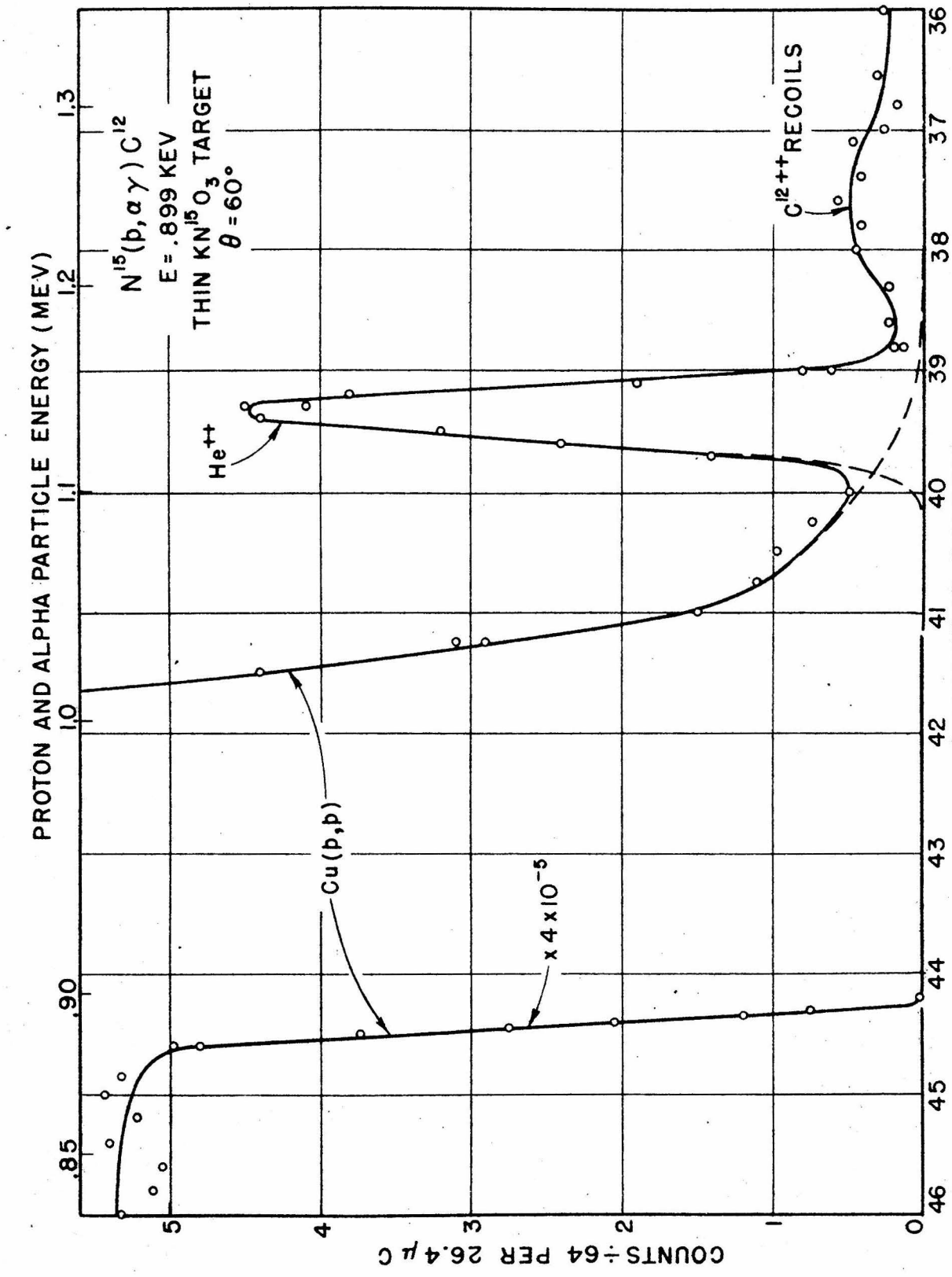
PROTON AND ALPHA PARTICLE ENERGY (MEV)
COUNTS ÷64 PER 26.4 μ C
FLUXMETER READING
N15(p,αγ)C12
E = .899 KEV
THIN KN15O3 TARGET
θ = 60°
He++
Cu(p,p)
x 4 x 10-5
C12++ RECOILS

FIGURE 14

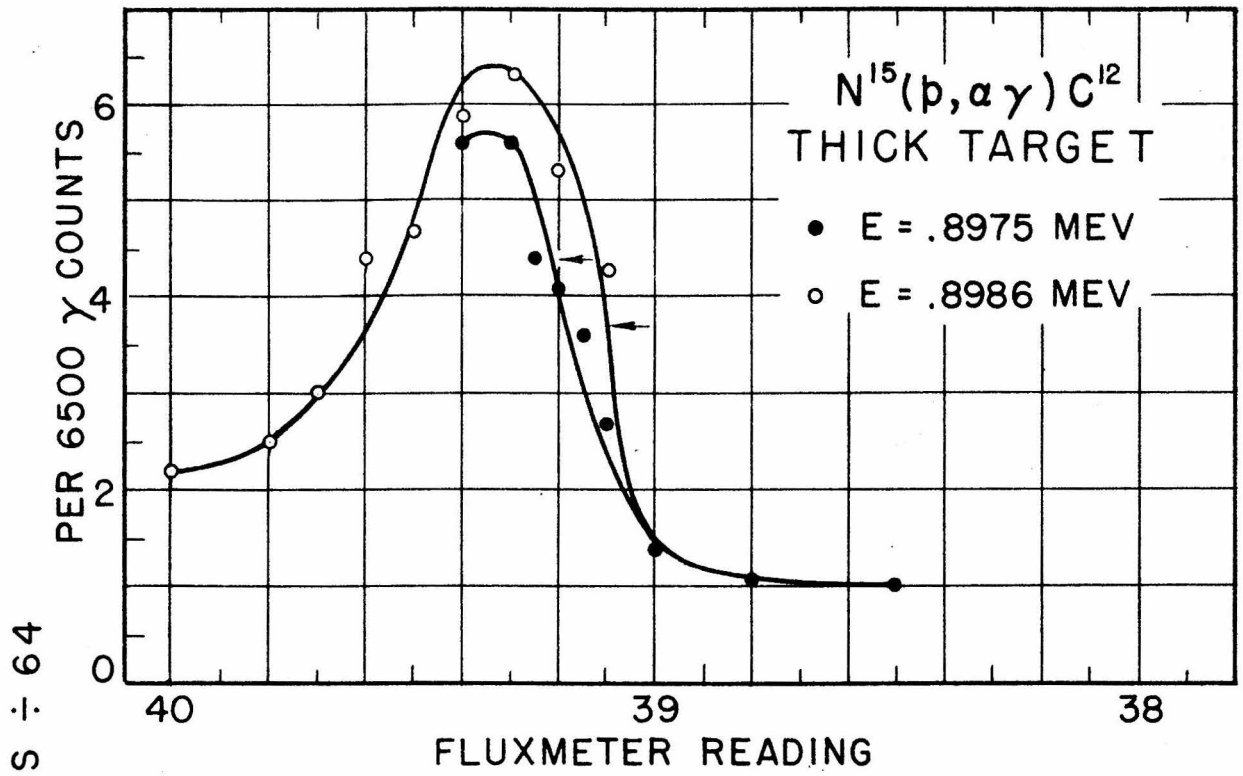
$N^{15}(p,\alpha\gamma)C^{12}$
THICK TARGET
E = .8975 MEV
E = .8986 MEV
PER 6500 γ COUNTS
0
2
4
6
40
39
38
FLUXMETER READING

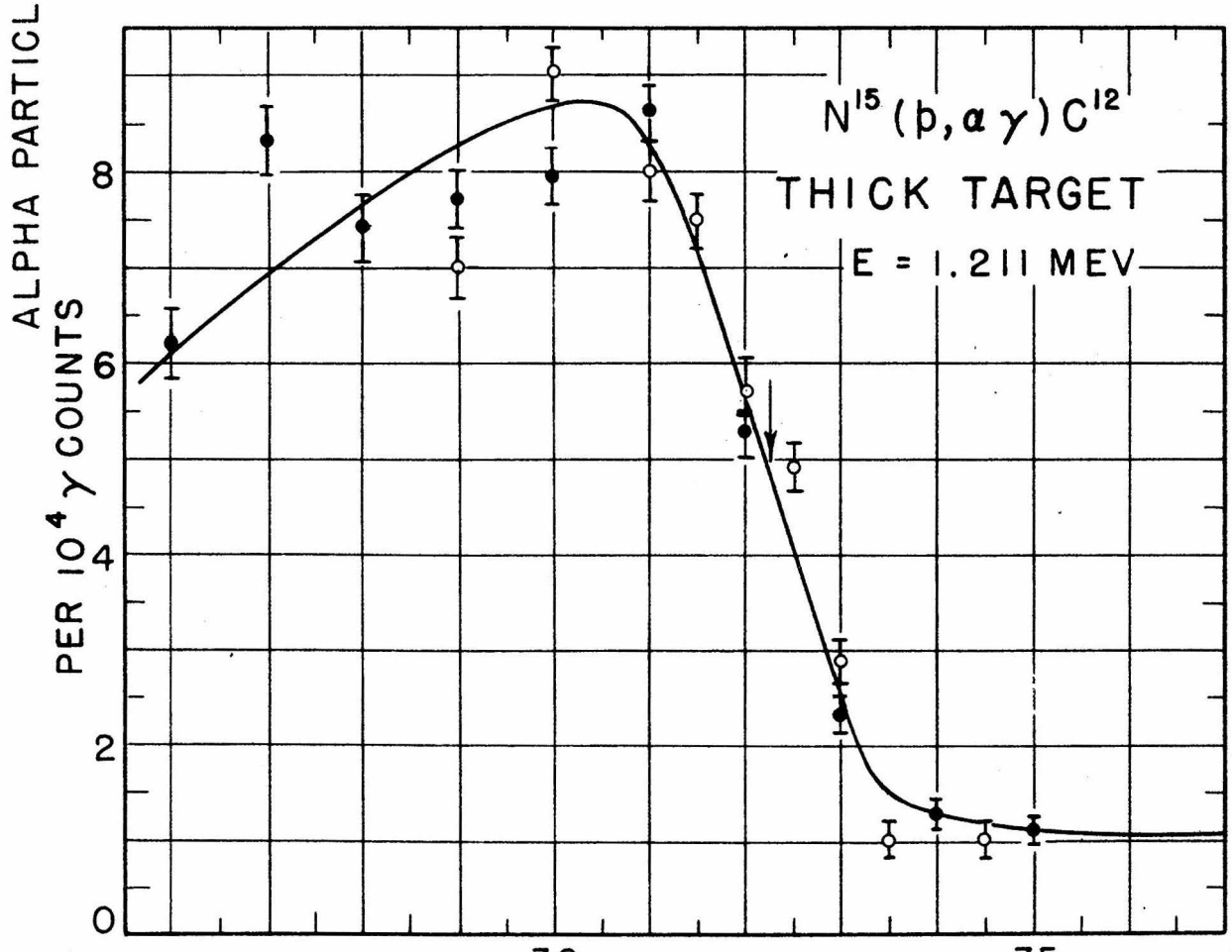
$N^{15}(p,\alpha\gamma)C^{12}$
THICK TARGET
E = 1.211 MEV
ALPHA PARTICLES ÷ 64
PER 10^4 γ COUNTS
0
2
4
6
8
36
35
FLUXMETER READING

FIGURE 15

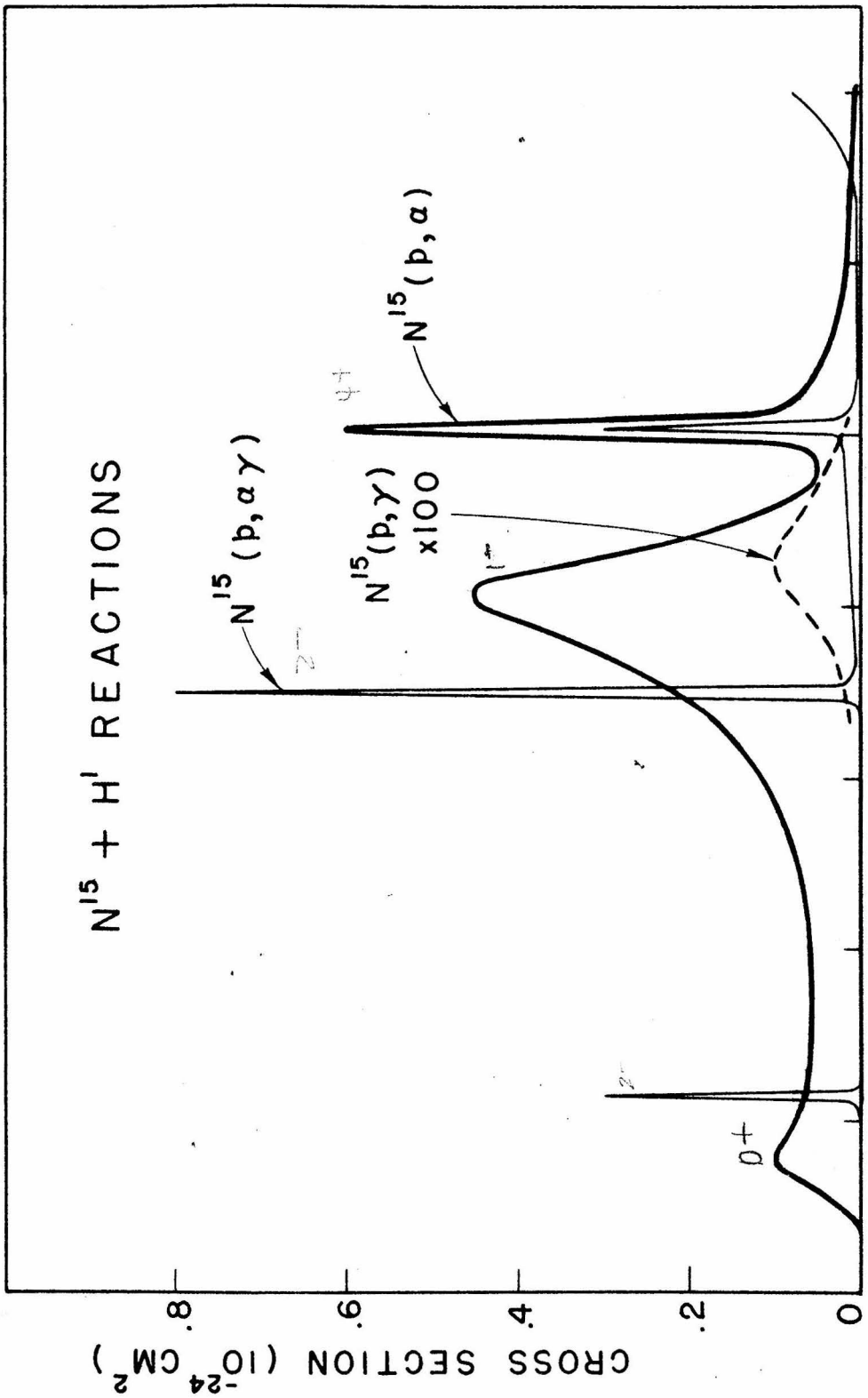
N^{15} + H' REACTIONS
$N^{15}(p,\alpha\gamma)$
$N^{15}(p,\gamma)$ x100
$N^{15}(p,\alpha)$
CROSS SECTION (10^{-24} CM^2)
PROTON ENERGY (MEV)
0
.2
.4
.6
.8
1.0
1.2
1.4
1.6

FIGURE 16

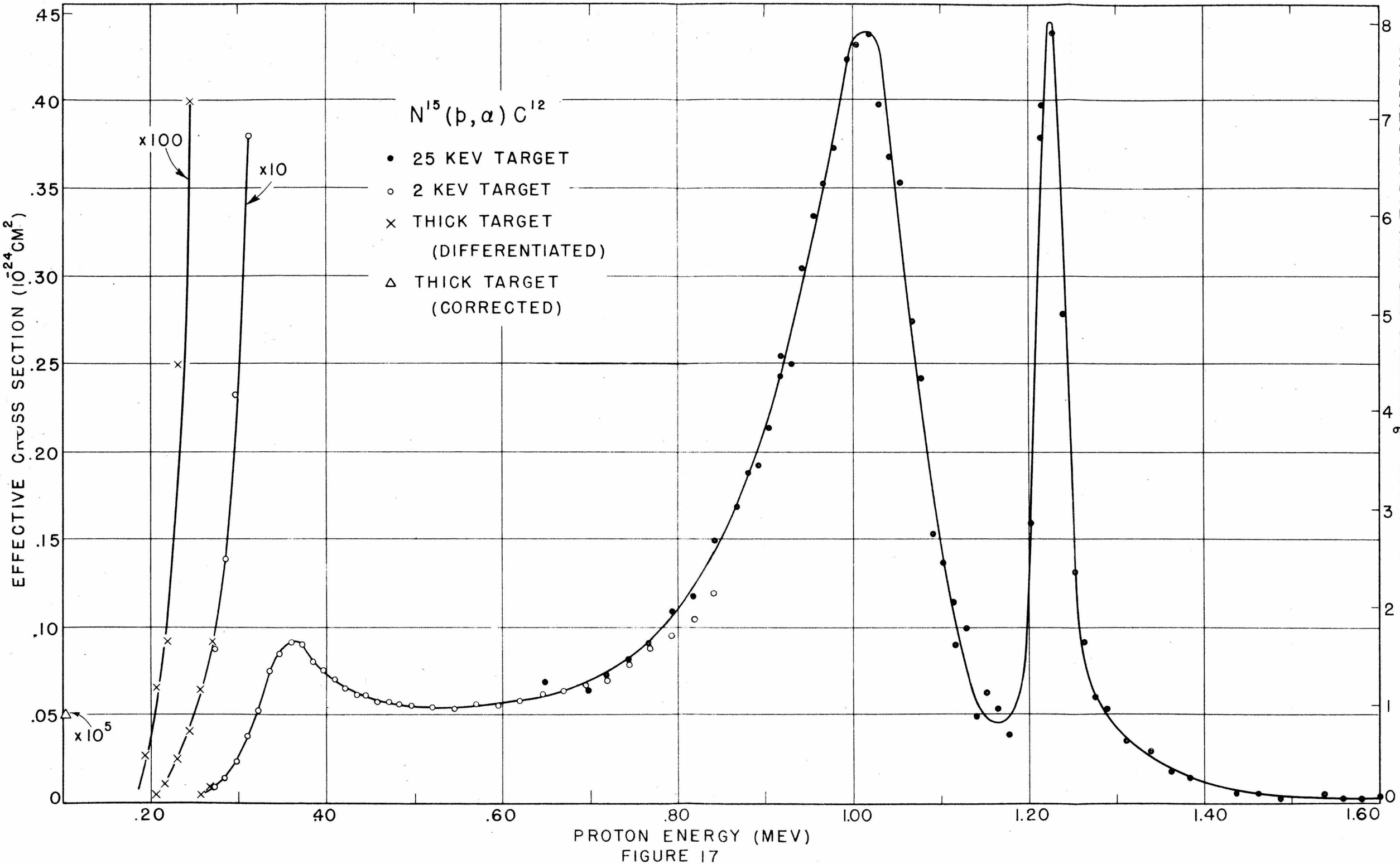
$N^{15}(p,\alpha)C^{12}$
25 KEV TARGET
2 KEV TARGET
THICK TARGET (DIFFERENTIATED)
THICK TARGET (CORRECTED)
x100
x10
x10^5
EFFECTIVE CROSS SECTION (10^{-24} CM^2)
YIELD IN ALPHAS PER 10^9 PROTONS PER KEV TARGET STOPPING
PROTON ENERGY (MEV)
.45
.40
.35
.30
.25
.20
.15
.10
.05
0
8
7
6
5
4
3
2
1
0
.20
.40
.60
.80
1.00
1.20
1.40
1.60

FIGURE 17

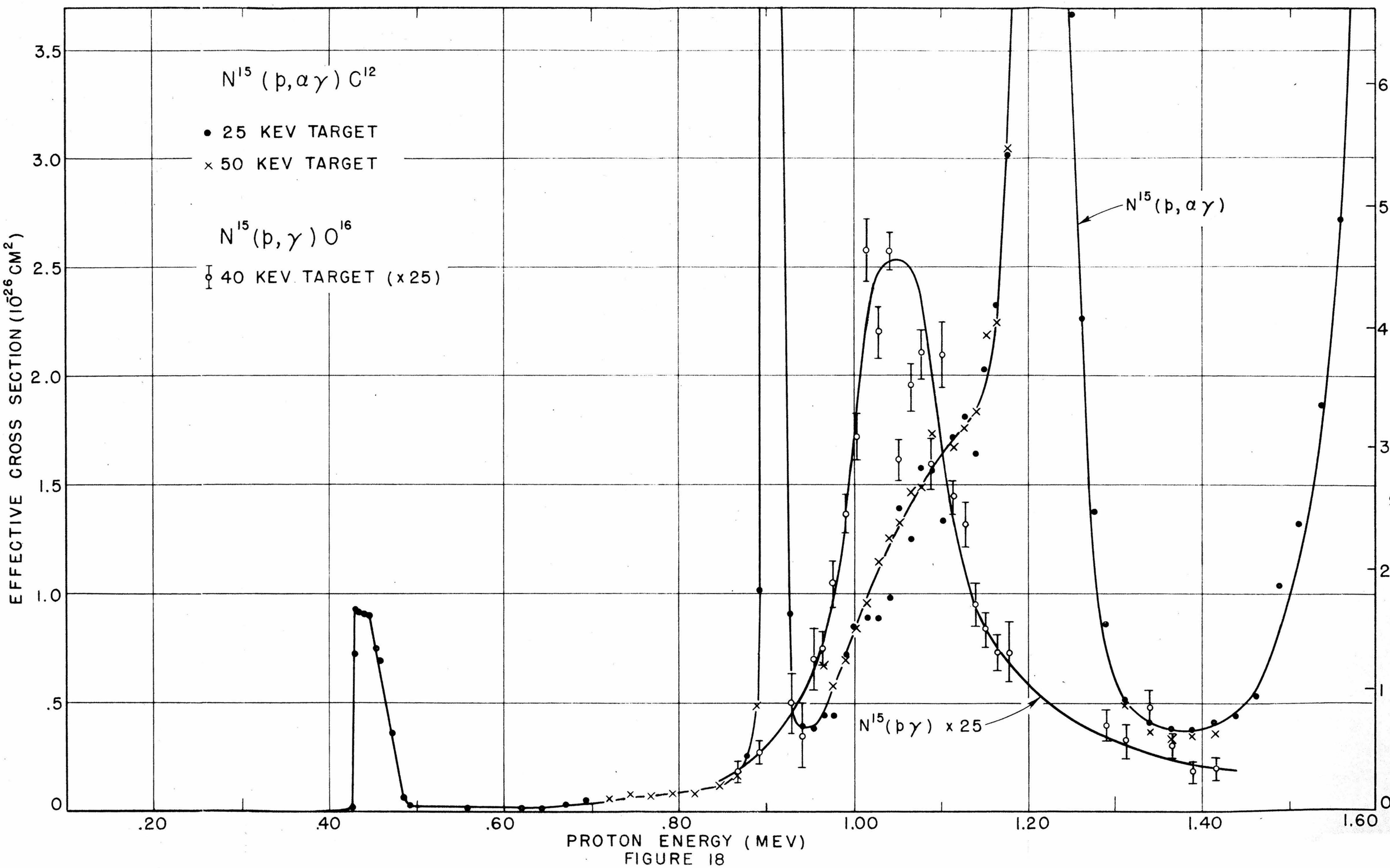
$N^{15}(p,\alpha\gamma)C^{12}$
• 25 KEV TARGET
× 50 KEV TARGET
$N^{15}(p,\gamma)O^{16}$
40 KEV TARGET (x25)
$N^{15}(p,\alpha\gamma)$
$N^{15}(p\gamma)$ x 25
EFFECTIVE CROSS SECTION (10^{-26} CM^2)
YIELD IN QUANTA PER 10^{10} PROTONS PER KEV TARGET STOPPING
PROTON ENERGY (MEV)
0
.5
1.0
1.5
2.0
2.5
3.0
3.5
0
1
2
3
4
5
6
.20
.40
.60
.80
1.00
1.20
1.40
1.60

FIGURE 18

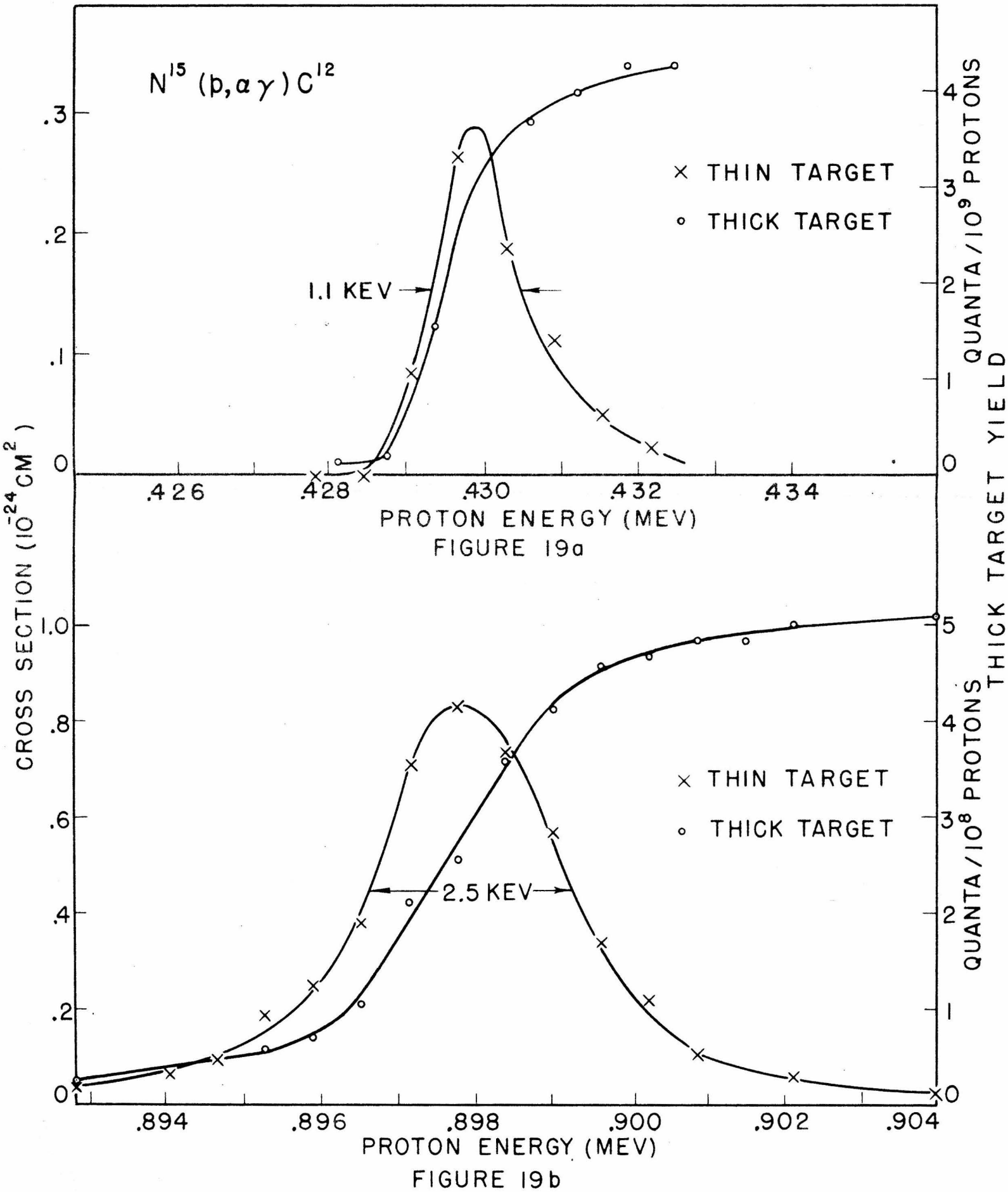

FIGURE 19a

FIGURE 19b

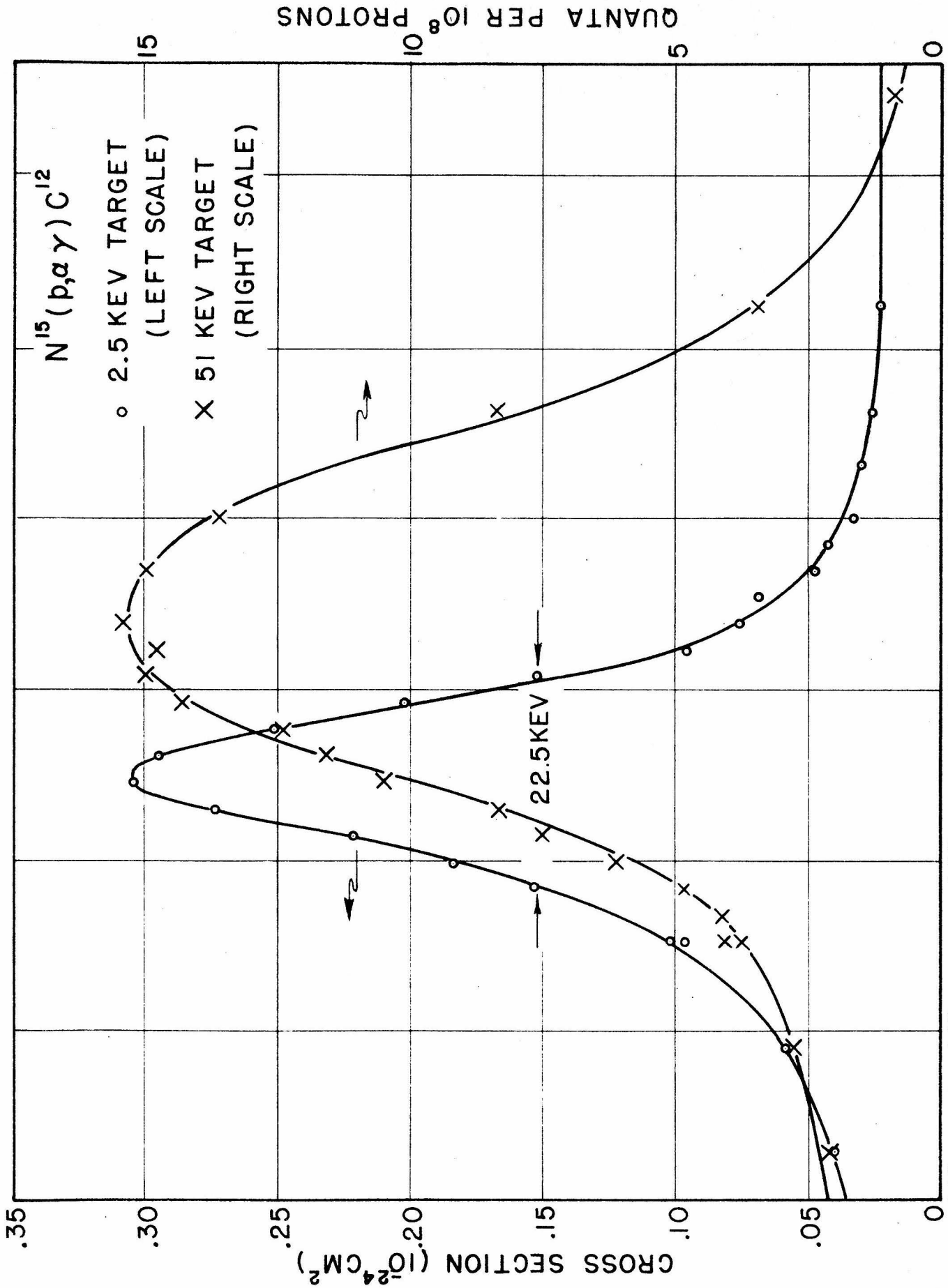
$N^{15}(p,\alpha\gamma)C^{12}$
○ 2.5 KEV TARGET (LEFT SCALE)
× 51 KEV TARGET (RIGHT SCALE)
22.5KEV
CROSS SECTION (10^{-24} CM^2)
QUANTA PER 10^8 PROTONS
PROTON ENERGY (MEV)
0
.05
.10
.15
.20
.25
.30
.35
5
10
15
1.16
1.18
1.20
1.22
1.24
1.26
1.28

FIGURE 20

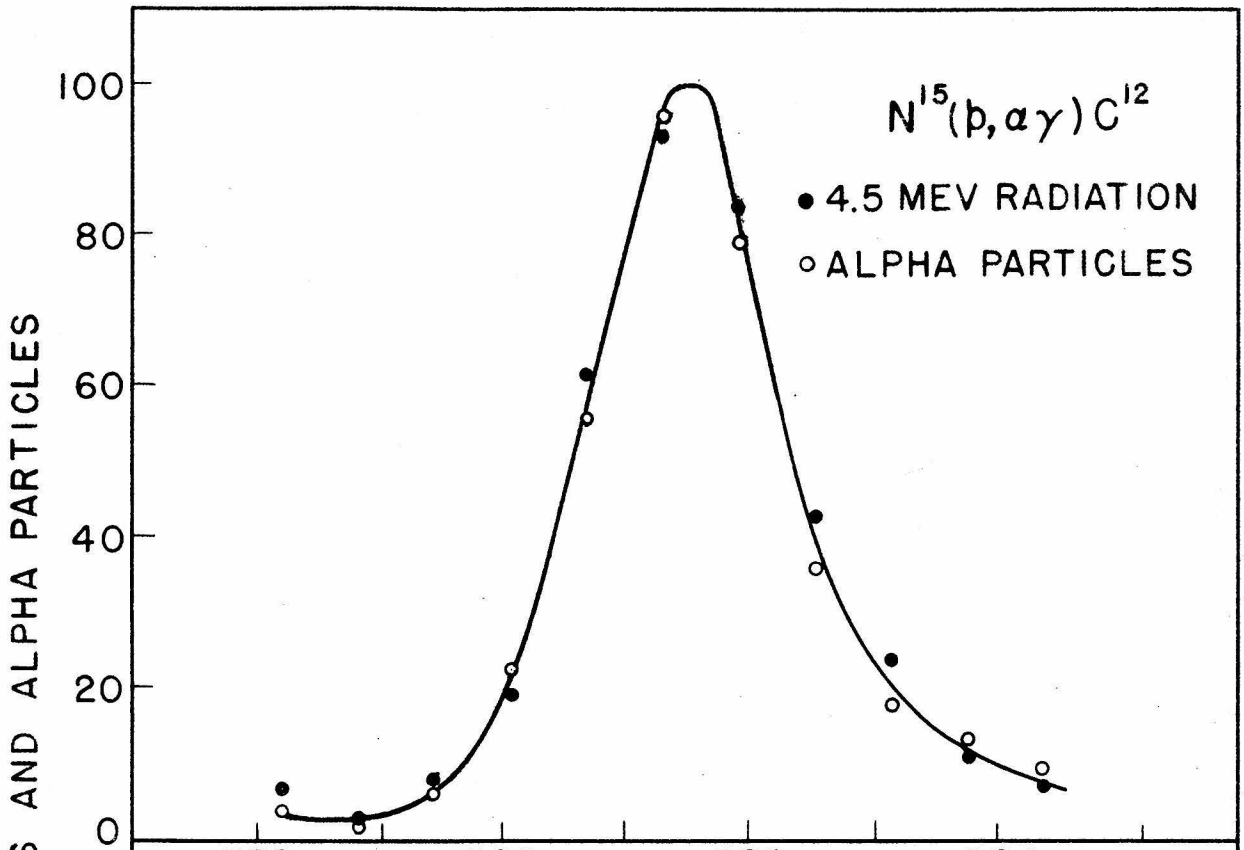

FIGURE 21a

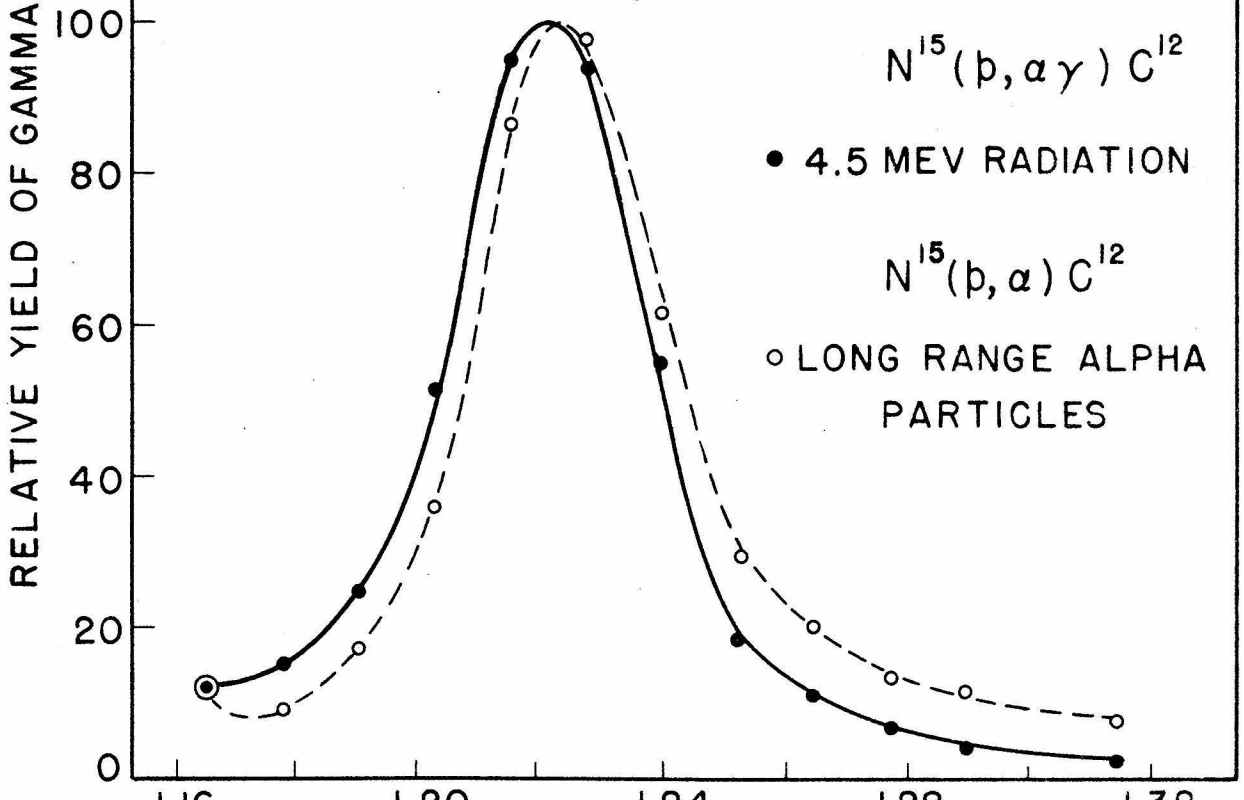

FIGURE 21b

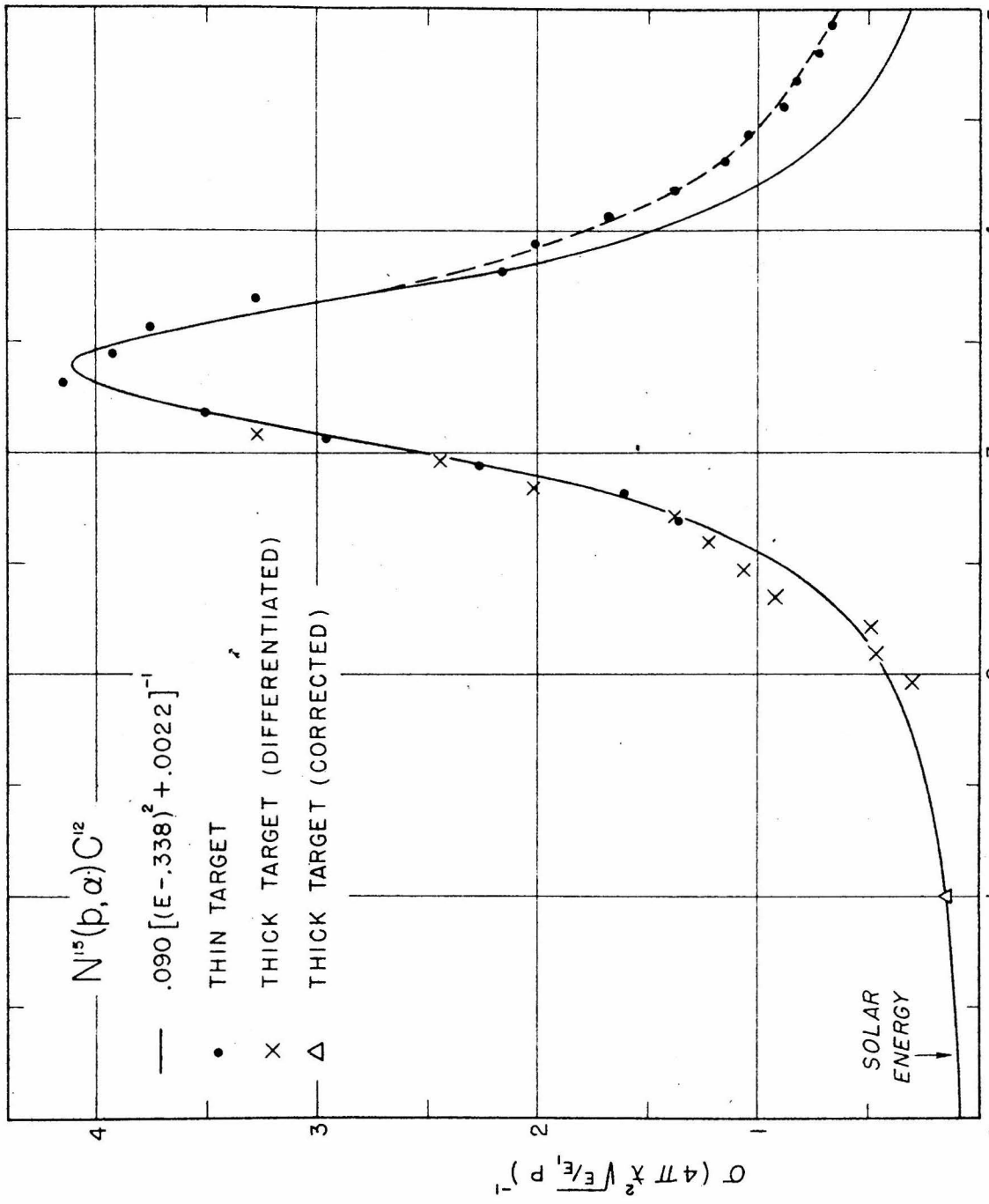
$N^{15}(p,\alpha)C^{12}$
$.090\,[(E-.338)^2+.0022]^{-1}$
THIN TARGET
THICK TARGET (DIFFERENTIATED)
THICK TARGET (CORRECTED)
SOLAR ENERGY
$\sigma\,(4\pi\lambda^2\sqrt{E/E_1}\,P)^{-1}$
PROTON ENERGY (MEV)
0
1
2
3
4
.1
.2
.3
.4
.5

FIGURE 22

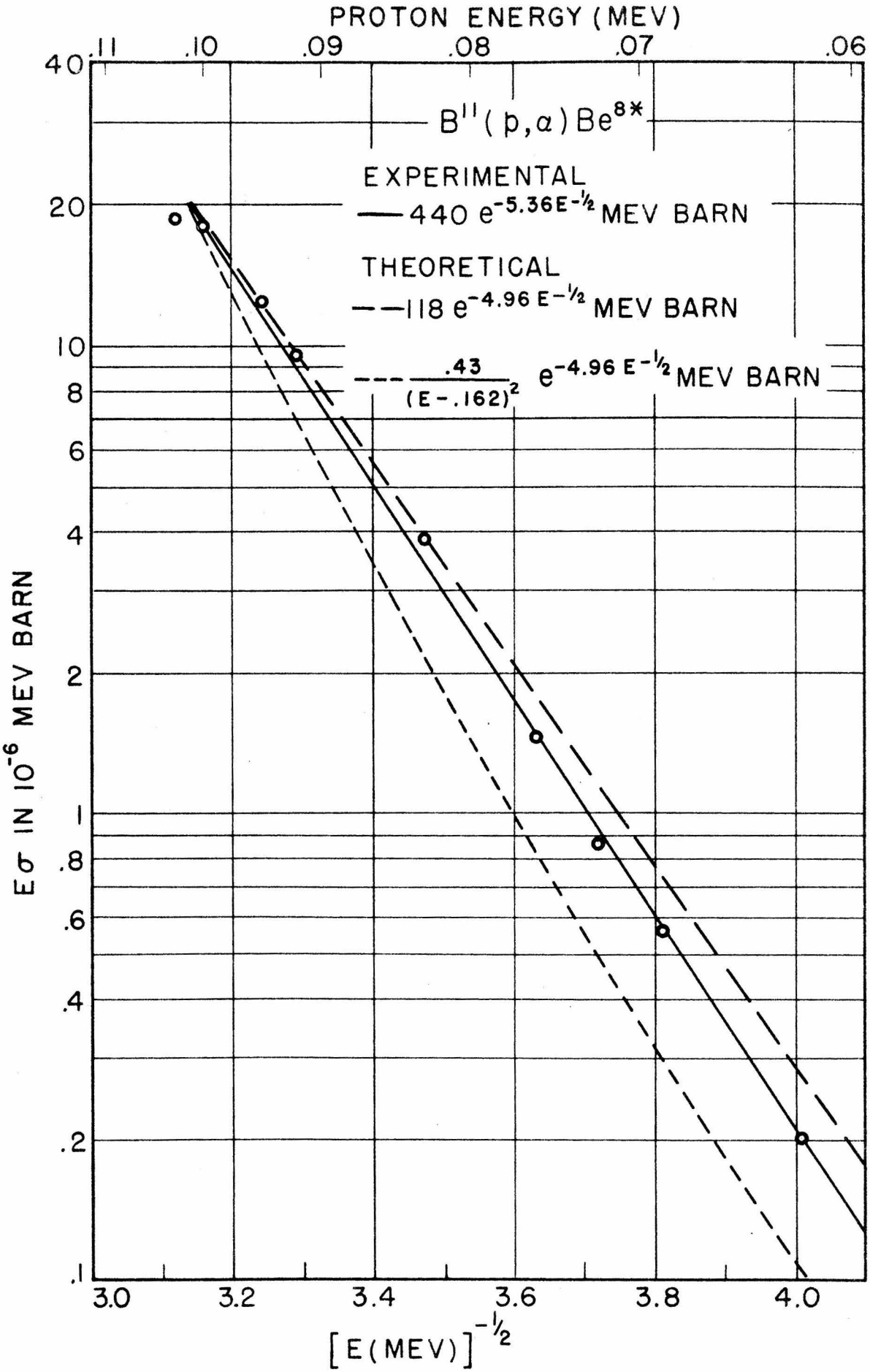
PROTON ENERGY (MEV)
.11
.10
.09
.08
.07
.06
$B^{11}(p,\alpha)Be^{8*}$
EXPERIMENTAL
$440\ e^{-5.36E^{-1/2}}$ MEV BARN
THEORETICAL
$118\ e^{-4.96\,E^{-1/2}}$ MEV BARN
$\frac{.43}{(E-.162)^2}\ e^{-4.96\,E^{-1/2}}$ MEV BARN
$E\sigma$ IN 10^{-6} MEV BARN
40
20
10
8
6
4
2
1
.8
.6
.4
.2
.1
3.0
3.2
3.4
3.6
3.8
4.0
$[E(MEV)]^{-1/2}$

FIGURE 23

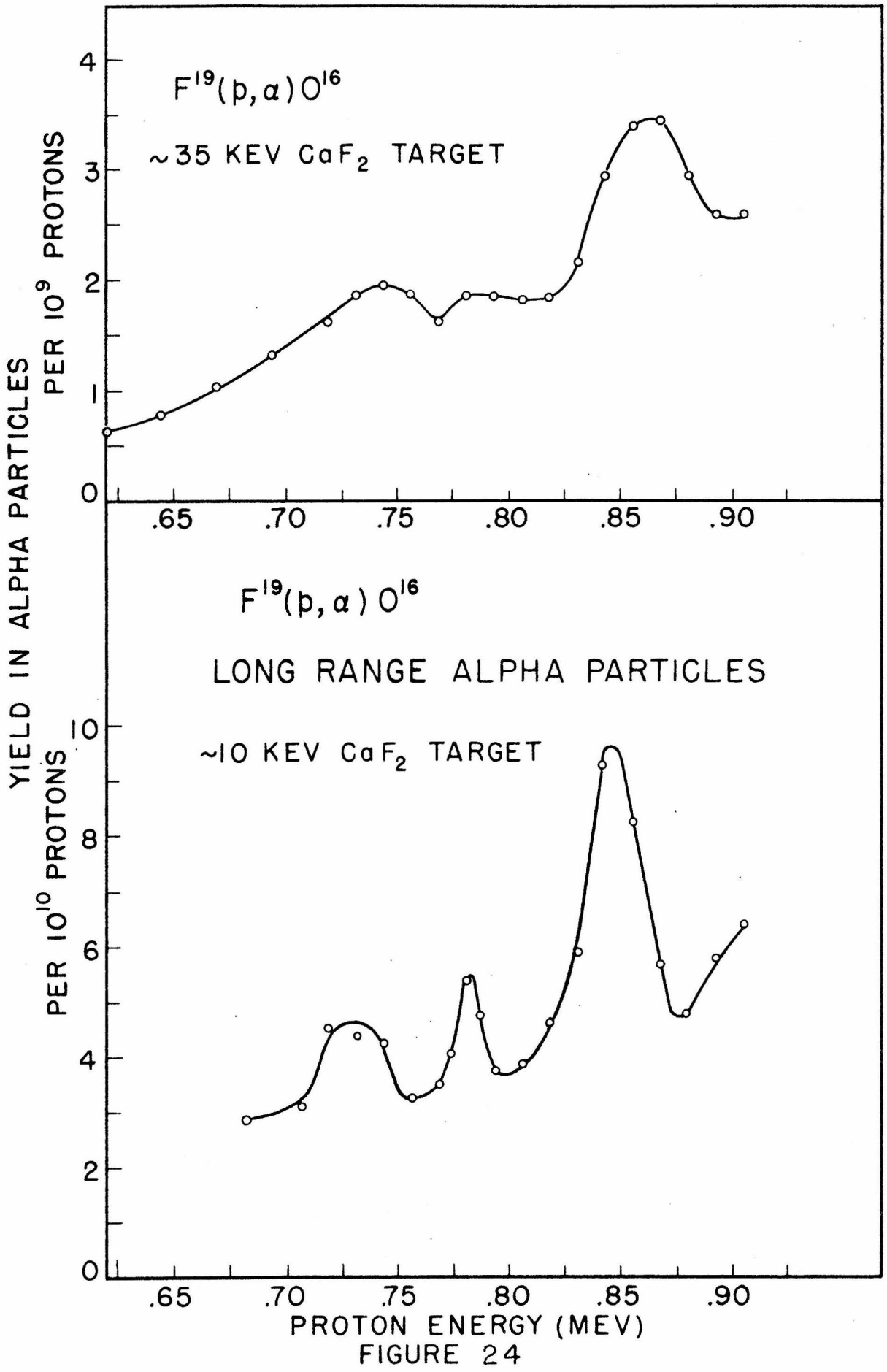
$F^{19}(p,\alpha)O^{16}$
~35 KEV CaF_2 TARGET
$F^{19}(p,\alpha)O^{16}$
LONG RANGE ALPHA PARTICLES
~10 KEV CaF_2 TARGET
YIELD IN ALPHA PARTICLES
PER 10^9 PROTONS
PER 10^{10} PROTONS
0
1
2
3
4
2
4
6
8
10
.65
.70
.75
.80
.85
.90
PROTON ENERGY (MEV)

FIGURE 24

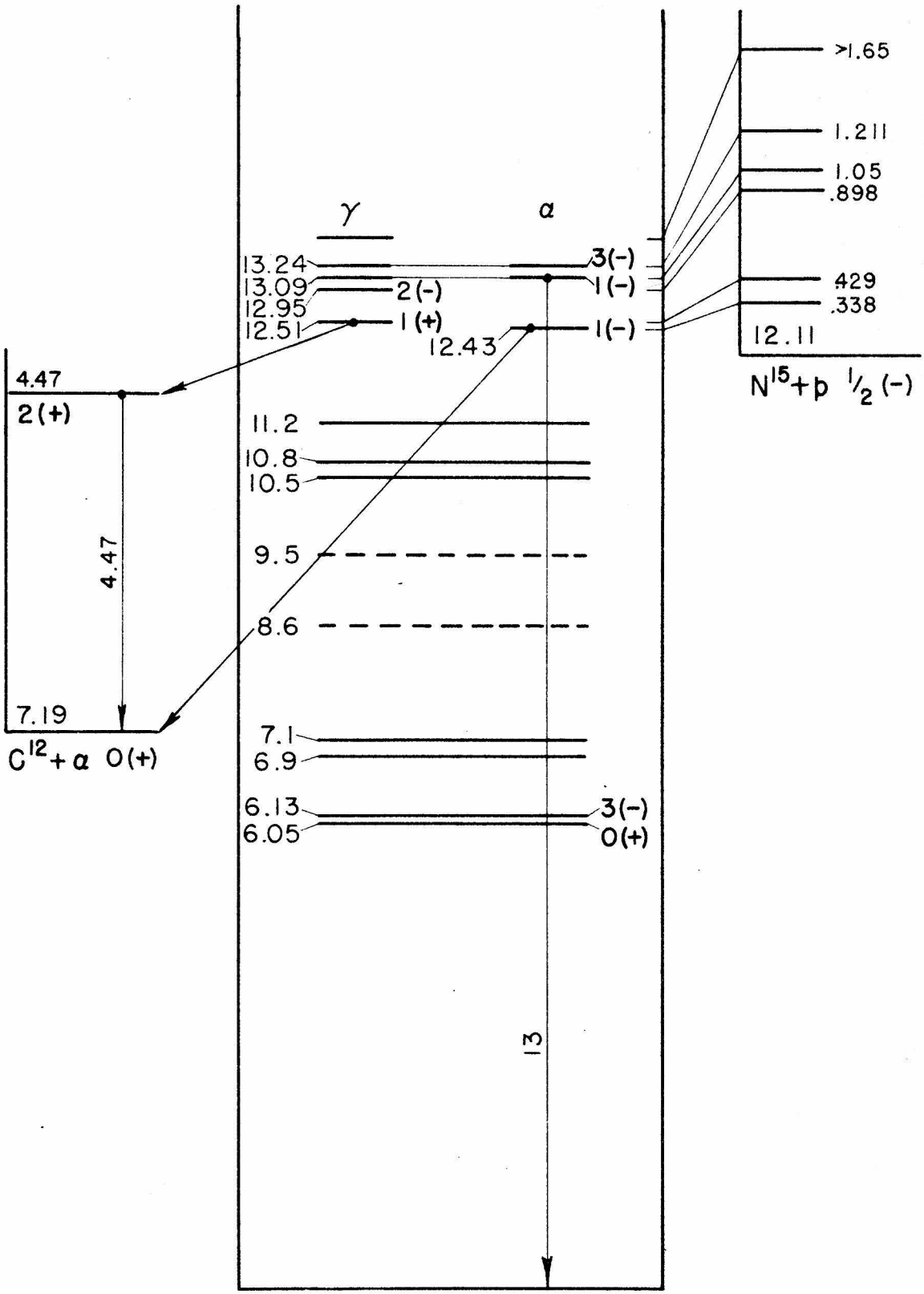
γ
α
13.24
13.09
12.95
12.51
12.43
3(-)
1(-)
2(-)
1(+)
1(-)
>1.65
1.211
1.05
.898
429
.338
12.11
N15+p 1/2(-)
4.47
2(+)
4.47
7.19
C12+α 0(+)
11.2
10.8
10.5
9.5
8.6
7.1
6.9
6.13
6.05
3(-)
0(+)
13
O16 0(+)

FIGURE 25

Table I

Resonance Energy (Mev)	Γ Kev	σ (p,α) barns	σ (p,$\alpha\gamma$) barns	Y (p,$\alpha\gamma$) quanta/proton*	σ (p,γ) barns
0.338**	94	0.075	---	---	---
0.429 ± .001	0.9	---	0.3	4×10^{-9}	---
0.898 ± .001	2.2	---	0.8	5×10^{-8}	---
1.05	~150	0.5	0.015	---	0.001
1.210 ± .003***	22.5***	0.6	0.3	1.8×10^{-7}	---

* Yield is for KNO_3 target containing 61 atom per cent of N^{15}.

** Experimental data has been corrected for S-wave penetration factor.
E_{max} = 0.36 Mev σ_{max} = 0.09 barn

*** These values were measured from the σ (p,$\alpha\gamma$) curve and may be different for σ (p,α).

TABLE II

Proton Energy (Mev)	Relative α Energy (Mev)	Penetration factor for short range alpha particles			
		S wave	P wave	D wave	F wave
0.429	0.954	4.1×10^{-5}	1.6×10^{-5}	2.7×10^{-6}	2.9×10^{-7}
0.898	1.423	2.4×10^{-3}	1.2×10^{-3}	2.0×10^{-4}	2.2×10^{-5}
1.05	1.58	6.3×10^{-3}	3.1×10^{-3}	6.6×10^{-4}	7.6×10^{-5}
1.21	1.74	1.3×10^{-2}	5.8×10^{-3}	1.3×10^{-3}	1.6×10^{-4}

TABLE III

Resonance Energy (Mev)	Proton Wave	State in O16	Γ_p kev	Q_p Mev	Long Range α Particles: partial wave	Long Range α Particles: Γ_α kev	Γ_α, kev	SHORT RANGE ALPHA PARTICLES leading to 4.5 Mev State in C12: 1(+) State: partial wave	1(+) State: Q_α, Mev	1(-) State: partial wave	1(-) State: Q_α, Mev	2(+)* State: partial wave	2(+)* State: Q_α, Mev	2(-) State: partial wave	2(-) State: Q_α, Mev	3(+) State: partial wave	3(+) State: Q_α, Mev	3(-) State: partial wave	3(-) State: Q_α, Mev	Capture Radiation: Γ_γ ev.	Capture Radiation: transition
0.338	S	1(-)	1.1	0.50	P	94															
"	P	0(+)	3.2	9.1	S	94		—	—					—	—	—	—				
"	P	2(+)	0.64	1.8	D	94															
0.429	S	0(-)	0.9	0.12	—	—	0.015	P	0.97	—	—	—	—	D	5.7	F	52	—	—		
"	P	1(+)	0.9	0.64	—	—	0.005^2	S	0.13	P	0.32	D	1.9	P	0.32	D	1.9	F	18		
"	D	2(-)	0.9	17	—	—	0.0031	P	0.19	D	1.1	P	0.19	S	0.075	P	0.19	D	1.1		
0.898	P	1(+)	1.1**	0.032	—	—	1.1	S	0.46	P	0.92	D	5.5	P	0.92	D	5.5	F	50		
"	D	2(-)	1.6	0.60	—	—	0.57	P	0.48	D	2.9	P	0.48	S	0.24	P	0.48	D	2.9		
" "	D	2(-)	0.57	0.21	—	—	1.6	P	1.33	D	8.0	P	1.33	S	0.67	P	1.33	D	8.0		
"	F	3(+)	1.8	18	—	—	0.35	D	1.8	F	16	D	1.8	P	0.29	S	0.15	P	0.29		
"	F	3(+)	0.35	3.5	—	—	1.8	D	9.0	F	82	D	9.0	P	1.5	S	0.75	P	1.5		
1.05	S	1(-)	105	0.58	P	45	1.5	P	0.48	S	0.24	P	0.48	D	2.3	F	20	D	2.3	100	el. dip.
"	S	1(-)	45	0.25	P	105	3.5	P	1.1	S	0.55	P	1.1	D	5.3	F	46	D	5.3	230	" "
"	P	2(+)	128	2.2	D	22.5	0.74	D	1.1	P	0.24	S	0.12	P	0.24	D	1.1	P	0.24	50	el. quad.
"	P	2(+)	23	0.39	D	125	4.2	D	6.4	P	1.3	S	0.67	P	1.3	D	6.4	P	1.3	280	" "
"	D	3(-)	135	27	F	15	0.50	F	6.6	D	0.76	P	0.16	D	0.76	P	0.16	S	0.08	33	el. oct.
"	D	3(-)	15	3.0	F	135	4.5	F	59	D	6.8	P	1.45	D	6.8	P	1.45	S	0.71	300	" "
1.21	P	2(+)	1.1**	0.012	D	7.6	3.7	D	2.8	P	0.64	S	0.28	P	0.64	D	2.8	P	0.64		
"	D	3(-)	16	1.7	F	4.5	2.2	F	14	D	1.7	P	0.38	D	1.7	P	0.38	S	0.17		
"	D	3(-)	6.7	0.71	F	11	5.2	F	33	D	4.0	P	0.90	D	4.0	P	0.90	S	0.40		

— Transition forbidden by selection rules.
* Lowest excited state of C^{12} predicted by alpha particle model.
** Observed yield 25% larger than maximum possible yield.

TABLE IV

Resonance Energy (Mev)	Proton Wave	State in O^{16}	Alpha Wave* α_o	Alpha Wave* α'	Nuclear Width in Mev G_p'	Nuclear Width in Mev Γ_{α_o}	Nuclear Width in Mev $G\alpha'$	Capture Radiation Γ_γ in ev
0.338	S	1 (-)	P		0.50	0.094		
0.429	P	1 (+)	—	D	0.64	—	1.9	
0.898	D	2 (-)	—	D	0.60	—	0.48	
1.05	S	1 (-)	P	P	0.58	0.045	0.48	100
1.210	D	3 (-)	F	P	0.71	0.011	0.90	

* α_o refers to long range alpha particles and α' to short range alpha particles.